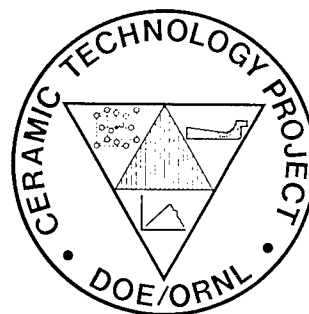# ornl

OAK RIDGE
NATIONAL
LABORATORY

MARTIN MARIETTA

Transformation-Toughened
Silicon Nitride

Final Report

H. W. Carpenter

*CERAMIC TECHNOLOGY FOR
ADVANCED HEAT ENGINES*

$D142154$

$BmDo$

19980123 003

TRANSFORMATION-TOUGHENED SILICON NITRIDE

Final Report

H. W. Carpenter

Date Published — August 1988

Prepared by
Rockwell International
Rocketdyne Division
6633 Canoga Avenue
Canoga Park, CA 91304
Under Subcontract 86X-22009C

Prepared for
U.S. Department of Energy
Assistant Secretary for Conservation and Renewable Energy
Office of Transportation Systems
Advanced Materials Development Program
(EE 04 00 00 0)

for
OAK RIDGE NATIONAL LABORATORY
Oak Ridge, Tennessee 37831
operated by
MARTIN MARIETTA ENERGY SYSTEMS, INC.
for the
U.S. DEPARTMENT OF ENERGY
under Contract DE-AC05-84OR21400

FOREWORD

Work described herein was performed by the Rocketdyne Division of Rockwell International for Martin Marietta, Oak Ridge National Laboratory (ORNL) under the sponsorship of the U.S. Department of Energy, Ceramic Technology for Advanced Heat Engine Program, Contract No. 86X-22009C. This work was performed over the period 1 June 1985 through 31 August 1987. Dr. G. D. Schnittgrund of Rocketdyne Division Advanced Programs was Program Manager and H. W. Carpenter of Rocketdyne's Materials Engineering and Technology was Project Engineer. Major technical contributions were provided by Dr. F. F. Lange, formerly of Rockwell Science Center, Thousand Oaks, CA, and presently on the faculty at the University of California at Santa Barbara. T. N. Tiegs was the ORNL Program Monitor.

CONTENTS

ILLUSTRATIONS

TABLES

vii

ACKNOWLEDGMENTS

ABSTRACT

Composites, consisting of a silicon nitride (Si_3N_4) matrix containing dispersions of phase-stabilized zirconia (ZrO_2), were prepared by colloidal processing and sintering to near full density. These materials exhibited improved strength and increased fracture toughness relative to the matrix alone. The effects of ZrO_2 content, phase-stabilizer type and amount, and processing conditions on mechanical and thermophysical properties of the resultant composites were determined. The possibility of high-volume, low-cost production was demonstrated by successfully injection molding samples.

Specific systems that appear promising for various alternative applications were developed. A composite containing 45 w/o (~30 v/o) ZrO_2 phase-stabilized with Y_2O_3 exhibited a 50% improvement in fracture toughness, (6 MPa m$^{1/2}$), high room temperature flexural strength (1000 MPa), low thermal expansion, and low thermal conductivity. Use of Y_2O_3 plus SiO_2 as sintering aids with this composite was shown to maintain high strength to temperatures of 1400 C. A second system containing from 30 w/o (~20 v/o) to 45 w/o (~30 v/o) ZrO_2 phase-stabilized with CaO also exhibited high fracture toughness and high strength. Further improvements (up to threefold) in fracture toughness were obtained by heat treatment. The CaO-containing system is limited to relatively low use temperatures of less than 700 C.

Probable toughening due to the martensitic tetragonal to monoclinic transition of zirconia has been hypothesized. Potential applications for these toughened systems include cryogenic turbopump bearings, intermediate use temperature applications in diesel engines, and high-temperature turbine uses. Materials will have to be tailored and optimized for each of these areas.

1

3

SUMMARY

A family of toughened structural ceramic composites consisting of a Si_3N_4 matrix plus dispersions of ZrO_2 or HfO_2 was developed that offers a combination of unique properties which, compared to monolithic Si_3N_4, include:

- Increased fracture toughness
- Increased strength
- Significantly higher toughness and strength by heat treatment for low and intermediate temperature applications
- Lower thermal conductivity
- Lower thermal expansion

These materials further offer:

- Adaptability to conventional fabrication methods
- Excellent figure of merit for resistance to thermal shock
- Potential as a matrix for whisker- or filament-reinforced composites.

Colloidal processing methods were used in this program to break up soft agglomerates and to eliminate hard agglomerates. Thus, particle size was controlled to provide a homogeneous, fine-grain microstructure free from agglomerates, and one that readily sintered to near full density. Colloidal processing also allowed complete dispersion of the second phase, and it is compatible with conventional low-cost fabrication methods such as sli) casting and injection molding.

Two approaches were successfully used to achieve composite compositions that exhibited increased toughness with concomitant increased strength and that did not exhibit microcracking when oxidized at intermediate temperatures.

The first approach used dispersed ZrO_2 particles stabilized with Y_2O_3. The presence of yttrium cation in the ZrO_2 lattice inhibited the formation of zirconium oxynitride, which was determined to be the probable cause of the intermediate temperature cracking problem. The second approach was to use

ZrO_2 particles stabilized with CaO. The CaO stabilization did not prevent the formation of zirconium oxynitride but the subsequent surface stresses, that normally caused microcracking, could be controlled by heat treatment to provide useful structural compositions with increased strength and significantly increased apparent toughness. Partial dissolution of CaO and the presence of CaO in the grain boundaries, however, limits this material to low to intermediate temperatures, less than 700 C.

Average room temperature strength and fracture toughness values of these composites are listed in Table 1. Values for Si_3N_4 matrix without any toughening and values for Si_3N_4 toughened with SiC whiskers are provided for comparison. Room temperature strength of all transformation-toughened composite systems was higher than 800 MPa and strength could be increased as much as 40% by heat treatment. The strength gained by heat treatment, however, would not be useful for high-temperature service. Compositions of Si_3N_4 plus $ZrO_2(Y_2O_3)$ sintered with selected mixtures of Y_2O_3 and SiO_2 showed no loss of strength at 1400 C. Room temperature strength was low, however, due to processing difficulties that were attributed to the character of the starting powders and to metal inclusions originating from erosion of the sonic mixing equipment. Strength of the same composition, but prepared using a colloidal processing method and sintered using 4 w/o Al_2O_3 as a sintering aid, was 700 MPa at 1000 C and 360 MPa at 1200 C, which is a retention of 75 and 60% of room temperature strength, respectively. Strength decreased above 1200 C for these samples.

Fracture toughness of the Si_3N_4 + 45 w/o (~30 v/o) $ZrO_2(Y_2O_3)$ composite increased above the level of the Si_3N_4 matrix when the Y_2O_3 alloy content in the ZrO_2 particles was reduced below 9 w/o. The toughness increased linearly to 6 MPa m$^{1/2}$ at a Y_2O_3 content of 4.5 w/o. The presence of ZrO_2 particles in the Si_3N_4 matrix also influenced thermal properties. Thermal diffusivity was significantly lower, which indicates lower thermal conductivity, for these composites than that predicted by rule of mixtures. A low thermal conductivity is necessary for some heat engine applications. Thermal expansion, on the other hand, followed the rule of mixtures, and the resultant low thermal

Table 1. Summary of Results

Toughening Mechanism	Material	Flexural Strength, MPa	Fracture Toughness, MPa m$^{1/2}$
None	Si_3N_4 matrix	700-965	4
Whisker reinforcement	Si_3N_4 + SiC whiskers*	700	5-6
Transformation toughening	Si_3N_4 + $ZrO_2(Y_2O_3)$	800-1000	4-6
Transformation toughening	Si_3N_4 + $ZrO_2(CaO)$	900-1200	7-14
NA	Si_3N_4 + $HfO_2(Y_2O_3)$	915	NA

*Typical Properties

expansion contributes favorably to the figure of merit for thermal shock resistance. Thus, additions of 30 and 45 w/o $ZrO_2(Y_2O_3)$ had a synergistic effect on the Si_3N_4 matrix in that composites exhibited increased strength, a large increase in toughness, a large decrease in thermal diffusivity (Fig. 1), and a high figure of merit for resistance to thermal shock.

$HfO_2(Y_2O_3)$ dispersions were substituted for ZrO_2 dispersions to demonstrate that Si_3N_4 + HfO_2 composites could be sintered to near theoretical density with similar properties to the Si_3N_4 + ZrO_2 composites. A composition of Si_3N_4 + 69 w/o HfO_2(10 m/o Y_2O_3) + 4 w/o Al_2O_3 sintered to high density with an average room temperature flexural strength of 915 MPa. High-temperature strength was slightly higher than that of comparable compositions containing ZrO_2 dispersions. Transformation toughening was not expected, however, because the HfO_2 (Y_2O_3) dispersion was fully stabilized.

The average strength and toughness values for composites composed of Si_3N_4 matrix containing ZrO_2 particles alloyed with CaO also are listed in Table 1. Strength at room temperature was as high as that for the compositions made using ZrO_2 dispersions alloyed with Y_2O_3, but strength began decreasing above 700 C. Toughness of these composites in the as-densified

HIGH TOUGHNESS

Si_3N_4 ZrO_2

LOW THERMAL DIFFUSIVITY

Si_3N_4 ZrO_2

LOW THERMAL EXPANSION

Si_3N_4 ZrO_2
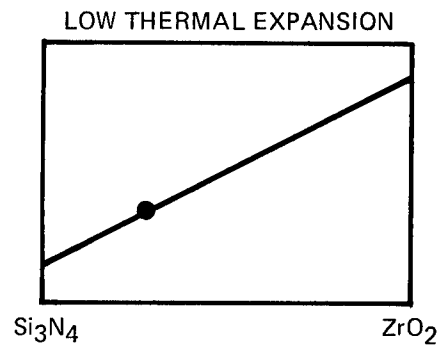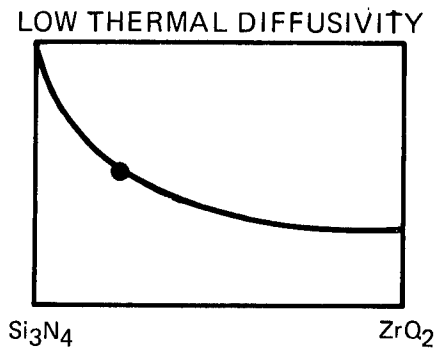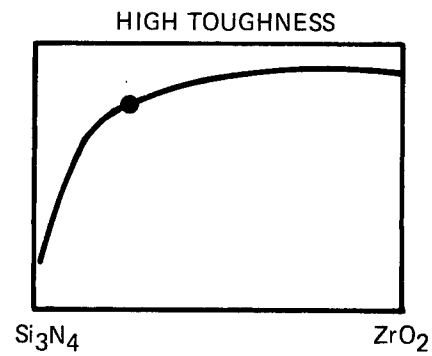
Figure 1. Benefits of Adding Small
Amounts of ZrO_2 Particles
to Si_3N_4 Matrix

condition was almost double that of the Si_3N_4 matrix, and toughness was increased to as high as 14 MPa $m^{1/2}$ by heat treatment. This increase was not an increase in inherent toughness, rather, it was the result of increased surface compressive stresses caused by the oxidation of zirconium oxynitride and the subsequent formation of monoclinic ZrO_2. Thermal diffusivity of this composition was higher than that for the composition made with ZrO_2 stabilized with Y_2O_3. Thermal diffusivity values were more in line with results predicted by the rule of mixtures. These composites offer a unique combination of high strength and very high toughness for applications at temperatures less than 700 C.

Injection-molded samples of Si_3N_4 + 45 w/o ZrO_2(9 w/o Y_2O_3) + 4 w/o Al_2O_3 were fabricated to demonstrate the feasibility of high-volume, low-cost production. Injection molding characteristics of this composition were the same as for Si_3N_4 without the ZrO_2 dispersion. Average flexural strength values for injection-molded samples were lower than those for colloidally processed material. The bend bar geometry used, pick-up of metallic inclusions during processing, and inhomogeneous distribution of the injection molding plasticizer are all considered sources of the reduced strength.

TECHNICAL BACKGROUND

The fracture toughness of Si_3N_4 can be increased by:

1. The addition of high-strength and elastic modulus, high aspect ratio, small-diameter SiC whiskers

2. The addition of a lower thermal expansion coefficient second phase

3. Heat treatment to grow acicular β-Si_3N_4 grains

4. Inclusion of dispersions that toughen by a phase transformation mechanism.

Toughening by the addition of SiC whiskers occurs principally by crack deflection and whisker pullout which limits toughness increases to about 50% over the matrix. Best results are achieved with high whisker loadings; however, processing becomes more difficult at high loadings. Uniform dispersion of the whiskers becomes increasingly difficult as the concentration increases. There is also a tendency for the whiskers to orient due to shear forces resulting in anisotropic properties. The net result of such processing difficulties is a subsequent inability to maintain strength and isotropy at the high loadings needed to improve toughness.

Toughening by a dispersed second phase having a lower thermal expansion coefficient than the matrix will theoretically result in toughening due to the residual stress fields around the second phase. The hoop tension field, as shown in Fig. 2, attracts passing cracks rather than deflecting them away. There is more dissipation of energy compared to the case in which the thermal expansion coefficient of the particle is higher than the matrix and in which the passing crack is deflected away from, rather than into, the particle. This method has not been demonstrated due to the lack of a suitable second phase that (1) has a lower thermal expansion coefficient than Si_3N_4, (2) is stable, and (3) is compatible with Si_3N_4 at elevated temperatures.
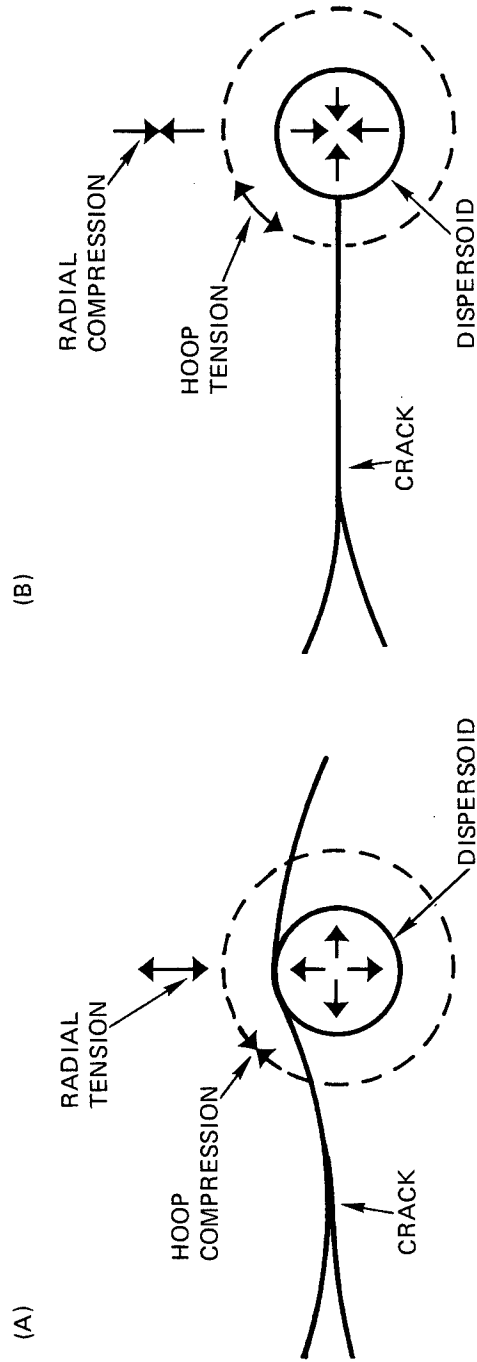
Figure 2. Dispersion-Toughened Material Containing Particles with:
(a) Higher Thermal Expansion Coefficient and (b) Lower Thermal
Expansion Coefficient

The use of transformation toughening in the Si_3N_4 matrix, on the other hand, increased toughness by as much as threefold over that of the Si_3N_4 matrix and there is no decrease in strength. In fact, in some cases, strength is 40% higher than that of the matrix material.

Transformation toughening is the basis for a new group of commercial materials based on partially stabilized zirconia (PSZ). Zirconia undergoes a martensitic, athermal phase transformation on cooling over the range from about 1400 to 1000 C. This phase change from the tetragonal phase to the monoclinic phase is accompanied by a 5% volume increase. Toughened materials can be obtained by inhibiting the phase change during fabrication so that the resultant material retains the metastable tetragonal phase at room temperature. When the phase change is triggered by the strain of an advancing crack, compressive loading occurs in the lattice around and ahead of the advancing crack tip. The result is an increase in toughness in the PSZ material from as low as 2 MPa $m^{1/2}$ in the untoughened matrix to as high as 13 MPa $m^{1/2}$ in the toughened composites.

Si_3N_4 is one desirable matrix material due to its inherent high strength, high modulus, and superior resistance to thermal shock. Although Si_3N_4 is a leading candidate for heat engine applications, its use is limited in some designs because Si_3N_4 has high thermal conductivity. Additions of small amounts of ZrO_2 to Si_3N_4 can substantially reduce the thermal conductivity of the composite while yielding significant gains in fracture toughness.

Lange (Ref. 2) reported increased surface toughness in the Si_3N_4/ZrO_2 system resulting from an oxidation-induced phase change. Reactions leading to increased toughness begin with the formation of Zr-oxynitride during the densification process. When the composite is later heated in an oxidizing environment, the surface Zr-oxynitride converts to ZrO_2. The formation of ZrO_2, which is associated with a volume increase of about 5%, causes compressive surface stresses. These surface stresses can be beneficial, but when the volume content of ZrO_2 is more than 10%, severe microcracking and spalling occur.

Gilles (Ref. 3) determined that the Zr-oxynitride structure was associated with an ordered array of oxygen deficiencies in the lattice. Lange et al. (Ref. 4) reasoned that the addition of an alloying agent to the ZrO_2 with a valence different from that of Zr would disrupt the oxygen-deficient lattice structure and thereby reduce or eliminate the formation of Zr-oxynitride. Results of this study indicated that Y_2O_3 alloy additions in the ZrO_2 did reduce or eliminate the Zr-oxynitride phase and inhibited microcracking.

PROCEDURE

COLLOIDAL POWDER PROCESSING

Silicon nitride composites containing dispersed ZrO_2 must be fine grained, exhibit complete dispersion of the ZrO_2 particles, and be free of large flaws. For these reasons, composites were made using colloidal processing methods. Colloidal processed material produced microstructures that exhibited homogeneity and excellent dispersion of the ZrO_2 particles (Fig. 3). With proper controls, the microstructure can be made with a very low flaw population and very small flaw sizes. The colloidal method can also be compatible with high-volume, low-cost production methods, such as injection molding and slip casting. Another advantage of colloidal processing is that slurry mixtures of two or more powders have long shelf lives. Mixtures can be stored in the flocced state without concern of powder segregation.

Each component, e.g., Si_3N_4, ZrO_2, or selected sintering aids, was separately suspended in dilute water solutions of less than 5 v/o solids to break up soft agglomerates and to remove hard agglomerates by sedimentation. Suspension was achieved by controlling pH. A pH of 10 was used to suspend Si_3N_4 and a pH of 2 was used to suspend ZrO_2 powders. Based on Stoke's Law calculations, the dilute solutions were allowed to settle to remove all particles over 1 micron. Settling duration was typically 24 h for Si_3N_4 and 16 h for ZrO_2 powders. The slurry containing particles less than 1 micron was siphoned into a clean container (Fig. 4), washed, and flocculated so that the excess water could be removed. The coarse sediment left on the bottom of the original container, which was usually a relatively hard cake, was re-suspended. An ultrasonic horn was used to break up the hardened cake and to re-suspend the powder. The suspension was again allowed to settle and the submicron powder was again siphoned off into a clean container. This process was repeated until most of the submicron powder was separated. Usually four separation cycles were sufficient.

Figure 3. Typical Microstructure Showing Good Dispersion of the Second Phase and Lack of Agglomerates
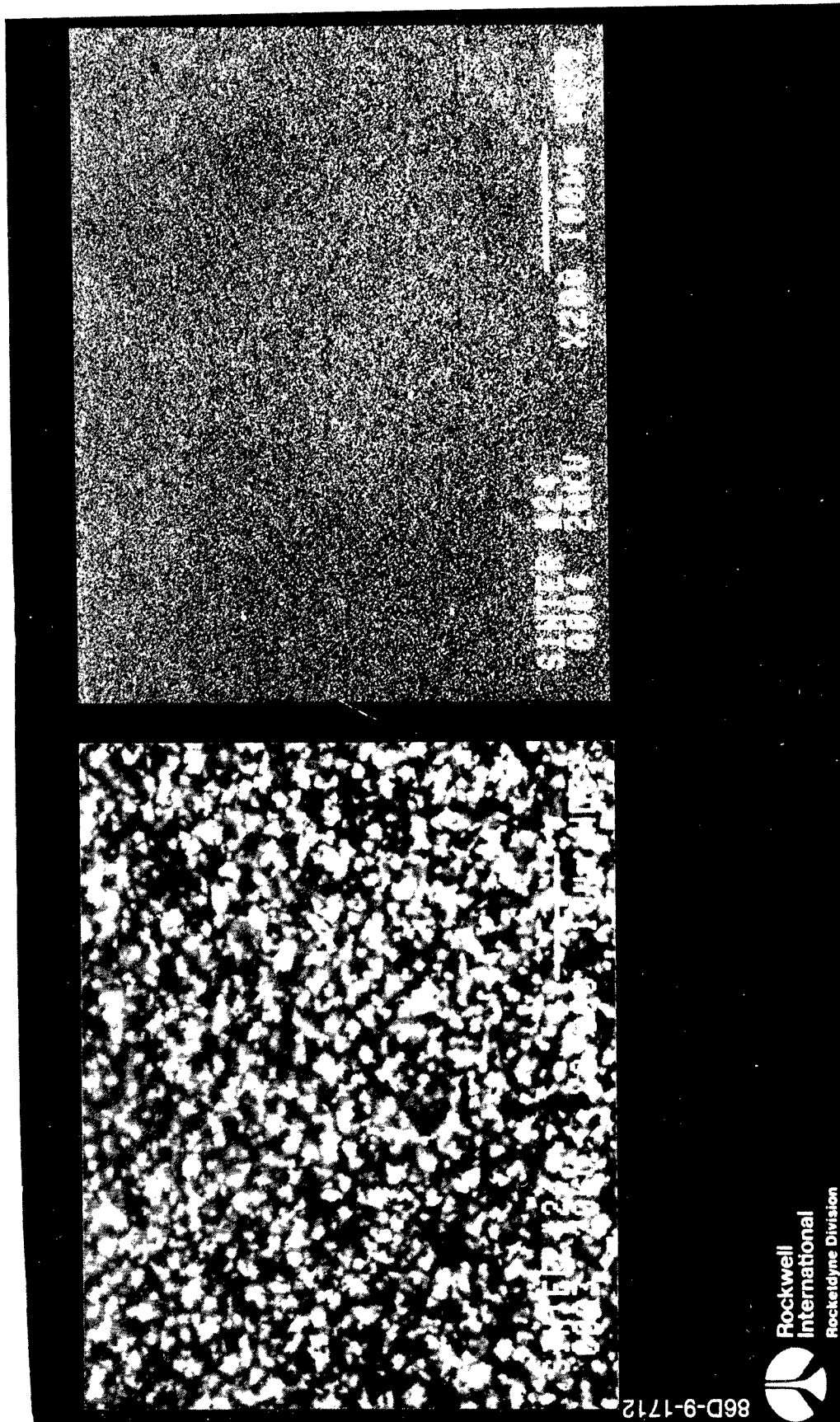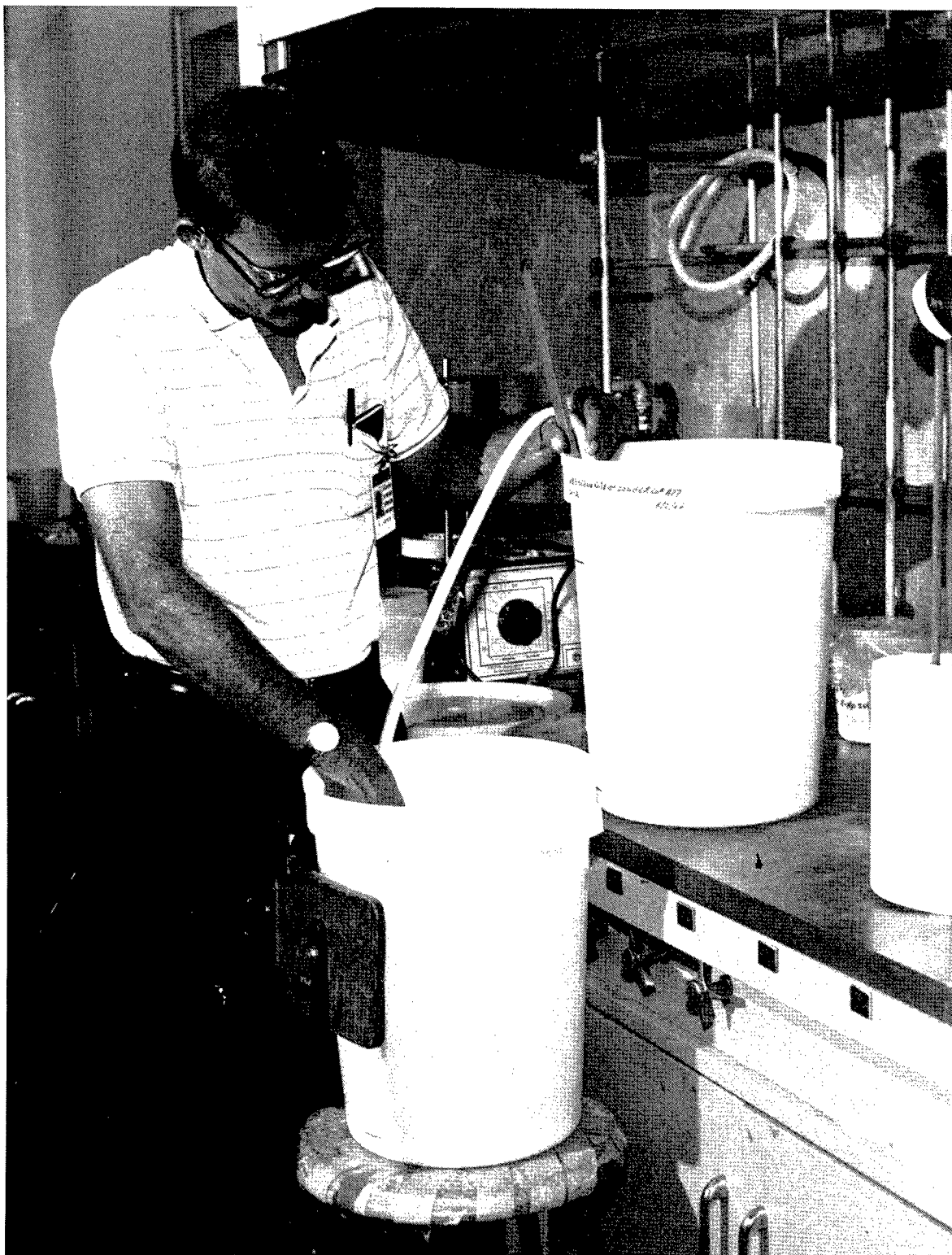
Figure 4. Siphoning the Slurry Containing Less
Than 1 Micrometer Particles

The concentration of solids in the slips was determined by measuring the slip specific gravity from which concentration was calculated. The desired quantity of the specified, flocculated slip was then weighed into a separate beaker. Each of the ingredients was then mixed together by manually stirring. The mixture was then pumped back and forth through a small ultrasonic mixing chamber* for a total of four passes (Fig. 5). Controlled parameters included pumping speed and power input to the ultrasonic horn. A photomicrograph of a typical composite (Fig. 3) illustrates the good dispersion of the second phase, good homogeneity, and the lack of inclusions in the microstructure.

High-purity, submicron powders were used whenever possible to make colloidal processing both practical and possible. Exceptions are noted in the text. All composites were based on a single Si_3N_4 matrix powder source (Table 2). ZrO_2 and HfO_2 were obtained from five different sources to obtain a range of alloying compositions and levels. Characteristics and chemistries of these powders are given in Table 3.

Table 2. Si_3N_4 Powder Characteristics

Composition	Si_3N_4
Source	UBE Industries, Ltd.
Grade	SN-E-10
Lot	A-77
Particle size	0.1 to 0.3 microns
Surface area	14 m^2/g
Degree crystallinity	100%
Phase content, $\dfrac{beta}{(alpha + beta)}$	3.5%

---

*Fischer Sonic Dismembrator Model 300
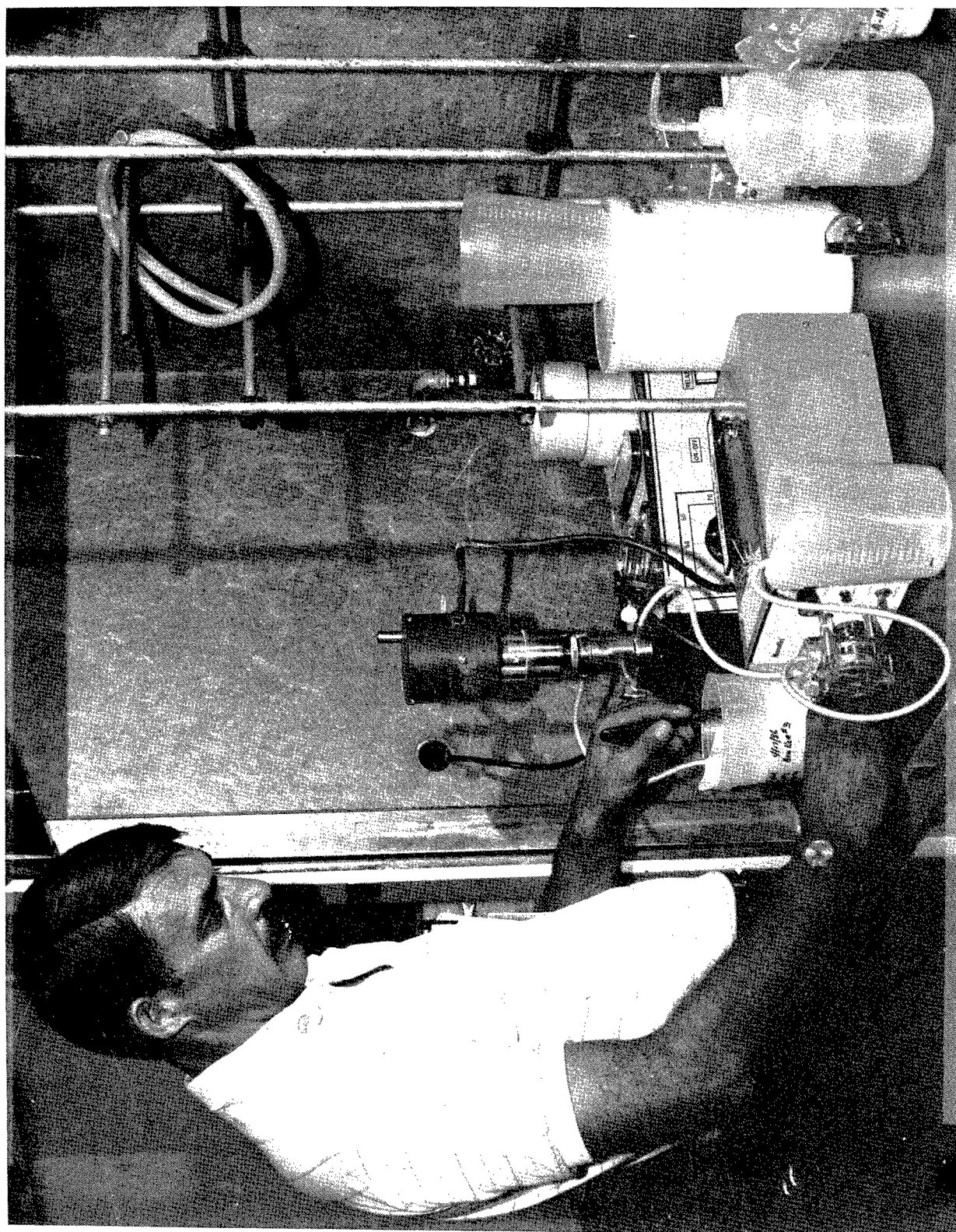
Figure 5. Pumping Slurry Through the Sonic Mixing Chamber

Table 3. Powder Characteristics
(Sheet 1 of 3)

Zirconia

Composition – ZrO_2 (Y_2O_3)

Source – Toyo Soda Mfg. Co. Ltd., Tokyo

Grade	TZ-4Y	TZ-6Y	TZ-8Y
Lot	Z405117P	Z605106P	Z805125P
Crystallite size (Angstroms)	220	220	220
Specific surface area (m^2/g)	20	19	23
Chemical analysis (w/o)			
Y_2O_3	7.02	10.37	13.25
Al_2O_3	0.06	0.056	0.007
SiO_2	0.005	0.005	0.007
Fe_2O_3	0.003	0.003	0.006
Na_2O	0.003	0.006	0.006
Ignition loss	0.5	0.8	0.5

Zirconia

Source – Zircoa Products, Corning Glass Works, Solon, OH

Type – Zircoa-B fully stabilized 5 w/o CaO

4.69 μm average particle size (-325 mesh)

SiO_2	0.68 w/o
CaO	5.12
MgO	1.16
Fe_2O_3	0.07
Al_2O_3	0.12
TiO_2	0.11

Zirconia

Source – Zircar, Florida, NY

Lot	P-298-B	P-298-C	P-301
Chemical Analysis (w/o)			
CaO	3.30	6.75	9.93
Loss on ignition	3.80	9.74	5.90

Table 3. Powder Characteristics
(Sheet 2 of 3)

<u>Zirconia</u>

Source - Zircar, Florida, NY

Type - ZYP Stabilized

	4.5 w/o Y_2O_3	8.0 w/o Y_2O_3	12.0 w/o Y_2O_3
Al_2O_3	0.019	0.019	0.019
SiO_2	0.2	0.2	0.2
TiO_2	0.22	0.22	0.22
Fe_2O_3	0.039	0.039	0.039
CaO	0.020	0.020	0.020
MgO	0.021	0.021	0.021
Cl	0.10	0.18	0.26
Na_2O	0.03	0.04	0.06
SO_4	0.11	-	-
H_2O	1.0	1.0	1.0
LOI	1.0	1.0	1.0

Agglomerate Size Distribution (%)

<1 μm	97
<0.7 μm	85
<0.5 μm	72
<0.3 μm	50
<0.1 μm	30
Crystallite size	0.02-0.03 μm
Surface area	30-45 m^2/gram

Table 3.   Powder Characteristics
(Sheet 3 of 3)

<u>Zirconia</u>

Source - Nippon Shokubai Kagaba Koggo Co., Ltd.

Grade - NS-8Y

Y_2O_3 8 mol %

Surface area   80 m^2/g

Particle diameter   130 angstroms

Chemical analysis (w/o)

  Y_2O_3 13.7

  SiO_2 0.03

  Al_2O_3 0.09

  TiO_2 0.03

  Fe_2O_3 0.006

<u>Hafnium Oxide</u>

Source - Teledyne Wah Chang

Grade - S

Type - K-906

1 to 2 microns powder

10 mole percent Y_2O_3

SAMPLE PREPARATION

Disk-shaped samples, 5 cm in diameter x 1 to 2 cm thick, were prepared by pressing the water out of flocced slurries in a special metal die (Fig. 6). One, or both (at the option of the technician) ends of the plunger was fitted with a porous metal filter to allow the water from the slurry to escape under pressure. A layer of coarse filter paper was placed over the metal filter to keep the fine powder from plugging it. A pressure of about 0.5 MPa (70 psi) was used to force the water out. Lower pressures took too long to remove the water, while higher pressures usually produced samples that cracked during drying.
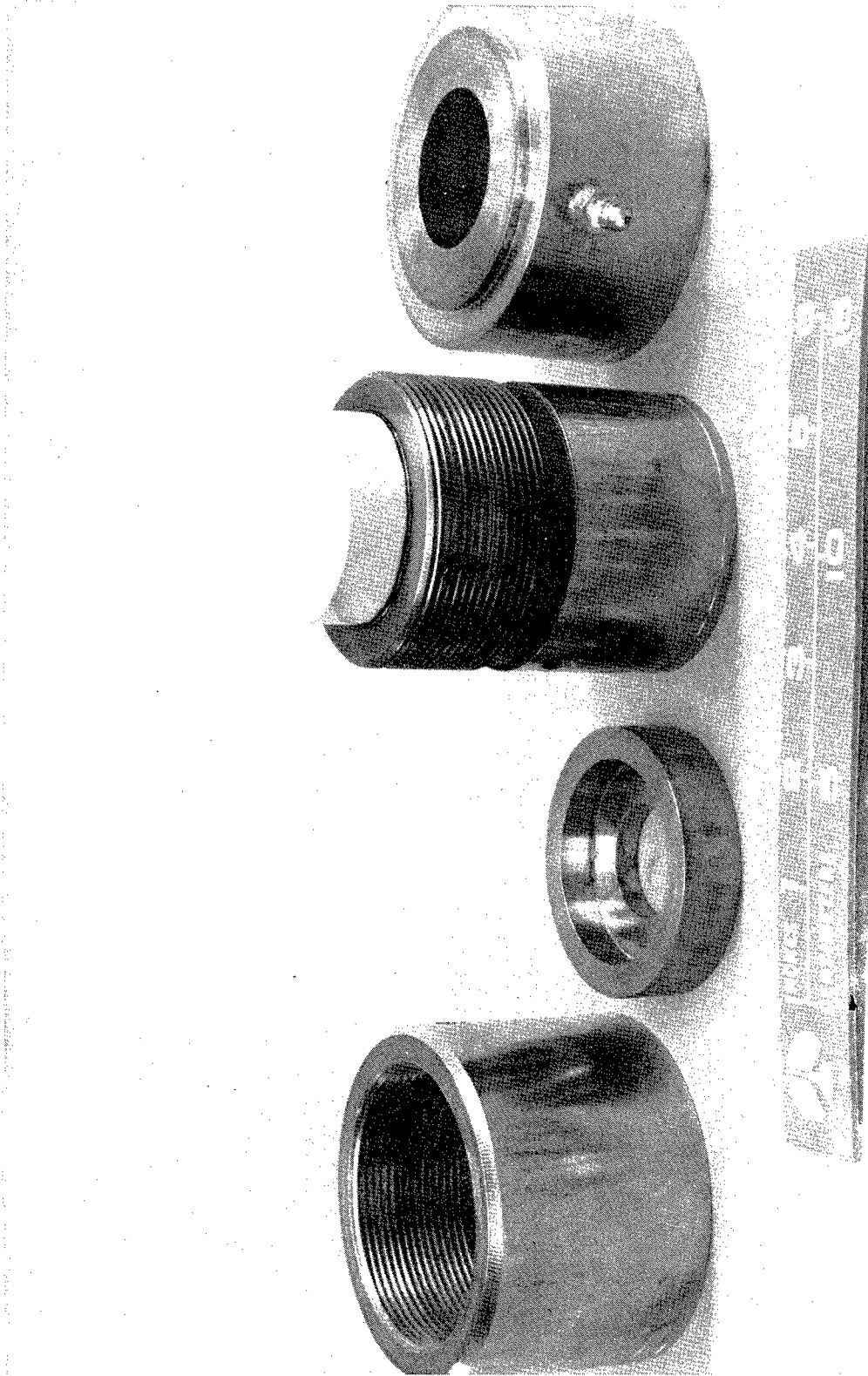
Figure 6. Pressure Filtration Die with Pressed Sample

The samples were air dried slowly then placed in a vacuum oven at 60 C. Green density was typically about 40% of theoretical, but this was increased to about 50% by isostatic pressing to pressures as high as 350 MPa.

Samples were densified by either pressureless sintering or hot pressing. Pressureless sintering was performed under 1 atm of nitrogen in a carbon resistance furnace. Samples were placed in a Si_3N_4 crucible and packed in a seasoned Si_3N_4 powder. Hot pressing was performed under 1 atm of nitrogen using graphite dies and varying compaction pressures from 26 to 52 MPa. The rate of heating and cooling for both densification routes was rapid, typically 1 h from room temperature to the sintering temperature, which ranged from 1700 to 1860 C, hold for 1 h, and furnace cool.

EVALUATION OF SAMPLES

Samples were characterized by the following techniques after densification. Density and porosity were measured by a modified-Archimedes method. X-ray diffraction analyses were performed on diamond-ground or diamond-cut surfaces using a General Electric X-ray diffraction unit with Cu-Kα radiation.

MOR bars with a cross section of 2.0 x 2.5 mm were made by diamond grinding to a surface finish of 10 μinch. MOR bar length ranged from 18 mm to 40 mm and varied depending on stock. All diamond grinding was in the long direction and edges were chamfered. Due to the short length of the average MOR bar and the large number of MOR tests that were required, 3-point bend tests with a span of 15.2 mm were used for most of the initial evaluations. Four-point tests were performed when a large sample population was available and when the sample length was adequate. Two fixtures were used for 4-point bend tests, one with spans of 23 and 8 mm, and one with spans of 32 and 11 mm. The larger fixture was made of SiC and was used for all tests at elevated temperatures. The span on 3-point tests was 15.2 mm. Crosshead rate was 0.05 cm/min.

Fracture toughness was measured by the diamond indentation method after Anstis (Ref. 5) and by breaking pre-indented MOR bars after Cook and Lawn (Ref. 6). Crack length measurements on indented samples were made using a light microscope and a side-angle lighting technique to define the crack tip.

Heat treatments performed on samples were conducted in a resistance heated furnace (SiC heating elements) in static air.

TECHNICAL DISCUSSION

The experimental work in this program was conducted on five families of composites. These composites included an Si_3N_4 matrix, a sintering aid, and from 10 to 30 v/o of one of the following additives as a dispersed phase:

1. ZrO_2(4.0 w/o to 13.5 w/o Y_2O_3)

2. ZrO_2 (3.5 w/o to 10 w/o CaO)

3. ZrO_2 (5 w/o MgO)

4. HfO_2 (10 m/o Y_2O_3)

5. 60 m/o HfO_2 + 20 m/o ZrO_2 + 20 m/o TiO_2.

Each of these five families of compositions is discussed in a separate section of this report. Most of the experimental work was conducted on the first two compositions because of the highly promising early results. The third composition was of interest because it is more refractory, but investigation of this composition was not pursued because the initially densified samples cracked during the hot pressing operation. The fourth composition contained fully stabilized HfO_2 as a dispersed phase. Testing of the fifth composition was discontinued because the oxide alloy reacted with the Si_3N_4 matrix and cracked excessively when oxidized.

$ZrO_2(Y_2O_3)$

Composites of Si_3N_4 +30 w/o (~20 v/o) or 45 w/o (~30 v/o) ZrO_2 (Y_2O_3) with sintering aids offer a combination of unique attributes: (1) as-fabricated toughness 50% higher than the Si_3N_4 matrix, (2) high strength, (3) beneficial surface compressive stresses following oxidation, (4) reduced thermal conductivity, and (5) the absence of Zr-oxynitride phase which is a leading cause of microcracking at intermediate temperatures.

Oxidation Degradation Stability

Microcracking at intermediate temperatures (500 to 1000 C) is a problem that has precluded Si_3N_4/ZrO_2 composites from consideration as structural materials in spite of high strength and increased toughness. Three approaches were used in this program to reduce or to eliminate microcracking. The first approach was to alloy the ZrO_2 with a sufficient amount of Y_2O_3 as suggested by Lange (Ref. 4). The second was to preoxidize the sample at an elevated temperature before exposure to the intermediate temperature. The third was to sinter the composite at higher temperatures.

Near-theoretical density values were obtained for samples sintered at 1700 C for 1 h. In this study, samples were sintered at temperatures to 1800 C to determine the effect on oxidation resistance. The Y_2O_3 alloying content and total ZrO_2 content also were varied. Oxidation was carried out at 700 C for periods from 64 to 1008 h. Samples were observed after oxidation for the appearance of microcracks. Results of these studies are summarized in Table 4.

For samples sintered at 1750 C, there was a high incidence of microcracking with only the 12 w/o Y_2O_3 stabilized material not exhibiting microcracks after 1008 h. For samples sintered at 1800 C, results were more encouraging with microcracking observed only for the 8 w/o Y_2O_3 stabilized sample after 255 h exposure.

The longer exposures appeared to result in less observed microcracking. This is not readily explained unless there is an associated crack healing occurring during extended oxidation. Also, since at least part of the Y_2O_3 is believed to enter into the grain boundary phase, it would be expected that the Y_2O_3 content should also affect microcracking and healing mechanisms. From the data available, it appears as if increasing Y_2O_3 content could be inhibiting healing, so that the higher Y_2O_3 content samples require longer oxidation times to eliminate the appearance of microcracks. The possibility of crack healing and the role of Y_2O_3 is speculative at present and would require further study for confirmation.

Table 4. Intermediate-Temperature Stability Results

Sintering Temperature, C	Sample Identification No.	ZrO2 Content, w/o	Y$_2$O$_3$ Content In ZrO$_2$, w/o	Duration At 700 C, h	Microcracking Observed
1750	21	45	9	284	Yes
	25	45	9	64	Yes
	35	30	12	1008	No
	35	45	12	1008	No
	24	45	13.5	504	Yes
1800	51	45	4.5	255	No
	51	45	6.9	255	No
	53	45	8	255	Yes
1800	54	45	6.9	500	No
	54	45	8	500	No
1800	34	30	9	1008	No
	34	45	9	1008	No

0099a/tab

Preoxidation at an elevated temperature was another method that was successful in reducing or preventing microcracking at intermediate temperatures. The rationale was that microcracking did not occur at elevated temperatures where the body could accommodate the small amount of plastic deformation and, then, when the body was later exposed to oxidation at intermediate temperatures, the oxide layer protected the surface from further oxidation because the oxidation rate through the protective layer was negligible. This approach was used more for compositions containing ZrO_2 stabilized with CaO, and these results are reported later. The limited results for compositions containing ZrO_2 stabilized with Y_2O_3 were as follows. Samples of a composition containing 45 w/o ZrO_2 stabilized with 13.5 w/o Y_2O_3 exhibited microcracking at 700 C after 500 h. When samples were preoxidized at 1200 C for 2 h, however, no microcracking was observed and the strength was retained after exposure in air at 700 C for 570 h.

An attempt was made to characterize the compositions that did and did not exhibit microcracking at intermediate temperatures. Understanding the difference between these so called "good" or "bad" materials is essential so that composition and fabrication history can be controlled to ensure that microcracking will not occur. The difference in appearance between these materials was obvious. All diamond-ground samples were dark grey. On heating at intermediate or elevated temperatures in air, the surfaces became white. The difference between the good and bad materials was in the nature of the white surface layers. The white surface layers on samples that did not microcrack were uniform in thickness, exhibited a distinct boundary line from white to grey, and the layers were thin. Layer thickness was about 25 microns after 100 h at 700 C, and 250 microns after 1000 h.

The white surface layers on samples that microcracked, on the other hand, were nonuniform in thickness, they exhibited a diffuse boundary line between the white and grey areas, and they were much thicker, often penetrating the sample as much as 1000 microns in 200 h.

X-ray diffraction analyses were performed on these materials but no differences between samples that did or did not microcrack were found. Two major phases were present, beta Si_3N_4 and cubic ZrO_2. Sometimes splitting was observed in the major ZrO_2 peaks, indicating the presence of tetragonal-prime ZrO_2 phase. Tetragonal-prime phase is a nontransformable phase that does not lead to toughening. Occasionally, a minor amount of monoclinic ZrO_2 phase was present. In every case, whether it was material sintered at 1750 or 1800 C, the results were similar.

Samples also were characterized using TEM, SEM, and AEM techniques. The analyses were performed on samples made from the same batch of Si_3N_4 + 45 w/o ZrO_2 (9 w/o Y_2O_3) + 4 w/o Al_2O_3. The differences between samples were that half were sintered at 1750 C and half were sintered at 1800 C. Samples sintered at 1750 C exhibited microcracking after 255 h at 700 C in air, while samples sintered at 1800 C did not microcrack after 1000 h at 700 C in air, the longest duration of exposure.

The purposes of this investigation were to identify the difference in the good and bad samples, to explain the color change between oxidation scale and the unreacted core region, and to provide an explanation of why those samples sintered at the lower temperature microcracked. Three possible mechanisms for microcracking were identified: (1) Si_3N_4 and ZrO_2 could react to form a zirconium oxynitride phase ($Zr_7O_{11}N_2$ or $Zr_7O_8N_4$) which would then undergo a destructive volume change on oxidation; (2) Zr metal precipitates, produced during sintering in a reducing environment, could oxidize and generate internal stresses; and (3) undesirable $Si_3N_4:Y_2O_3$ could collect at the grain boundaries (Ref. 12), which could explain the rapid oxidation, or it could precipitate as discrete islands inside the grain boundaries where oxidation would be much slower. $Si_3N_4:Y_2O_3:SiO_2$ phases could develop that undergo volume changes on oxidation. In hypothesis (2), for example, Zr metal could (a) collect in the grain boundaries (Ref. 12), in which case the oxidation rate would be high, or (b) precipitate inside the ZrO_2 grains, in which case the oxidation would be much slower and, possibly, less destructive. Analyses designed to isolate the actual mechanism(s) were undertaken. Specifically, analytical

electron microscopy (AEM) experiments were performed to identify the presence and location within samples of nitrogen, metallic Zr, and Y_2O_3.

The first direct observation was that scale formation was uniform in thickness only for the good samples while, for the poor quality samples, white material penetrated into the interior of samples nonuniformly with associated cracking. Attempts to prepare transmission electron microscope (TEM) specimens from scale regions by back ion-beam thinning were only partially successful. First, scale samples were poor quality, with little thin area. Second, the thin areas of the back-thinned samples appeared to have darkened, suggesting that they may have transformed back to the unoxidized darker structure in the vacuum of the ion beam thinner. There was insufficient time to overcome the problems of specimen preparation.

AEM characterization identified no significant differences between either the oxidized and unoxidized samples or between the good and bad samples. All samples examined contained a reasonably homogeneous distribution of electron-dense, zirconium-rich grains and electron-transparent, silicon-rich grains, and all grain boundaries and triple points contained a crystalline grain boundary phase.

Energy dispersive X-ray spectrometry (EDS) was performed using an ultra-thin-window detector for light element analysis. Yttria and oxygen were detected in the zirconium-rich grains (0.1 to 0.5 µm diameter), whereas some of the larger silicon-rich grains (5 µ) additionally contained oxygen. Convergent beam diffraction confirmed that the small grains were silicon nitride and that there were a few larger Si_2N_2O grains. The zirconium-rich grains typically contained 7 cation w/o Y and 93 cation w/o Zr. Some internal structure could be imaged by TEM in the Zr-rich grains, possibly consisting of small Zr metal precipitates. Sample thickness prevented analysis of these precipitates by either EDS or diffraction analysis. Monoclinic laths, traversing entire grains, were observed in some zirconia grains. Analysis of the grain boundary phases by EDS identified Si, Al, Y, and O in varying proportions. Although quantitative analysis of the crystalline grain boundary phase would be unreliable (there is

no guarantee that the beam would be contained entirely within the boundary phase), the presence of Y (absent within the Si-rich grains) and elevated levels of Al were confirmed.

Figure 7 shows a scheme of an analyzed area with the results of semiquantitative cation analysis for a number of analyzed points. The shaded grains were zirconia and unshaded grains were silicon nitride. Small pockets of grain boundary phase are also shown shaded.

Although the presence of Si_2N_2O was confirmed, analysis by thin window EDS is not sufficiently sensitive to detect nitrogen in $Zr_7O_{11}N_2$. Therefore, the hypothesis that the presence of Si_2N_2O formation could confirm the presence of $Zr_7O_{11}N_2$ could not be resolved. Similarly, the hypothesis that the dark color of as-sintered samples is due to the presence of Zr metal precipitates could not be confirmed.

Transformation Toughening

Transformation toughening without microcracking was not achieved for ZrO_2 (Y_2O_3) alloys until near the end of the program and further work is needed to confirm it. Thus, most of the samples made during the program did not exhibit toughening because they contained ZrO_2 stabilized with 9 w/o or more Y_2O_3. Nine weight percent Y_2O_3 alloy was thought to be necessary to prevent microcracking when these samples were heated in air at intermediate temperatures. Even though some of the Y_2O_3 comes out of the ZrO_2 lattice during sintering, there is enough Y_2O_3 to keep the composition well within the cubic or tetragonal-prime phase region of the phase diagram (Fig. 8). Tetragonal-prime phase does not undergo a phase transformation (Ref. 6), so there is no toughening mechanism in this composition. Nevertheless, this composition showed enough merit, because of high strength combined with low thermal conductivity, that characterization studies were conducted.
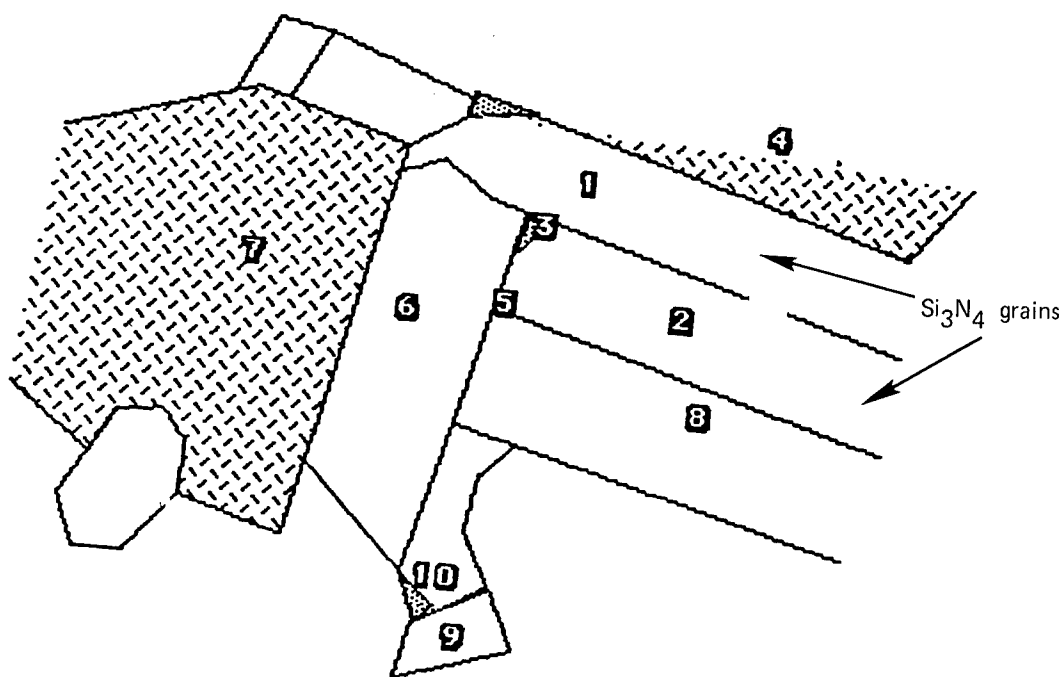
Semiquantitative Analysis*

No.	Zr	Y	Si	Al	
1	1	0	92	5	Si_3N_4 grain
2	1	0	94	4	Si_3N_4 grain
3	3	7	68	19	triple point
4	93	7			ZrO_2 grain
5	2	2	83	10	triple point
6	2	0	90	6	Si_3N_4 grain
7	93	7			ZrO_2 grain
8					
9					
10	2	0	89	6	triple point grain boundary

* Numbers signify cation w/o

Figure 7. AEM Analysis on a Si_3N_4 + 45 w/o ZrO_2
(9 w/o Y_2O_3) + 4 w/o Al_2O_3 Sample
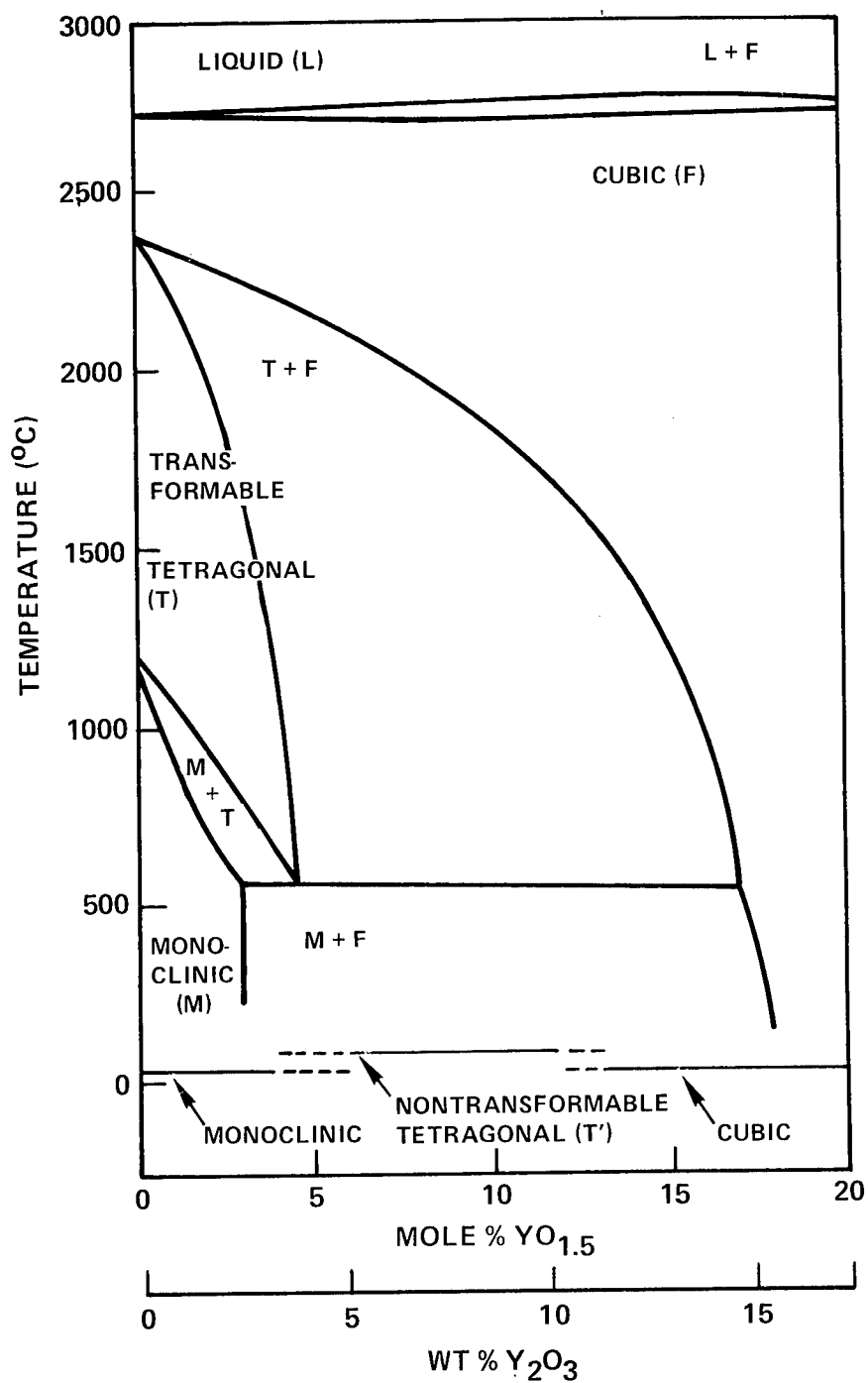
Figure 8. ZrO_2/Y_2O_3 Phase Diagram

Characterization studies late in the program showed that higher sintering temperatures allowed the use of lower Y_2O_3 stabilization without the appearance of microcracking and that use of lower Y_2O_3 stabilization did result in increased toughness. These results are shown in Fig. 9. The toughness for $Si_3N_4-ZrO_2$ composites containing 45 w/o ZrO_2 stabilized with 9 to 13.5 w/o Y_2O_3 was 4 to 4.5 MPa $m^{1/2}$, about the same as the Si_3N_4 matrix without ZrO_2. However, toughness increased with decreasing Y_2O_3 stabilizer content to 6.0 MPa $m^{1/2}$ at a Y_2O_3 content of 4.5 w/o. As shown in the phase diagram (Fig. 9), 4.5 w/o Y_2O_3 content is near the edge of the region in which transformable tetragonal phase is formed. In practice, the ZrO_2 with 4.5 w/o Y_2O_3 is probably within the transformable region after sintering because a portion of the Y_2O_3 content will diffuse into the grain boundaries.

A value of 6 MPa $m^{1/2}$ represents a 50% increase in toughness in material in the as-sintered condition. Higher measured toughness values can be expected for heat-treated samples based on the results (which are discussed in a later section) that show significant increases in strength. These increases are due to surface compressive stresses that should also cause an increase in toughness.

Fracture toughness also was measured using bars containing 3 diamond indentations lined up along the length within the constant stress region of a 4-point bend test (Ref. 6). These results (Tables 5 and 6) showed an increase in toughness in the Si_3N_4 + $ZrO_2(Y_2O_3)$ composites compared to NC-132 control samples, and it showed an increase in toughness when the Y_2O_3 alloy content was less than 9 w/o. But, it did not show as much increase as was evidenced when toughness was measured by the single indentation method (Fig. 9).

Fracture toughness also was measured by this method at 700 and 1000 C. The Y_2O_3 alloy content in these bars was 9 w/o so the transformation toughening effect would not be active. Toughness increased 50% at 700 C but it decreased at 1000 C to the level of the NC-132 reference sample.
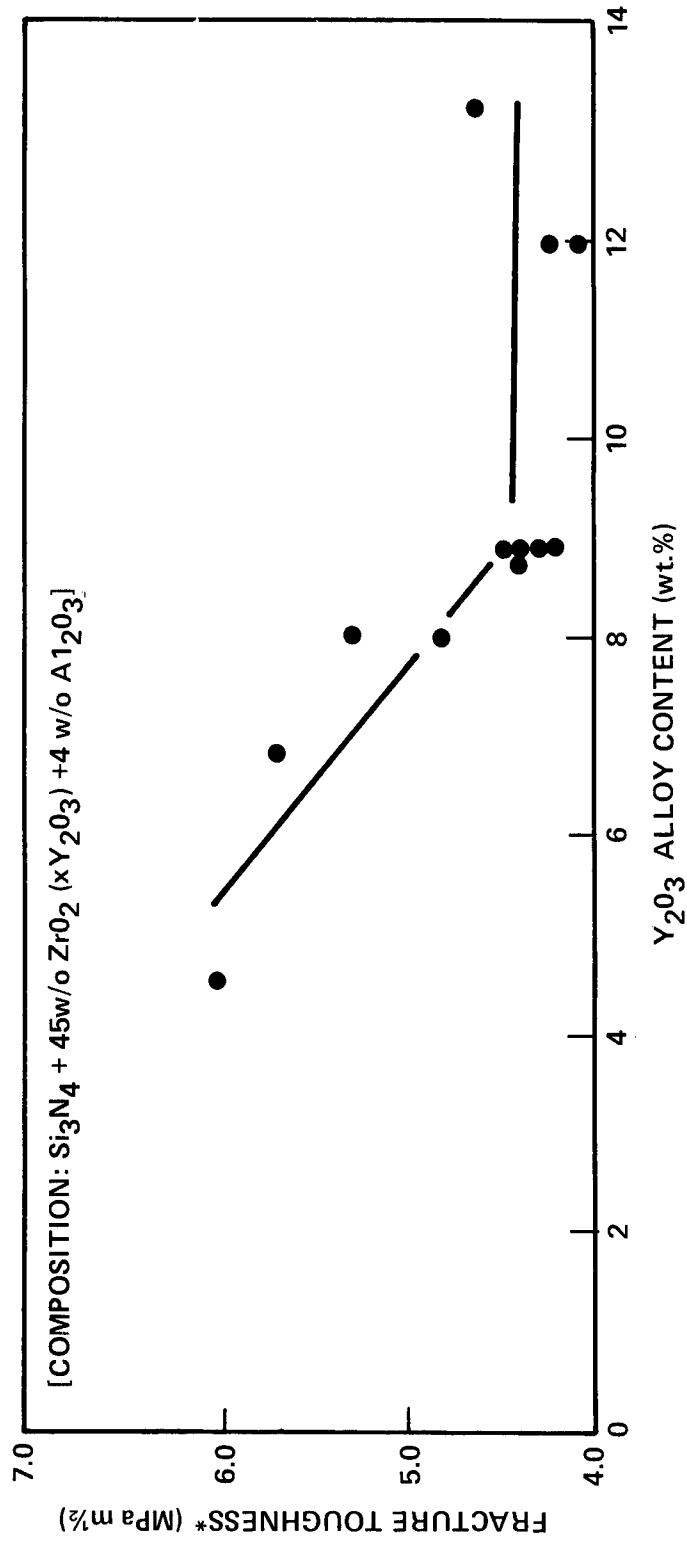
Figure 9.   Fracture Toughness vs Y_2O_3 Alloy Content in ZrO_2

*MEASURED BY THE DIAMOND INDENTATION METHOD

Table 5. Fracture Toughness Measured on Indented MOR Bars

ZrO_2 (Y_2O_3) Content, v/o (w/o)	Y_2O_3 Alloy Content (w/o)	Number of Samples	Test Temperature, C	Fracture Toughness (MPa $m^{1/2}$)
30 (45)	13.3	3	25	7.4
30 (45)	12	5	25	6.7
30 (45)	9	3	25	7.0
30 (45)	8	7	25	8.2
30 (45)	6.9	4	25	8.6
0	0	5	25	5.7*
30 (45)	9	1	25	6.1
30 (45)	9	2	700	8.9
30 (45)	9	1	1000	5.6

*NC-132 material

Sintered Density

Composites of Si_3N_4 + 30 or 45 w/o (20 or 30 v/o) ZrO_2 readily sintered to high densities at 1750 C in 1 h using 4 w/o Al_2O_3 as a sintering aid. Sintered density for 45 w/o ZrO_2 composites was typically 3.90 g/cm^3 and that for 30 w/o ZrO_2 composites was 3.50 g/cm^3. Sintered densities were estimated to be 96% of theoretical based on theoretical densities of 4.05 g/cm^3 and 3.65 g/cm^3, respectively. Theoretical values were based on calculations using the rule of mixtures and on measured densities of hot pressed samples (Table 7). Physical properties used for the rule of mixture calculation are listed in Table 8. Calculated values were 4.05 g/cm^3 and 3.76 g/cm^3. A theoretical density of 4.05 g/cm^3 for the 45 w/o ZrO_2 composition was reasonable compared to the average measured value of hot-pressed samples, which was 4.00 g/cm^3, but a theoretical value of 3.76 g/cm^3 for 30 w/o ZrO_2 compositions seemed high in relation to the results of hot-pressed samples. Therefore, a theoretical value 3.65 g/cm^3 was used for the 30 w/o ZrO_2 compositions. This value places the measured densities in agreement with the densities and porosities as determined by the modified Archimedes method.

Table 6. Test Data for Measuring Fracture Toughness
(Sheet 1 of 3)

SAMPLE IDENTIFICATION	HEIGHT (INCH)	WIDTH (INCH)	LOAD (LBS)
S#54:8Y-4A-117-852-D1-B48-1-1	0.074	0.099	27.6
	0.0735	0.099	27.7
	0.072	0.0985	25.9
	0.073	0.0985	26.8
S#54:4Y(6.9)-4A-106-852-D2-B47-2-1	0.0735	0.099	26.3
	0.073	0.099	26
	0.073	0.099	28.4
	0.0735	0.099	28.3
S#53:4Y-4A-117-852-D2-B45-3-1	0.074	0.099	25.7
	0.0735	0.0995	25.3
	0.074	0.0995	23.8
S#51:8Y(13.3) -4-73-852-D1-B44-4-1	0.074	0.0995	23.4
	0.074	0.099	25
	0.0735	0.099	24.5
S#39:12*Y-4A-168-795-D2-B26-5-1	0.073	0.099	23
	0.0735	0.0995	22.3
	0.0735	0.099	20.3
S#34:12*Y-4A-168-795-D1-B22-6-1	0.0725	0.098	20
	0.0735	0.099	20.3
S#32:12Y(9)-4A-105-795-D3-B29-7-1	0.071	0.099	19.7
	0.072	0.0985	21
	0.072	0.099	20.3
NC132	0.074	0.123	23.2
	0.074	0.122	25.3
	0.0745	0.115	23.2
	0.0745	0.103	20.3
	0.074	0.114	24.1
S#32:12T(9)-4A-105-795-D3-B29-9-1	0.073	0.099	14.1
	0		
S#32:12Y9-4A-105-795-D3-B29-10-1	0.073	0.099	21.8
700 C	0.072	0.0985	20.1
	0		
S#32:12y9(0-4A-105-795-D3-B29-11-1	0.0725	0.0985	19.7
1000 C			

Table 6. Test Data for Measuring Fracture Toughness
(Sheet 2 of 3)

4-PT MOR (KSI)	4-PT MOR (MPa)	2Cmax (UNITS)	2Cmin (UNITS)	CNVSN FTR (u/UNIT)	Cmax (MICRONS)	Cmin (MICRONS)
45.8	316	22.8	19.1	22.1	251.94	211.055
46.6	321	15.5	14.3	22.1	171.275	158.015
45.7	315	24.4	19.9	22.1	269.62	219.895
46.0	317	19.8	16.9	22.1	218.79	186.745
ERR	ERR			22.1	0	0
44.3	305	20.8	16.8	22.1	229.84	185.64
44.4	306	17.9	16.4	22.1	197.795	181.22
48.4	334	21	18.1	22.1	232.05	200.005
47.6	328	22.8	18.3	22.1	251.94	202.215
ERR	ERR			22.1	0	0
42.7	294	21.9	17.6	22.1	241.995	194.48
42.4	292	20.5	14.7	22.1	226.525	162.435
39.3	271	19.3	19.2	22.1	213.265	212.16
ERR	ERR			22.1	0	0
38.7	266	18	15.3	22.1	198.9	169.065
41.5	286	20.1	0	22.1	222.105	0
41.2	284	21.1	19.5	22.1	233.155	215.475
ERR	ERR			22.1	0	0
39.2	270	19.3	0	22.1	213.265	0
37.3	257	24.7	18.5	22.1	272.935	204.425
34.2	235	15.6	14.8	22.1	172.38	163.54
ERR	ERR			22.1	0	0
34.9	241	26.2	20.5	22.1	289.51	226.525
34.2	235	22.7	22.4	22.1	250.835	247.52
ERR	ERR			22.1	0	0
ERR	ERR			22.1	0	0
35.5	245	23.8	20.9	22.1	262.99	230.945
37.0	255	25.2	0	22.1	278.46	0
35.6	245	17	21.7	22.1	187.85	239.785
ERR	ERR			22.1	0	0
ERR	ERR			22.1	0	0
31.0	214	20.6	20.2	22.1	227.63	223.21
34.1	235	18.5	16.2	22.1	204.425	179.01
32.7	225	16.4	0	22.1	181.22	0
32.0	220	17.4	16.6	22.1	192.27	183.43
34.7	239	16.8	16.2	22.1	185.64	179.01
ERR	ERR			22.1	0	0
33.3	229	19.6	19.2	22.1	216.58	212.16
ERR	ERR			22.1	0	0
51.4	354	9.2	7.1	22.1	101.66	78.455
49.0	338	6.8	6.6	22.1	75.14	72.93
ERR	ERR			22.1	0	0
47.4	326	20.1	18.1	22.1	222.105	200.005
ERR	ERR			22.1	0	0
ERR	ERR			22.1	0	0

Table 6.   Test Data for Measuring Fracture Toughness
(Sheet 3 of 3)

Kc max (MPa m1/2)	Kc min (MPam1/2)	Kc avg
9.442134	8.584486	9.013310
7.810435	7.475153	7.642794
9.752483	8.741484	9.246983
8.779750	8.059577	8.419663
ERR	ERR	ERR
8.658385	7.712565	8.185475
8.001868	7.630144	7.816006
9.591676	8.856103	9.223889
9.840544	8.745325	9.292934
ERR	ERR	ERR
8.557422	7.601043	8.079232
8.193479	6.834077	7.513778
7.310304	7.289577	7.299940
ERR	ERR	ERR
6.906820	6.314703	6.610762
7.928622	-0.68	3.624311
8.081766	7.743018	7.912392
ERR	ERR	ERR
7.294800	-0.68	3.307400
7.905188	6.749972	7.327580
5.562272	5.400107	5.481189
ERR	ERR	ERR
7.595091	6.639797	7.117444
6.849971	6.800048	6.825010
ERR	ERR	ERR
ERR	ERR	ERR
7.338572	6.834182	7.086377
7.916320	-0.68	3.618160
6.110700	6.992200	6.551450
ERR	ERR	ERR
ERR	ERR	ERR
5.829494	5.765986	5.797740
6.102305	5.666715	5.884510
5.449058	-0.68	2.384529
5.487584	5.344132	5.415858
5.908668	5.789943	5.849305
ERR	ERR	ERR
6.135336	6.065433	6.100385
ERR	ERR	ERR
6.539224	5.661994	6.100609
5.232489	5.144892	5.188690
ERR	ERR	ERR
9.145917	8.644259	8.895088
ERR	ERR	ERR
ERR	ERR	ERR

Table 7.   Densities of Hot-Pressed Samples

ZrO$_2$ Content, v/o (w/o)	Y$_2$O$_3$ Alloy Content (w/o)	Hot Press Temperature (C)	Density (g/cm^3)
30 (45)	8	1800	4.07*
30 (45)	9	1700	3.96*
30 (45)	9	1700	4.05*
30 (45)	9	1700	4.01*
30 (45)	9	1700	4.04*
30 (45)	9	1700	3.88*
26 (30)	9	1700	3.65
*Avg. = 4.00			

Table 8.   Properties of Si$_3$N$_4$ and ZrO$_2$ for Calculation of Si$_3$N$_4$/ZrO$_2$ Composite Theoretical Density

	Si$_3$N$_4$	ZrO$_2$
Density (g/cm^3)	3.18	6.07
Elastic Modulus (GPa)	3.07	2.07

Compositions of Si$_3$N$_4$ + 15 w/o ZrO$_2$, on the other hand, did not sinter to a high density, even at a temperature of 1860 C. Sintered samples cracked and had a porosity in excess of 15%. Based on these results, it appears as if the ZrO$_2$ is acting as a sintering aid which has been previously determined by other researchers.

Room-Temperature Strength

Three-point MOR tests (Table 9) were generally used to obtain the most data from limited material. When there was sufficient material, 4-point MOR tests were performed. Evaluation of these data shows that 4-point flexural strength

41

Table 9. Density and Room Temperature Flexural Strength

Y2O3 Alloy Content (w/o)	Sintering Parameters	45 w/o (30 v/o) ZrO2										30 w/o ZrO2					
		Sintered Density (g/cm3)	Porosity (%)	3-Point MOR (MPa)			4-Point MOR (MPa)					Sintered Density (g/cm3)	Porosity	3-Point MOR (MPa)			
				$\bar{X}$	n	Std. Dev.	$\bar{X}$	n	Std. Dev.					$\bar{X}$	m	Std. Dev.	
13.3	1750C, 1h	3.93	0.03	782	14	142	730	6	83			–	–	–	–	–	
12	1750C, 1h	3.81	0.00	994	7	130	–	–	–			3.47	0.16	840	7	45	
12	1800C, 1h	3.92	0.01	957	8	54	–	–	–			3.53	0.02	1009	8	105	
12	1860C, 2h	3.89	0.16	812	7	138	–	–	–			–	–	–	–	–	
9	1750C, 1h	3.87	0.03	–	–	–	–	–	–			3.48	0.00	–	–	–	
9	1800C, 1h	3.85	0.00	–	–	–	–	–	–			3.48	0.70	–	–	–	
9	1800C, 1h	3.92	0.04	860	16	123	696	7	79			3.65	0.00	916	5	124	
8	1800C, 1h	3.96	0.01	–	–	–	–	–	–			–	–	–	–	–	
8	1860C, 1h	3.87	0.04	983	11	87	794	5	143			–	–	–	–	–	
6.9	1800C, 1h	3.91	0.22	908	9	161	840	5	79			–	–	–	–	–	
6.9	1860C, 1h	3.92	0.19	1003	8	114	898	4	98			–	–	–	–	–	
NA*	NA	NA	NA	854	5	45	806	5	70			–	–	–	–	–	

*NC132, Lot 1073, tested for reference

Notes: 3-Point MOR, $L_0 = 15.2$ mm
4-Point MOR, $L_0 = 23$ mm, $L_i = 7.2$ mm
Composition, Si3N4 + x ZrO2 (y*Y2O3) + 4 w/o Al2O3

0099a/tab

ranges from 7% to 19% lower than 3-point strength. The strength of a reference material, NC-132, was also measured. NC-132 grade of hot-pressed Si_3N_4 exhibited a difference of only 6% between 3- and 4-point test data.

The effects of sintering temperature on density and strength can be seen in Table 9 and Figs. 10 and 11. As sintering temperature is increased from 1750 to 1860 C for the 45 w/o ZrO_2 sample, there is no significant change in density, but strength decreases. For the 30 w/o ZrO_2 samples, there is a slight increase in density with increasing sintering temperatures and a substantial increase in strength. Based on previous considerations of the effect of ZrO_2 as a sintering aid, it appears as if the 45 w/o ZrO_2 samples could be progressively overfired at temperatures greater than 1750 C, while the lower ZrO_2 content materials require a higher sintering temperature of at least 1800 C to achieve their optimum properties.

There was no correlation between strength and Y_2O_3 stabilizer content in the ZrO_2 particles.

Strength increased significantly in samples that were aged in air at 700 C. A temperature of 700 C was an arbitrary temperature selected for evaluating microcracking in the 500 C to 1000 C range. This, of course, applies to material sintered at 1800 C or higher, in which no microcracking occurred. When samples were sintered at 1750 C, the strength of aged samples often decreased due to the microcracking phenomenon. However, when samples were sintered at 1800 C and aged at 700 C, strength increased. Strength in composites containing 45 w/o ZrO_2 peaked at 1082 MPa after 240 h, a 26% increase. The increase was even higher for composites containing 30 w/o ZrO_2, which peaked at 1254 MPa after 120 h, a 37% increase. Increased strength is due to residual compressive stresses that are formed on the surface. These increased strengths would not be observed at elevated temperatures, of course, as the compressive stresses would be relieved by plastic deformation, but these aged materials would be attractive for low-temperature applications, such as for high wear surfaces.
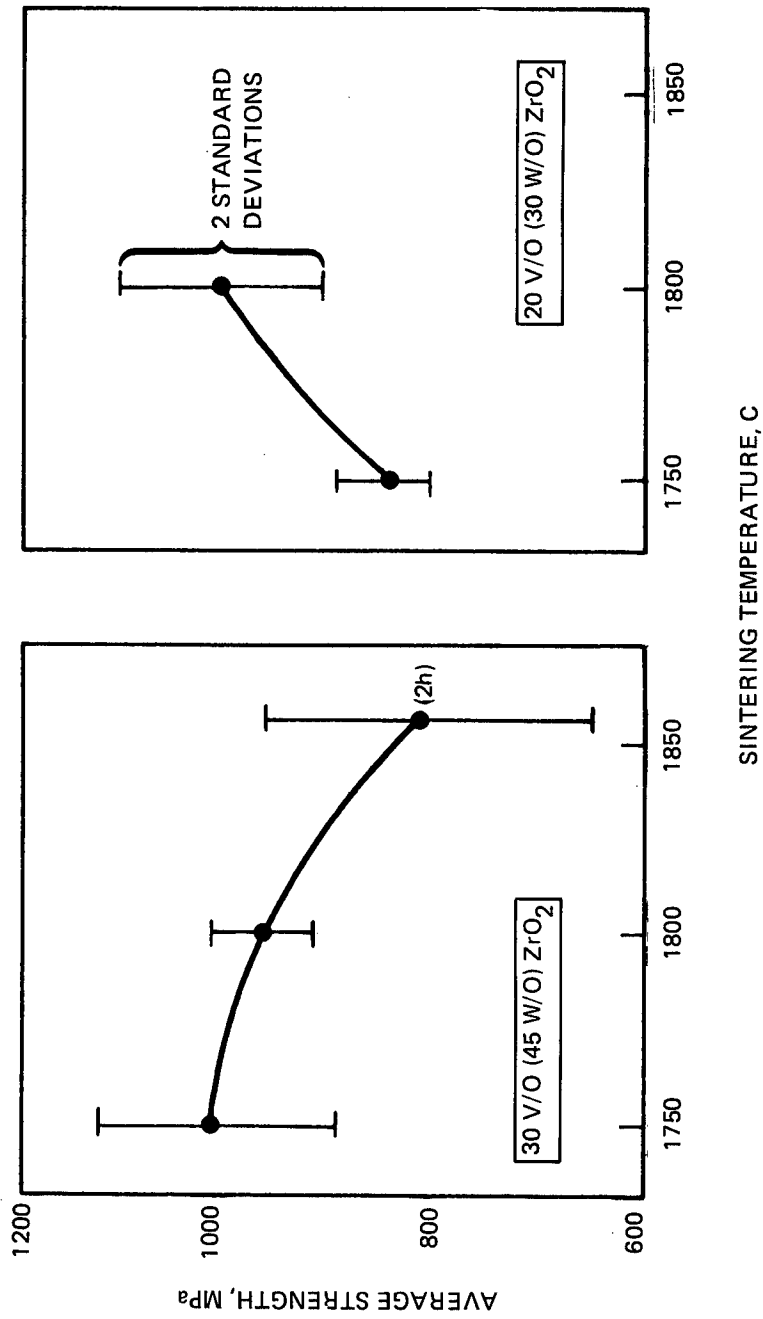
Figure 10. Si_3N_4 Room-Temperature Strength
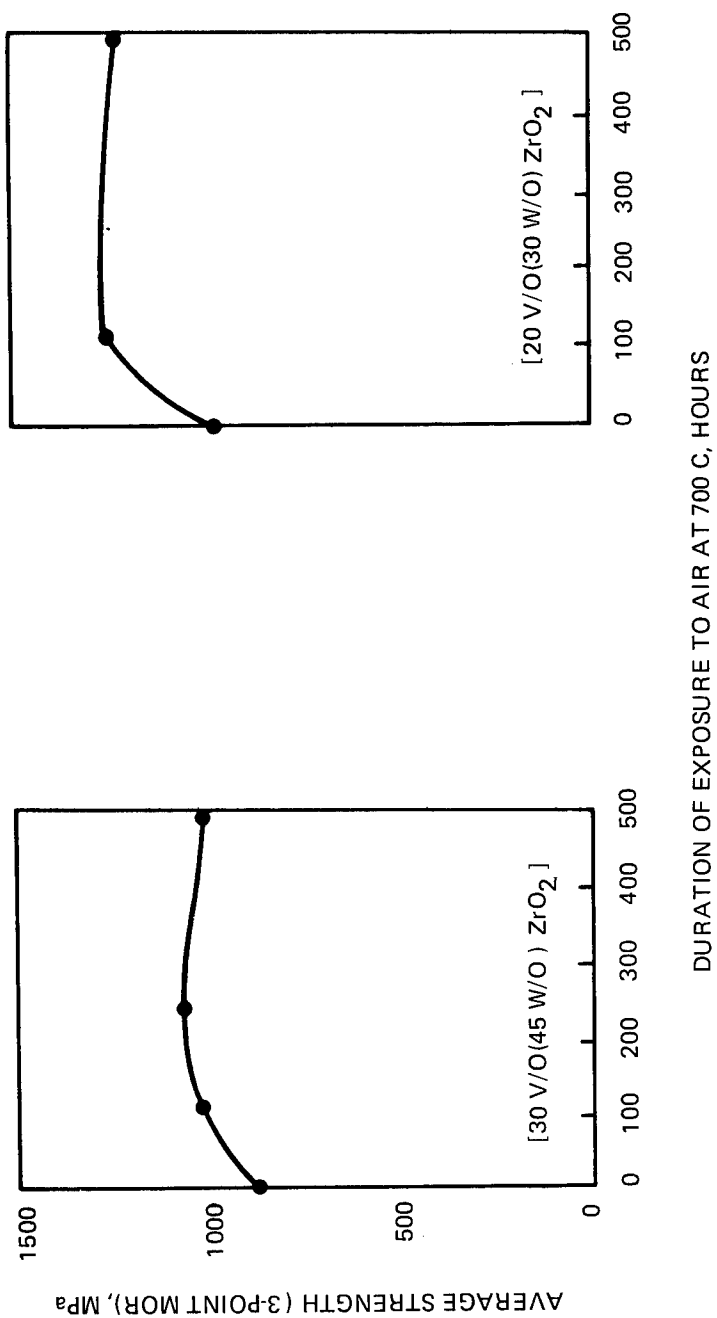
Figure 11. Effect on Room Temperature Strength of Exposure to an Oxidizing Environment of $Si_3N_4 + ZrO_2$ (9 w/o Y_2O_3) + 4 w/o Al_2O_3

High-Temperature Strength

The purpose of this program was to develop a tough Si_3N_4 composite with high strength at high temperatures. Four weight percent Al_2O_3 was used early in the program as a sintering aid for Si_3N_4 + ZrO_2 (Y_2O_3) systems because it was effective for obtaining dense samples for evaluation and for demonstration of concept. The Al_2O_3 sintering aid additions, however, did not meet the goals of the program because the resultant grain boundary phases are not sufficiently refractory at 1400 C. Thus, compositional changes were made in an effort to increase the strength at elevated temperatures. Three approaches were used: (1) the Al_2O_3 was replaced with selected mixtures of Y_2O_3 + SiO_2, (2) the Al_2O_3 content was reduced from 4 w/o to 2 w/o, and (3) an addition of 2 w/o Al_2O_3 + 6 w/o Y_2O_3 was used. The first approach was the most promising. Strengths at elevated temperatures were at the same level as strengths at ambient temperature, although the ambient strength was lower than expected because of processing complications. The second two approaches achieved a small amount of improvement in high-temperature strength compared to the 4 w/o Al_2O_3 reference composition, but the increases were far short of program goals.

Compositions with 4 w/o Al_2O_3 Sintering Aid. The high-temperature strength of compositions containing 4 w/o Al_2O_3 as a sintering aid are presented as a reference level for comparing compositions with sintering aids that were selected to provide more refractory compositions in the grain boundaries.

The results of both 3- and 4-point high-temperature strength measurements are listed in Table 10; 3-point data are plotted in Fig. 12.

Figure 13 shows that strength decreases linearly to 1000 C where it is 72 to 79% of the room-temperature level. Strength then drops at an increasing rate to between 53 and 57% of the room-temperature level at 1200 C, which is still at a level above 450 MPa for composites with 45 w/o ZrO_2 and above 524 MPa for composites with 30 w/o ZrO_2. Strength then drops rapidly to 161 MPa at

Table 10. High-Temperature Strength of Si3N4 + ZrO2 (Y2O3) Composites Containing 4 w/o Al2O3 as a Sintering Aid

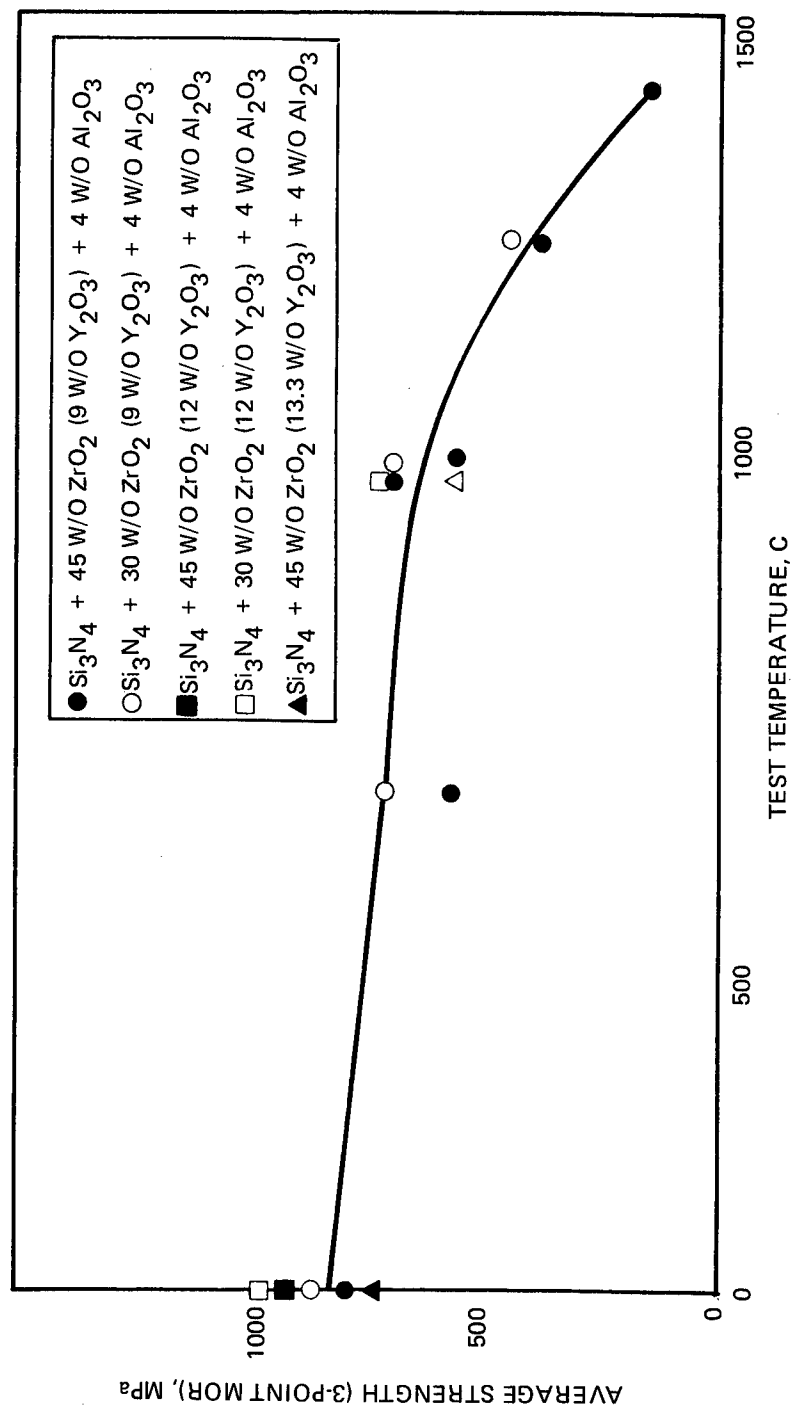| Composition				3-Point MOR (L = 15 mm)			4-Point MOR (L_o = 23 mm, L_i = 7.6 mm)				Strength Ratio (4-Point/3-Point)
Sinter Run No.	ZrO2 Content (v/o)	Y2O3 Content (w/o)	Test Temperature (C)	Number of Tests	Average Strength (MPa)	Retention of Room Temp. Strength (%)	L_o (mm)/L_i (mm)	Number of Samples	Average Strength (MPa)	Retention of Room Temp. Strength (%)	
22, 23	30	9	25	16	860	100	–	–	–	–	–
22, 23			700	1	613	71	–	–	–	–	–
22, 23			1000	2	623	72	–	–	–	–	–
22, 23			1200	5	458	53	30/10	3	360	–	.79
32			1400	4	161	19	–	–	–	–	–
22, 23	20	9	25	5	916	100	–	–	–	–	–
			700	1	785	86	–	–	–	–	–
			1000	2	706	77	–	–	–	–	–
			1200	1	524	57	–	–	–	–	–
32	20	9	25	10	749	100	30/10	4	609	100	.81
			1200	–	–	–	30/10	3	365	60	–
			1400	–	–	–	30/10	2	147	24	–
34	30	12	25	8	957	100	–	–	–	–	–
			1000	1	704	74	–	–	–	–	–
34	20	12	25	8	1009	100	–	–	–	–	–
			1000	2	728	72	–	–	–	–	–
24, 25		13.3	25	14	783	100	23/7.1	6	730	100	.93
			1000	2	617	79	–	–	–	–	–

Figure 12. Flexural Strength of Si_3N_4/ZrO_2 (xY_2O_3) Composites Using 4 w/o Al_2O_3 as a Sintering Aid
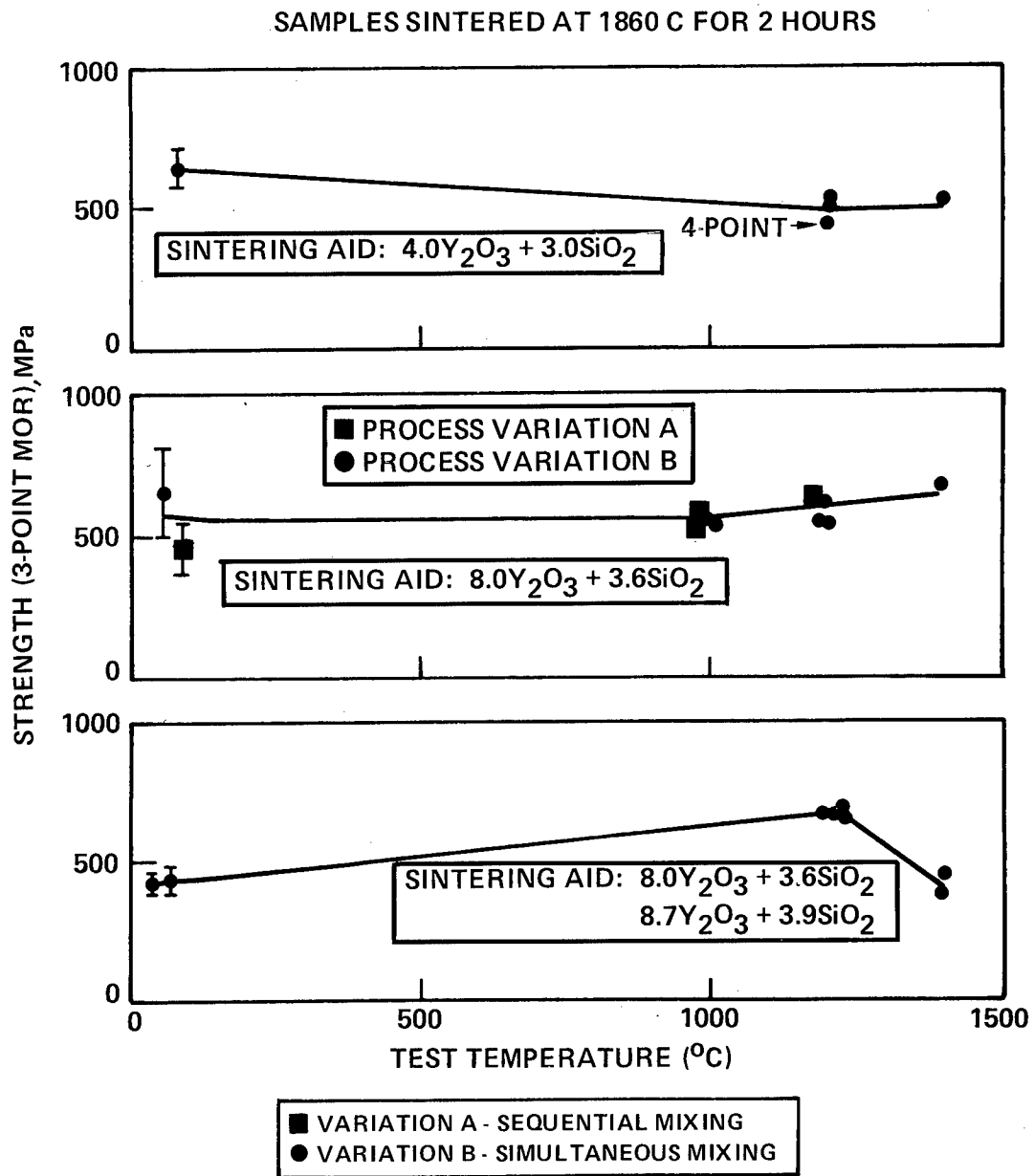
Figure 13. Strength of Si_3N_4 + 30 v/o ZrO_2 (12 w/o Y_2O_3) with Y_2O_3 and SiO_2 (w/o) as Sintering Aid

1400 C, which is only 19% of the room-temperature level. Thus, these compositions could be useful to 1000 C, or 1200 C at most, but they would not be structurally stable at higher temperatures.

Composites with Y_2O_3 + SiO_2 Sintering Aid. Selected mixtures of Y_2O_3 + SiO_2 can be used to sinter Si_3N_4 to near full densities and these compositions have demonstrated very little loss in strength at elevated temperatures (Ref. 8). Rocketdyne used this technology over 10 years ago to develop a composition, Si_3N_4 + 15.5 w/o Y_2O_3 + 7.0 w/o SiO_2, called "SN104", that sintered to near full density and exhibited no loss in strength at 1200 C (Ref. 9). It has been shown that SN104 exhibited excellent resistance to creep (Ref. 9), being second only to a hot-pressed material containing a much lower amount of Y_2O_3 densification aid and no added SiO_2. Studies at Rocketdyne and the Rockwell Science Center showed that high-temperature properties could be improved even more by heat treatment (Ref. 10). Heat treatment is believed to cause (1) undesirable cations to diffuse into the Si_3N_4 grains where they do not affect grain boundary softening or melting, and (2) crystallization of glassy phases in the grain boundary.

With this in mind, mixtures of Y_2O_3 + SiO_2 were selected for evaluation in this program. Compositions were selected based on adding sufficient sintering aid to promote densification while remaining in the Si_3N_4-Si_2N_2O-$Si_2Y_2O_7$ compatibility phase triangle. Certain compositions outside this triangle, containing Y_2O_3, undergo excessive volume increases on oxidation that lead to cracking and spalling. The oxygen content in the Si_3N_4 powder was taken into account in the calculation of batches, but the reported quantities are only the amount added during fabrication. Selected additions for this study contained as little as 4.04 w/o Y_2O_3 + 1.1 w/o SiO_2 to as high as 15.5 w/o Y_2O_3 + 7.0 w/o SiO_2 (Table 11).

The Y_2O_3 and SiO_2 powders could not be suspended so the colloidal processing method could not be used. These powders were ball-milled then blended with the Si_3N_4 and ZrO_2 powders using the sonic mixing chamber. Large disks 50 mm in diameter were prepared by pressure filtration. Most of the disks cracked on drying even when precautions were exercised, such as slow, controlled humidity

Table 11. Density and High Temperature Strength of Si_3N_4 + 45 w/o (12 w/o Y_2O_3) Containing Y_2O_3 + SiO_2 Sintering Aid

Sinter Run No.	Sintering Parameter	Sintering Aid Y_2O_3 (w/o)	SiO_2 (w/o)	Sintered Density (g/cm³)	Test Temperature (C)	Strength (3-Point MOR) (MPa)	Comments
38	1800 C, 1h	4.0	1.1	2.18	-	-	
		8.0	3.6	2.35	-	-	
42	1860 C, 1h	4.0	3.0	3.44	-	-	
		8.0	3.6	3.40	-	-	
		8.0	5.0	3.57	-	-	
		8.7	3.9	3.87	-	-	
		15.5	7.0	3.87	-	-	
39	1860 C, 2h	4.0	1.1	3.42	-	-	
		8.0	3.6	3.89	-	-	
40	1860 C, 2h	8.0	3.6	4.07	25	$\bar{x}$ = 455	n = 8, S.D. = 103 (Process Variation A)
					1000	516	
					1000	544	
					1200	618	
					1200	518	
				3.84	25	$\bar{x}$ = 655	n = 7, S.D. = 152 (Process Variation B)
					1000	526	
					1000	524	
					1200	613	
					1400	690	

$\bar{x}$ = mean
n = number of samples
S.D. = standard deviation

Table 11. Density and High Temperature Strength of Si_3N_4 + 45 w/o (12 w/o Y_2O_3) Containing Y_2O_3 + SiO_2 Sintering Aid (Continued)

Sinter Run No.	Sintering Parameter	Sintering Aid		Sintered Density (g/cm³)	Test Temperature (C)	Strength (3-Point MOR) (MPa)	Comments
		Y_2O_3 (w/o)	SiO_2 (w/o)				
44	1860 C, 2h	4.0	3.0	3.78	25	$\bar{X}$ = 662	n = 4, S.D. = 66
					1200	514	
					1200	503	
					1200	4-pt.: 448	4-Point MOR / 3-Pt. MOR = .89
					1400	508	
		8.0	3.6	4.12	25	$\bar{X}$ = 424	S.D. = 18
					1200	659	
					1200	666	
					1400	379	
					–	–	
		8.0	5.0	3.82			
		8.7	3.9	3.96	25	$\bar{X}$ = 469	n = 4, S.D. = 16
					1200	655	
					1200	700	
					1400	364	
					1400	421	
					–	–	
		15.5	7.0	3.93			

drying schedules and binder additives. For these reasons, large samples for fabricating MOR bars were difficult to obtain. As will be shown below, room-temperature strength levels were much lower than those of the compositions sintered using 4 w/o Al_2O_3. The reasons for this lower strength are believed to be flaws introduced from ball-milling debris and the lack of uncracked green disks.

High sintered densities were obtained with additions of 8.0 w/o Y_2O_3 + 3.9 w/o SiO_2 and sintering parameters of 1860 C for 2 h (Table 11). These are the same parameters, incidentally, that are required to sinter the SN104 composition. The only phases that were identified on ground surfaces were beta-Si_3N_4 and cubic ZrO_2.

Results of strength tests at ambient and elevated temperatures are listed in Table 11 and plotted in Figure 13. Strengths at 1400 C are the same as those at room temperature. There was no loss in strength at 1400 C.

Only one specimen was tested in 4-point loading because of the scarcity of long MOR bars. The 4-point strength was 11% below that of the 3-point data. Although there was only one sample tested under 4-point loading, an 11% difference is in agreement with other high-temperature tests.

Process variations A and B, shown in Fig. 13, refer to the mixing sequence. The ingredients were mixed sequentially in variation A. That is to say, that Y_2O_3 and SiO_2 powders were ball-milled; these powders were then mixed with the ZrO_2 powder in the sonic chamber, and these powders were, in turn, mixed with the Si_3N_4 powder in the sonic chamber. In variation B, the ball-milled mixture of Y_2O_3 and SiO_2 was mixed with the ZrO_2 and Si_3N_4 powders simultaneously in the sonic chamber. The reason for the increased room temperature strength is unknown, but all strength values measured after any heat treatment or at temperature were in line with the room-temperature strength of samples made by variation B.

Samples were aged in air at 700 C to determine whether microcracking occurred. Based on MOR results (Table 12), none had occurred after exposures as long as 500 h at 700 C.

Table 12. Strength After Heating in Air at 700 C for Composites of Si_3N_4 + 45 w/o ZrO_2 (12 w/o Y_2O_3) + x Y_2O_3 + y SiO_2

| Sinter Run No. | Sintering Aids | | Exposure Time at 700 C (h) | Room Temperature Strength | | |
	Y_2O_3 (w/o)	SiO_2 (w/o)		n	Std. Dev. (Mpa)	3-Point MOR (MPa)
40	8.0	3.6	0	8	110	445
			139	1	-	459
			273	1	-	430
			517	1	-	328
42	8.0	5.0	0	4	17	464
			98	1	-	584
			500	1	-	417
			500	1	0	443

*n = number of samples

Composites with 2 w/o Al_2O_3 Sintering Aid. Sintered compositions of Si_3N_4 + 45 w/o (~30 v/o) ZrO_2 (12 w/o Y_2O_3) exhibited inconsistent results. Two samples with identical composition and processing history were sint red together at 1800 C for 1 h. The densities were 2.92 g/cm_3 and 3.40 g/cm_3, v ich were 72 and 84% of theoretical. A third sample was sintered at 1860 C for 1 h, but the density was 3.11 g/cm^3, or 77% of theoretical. Despite the low densities, MOR bars were diamond ground from the latter sample and the results of the tests are listed in Table 13. Results of a similar composition, but containing 4 w/o Al_2O_3 as the sintering aid (Table 13), also are listed for reference (note that the Y_2O_3 content in the ZrO_2 is different, 12 w/o for the composition containing 2 w/o Al_2O_3 and 9 w/o for the composition containing 4 w/o Al_2O_3). The significance of this difference is that the

Table 13. High-Temperature Strength of Si_3N_4 + ZrO_2 (Y_2O_3) Composites Containing Sintering Aids

Sintering Aid	Sintered Density (g/cm^3)	Test Temperature (C)	Y_2O_3 Content in ZrO_2 (w/o)	Average 3-Point MOR L = 15 mm (MPa)	Retention of Room Temp. Strength (%)	Average 4-Point MOR L_o = 30 mm L_i = 10 mm	Retention of Room Temperature Strength (%)	Strength (4-Point/3-Point)
2 w/o Al_2O_3	3.13	25	12	752	100	499	100	0.66
		1200	12	413	55	418	83	1.0
		1400	12	–	–	197	39	–
6 w/o Y_2O_3 + 2 w/o Al_2O_3	3.97	25	12	773	100	707	100	0.91
		1200	12	477	62	–	–	–
		1400	12	125	16	–	–	–
4 w/o Al_2O_3	3.85	25	9	860	100	–	–	–
		1200	9	458	53	360	–	0.79
		1400	9	161	19	–	–	–

[Composition: Si_3N_4 + 45 w/o. ZrO_2 (12 w/oY_2O_3) + Sintering Aid Indicated]

grain boundary composition in these composites will be different, one containing more Y_2O_3 dissolved from the ZrO_2 (Y_2O_3) alloy. The grain boundary composition is believed to control high-temperature properties.

Three-point MOR results of tests conducted at 1200 C do not indicate that the lower Al_2O_3 content is of any benefit. The retention of room-temperature strength, 53%, was the same as that for the 4 w/o Al_2O_3 reference material. The 4-point MOR data, on the other hand, indicate that there is some improvement. The retention of room-temperature strength is 83%, but the room-temperature strength appears to be low. Moreover, the strength at 1400 C is very low, 197 MPa, so the approach of simply reducing the Al_2O_3 content did not result in any substantial increase in high-temperature strength.

<u>Composites with 6 w/o Y_2O_3 + 2 w/o Al_2O_3 Sintering Aid</u>. Use of a combination of 6 w/o Y_2O_3 + 2 w/o Al_2O_3 did not produce any better results than that for compositions containing 2 w/o or 4 w/o Al_2O_3. Retention of room-temperature strength at 1200 C was 62%, up from 53%, and at 1400 C it was 12%. These are far below the desired level.

HfO_2 (Y_2O_3)

The use of dispersed HfO_2 in place of, or in combination with, ZrO_2 is attractive because it should allow composites to be used at higher temperatures. It is well documented in the literature that transformation-toughened ZrO_2 materials do not exhibit the toughening mechanism at high temperatures, beginning at about 1000 C. The metastable tetragonal grains tend to transform at the lower end of the transformation temperature range (950 to 1200 C). HfO_2, on the other hand, transforms at a much higher temperature, beginning at 1400 C (Ref. 11). Stabilizer additions may reduce the transformation temperature, but a gain of 500 C in service temperature may be achievable. An increase in service temperature of this magnitude could allow transformation-toughened materials to be used in turbine applications.

Selected stabilizers of HfO_2 (Y_2O_3) and HfO_2 (MgO) were ordered but the powders were not received in time to be a part of this program. An Si_3N_4 + HfO_2 composite was made, however, using HfO_2 fully stabilized with 10 m/o Y_2O_3. Naturally, transformation toughening was not anticipated, but samples were made to demonstrate that the composition sintered to near full density and that it exhibited high strength.

The composition of the composite was Si_3N_4 + HfO_2 (10 m/o Y_2O_3) + 4 w/o Al_2O_3 and a batch was prepared using the colloidal method. No differences were noted using HfO_2 powder compared to ZrO_2 powder. Two disks, 50 mm in diameter, were prepared by pressure filtration, dried and sintered at 1800 C for 1 h. Sintered density was 4.99 g/cm^3 in both disks, average weight loss was 0.7%, and the open porosity was 0.1% in one and 0.01% in the other. Ground surfaces were uniform in appearance and dark grey. A photomicrograph showing the good dispersion of the HfO_2 grains is shown in Fig. 14. The microstructure was analyzed using TEM and AEM methods as described in the previous section. The microstructure appeared uniform and homogeneous, and similar to that of the comparable Si_3N_4 + ZrO_2 + 4 w/o Al_2O_3 composites. The size of the Si_3N_4 grains was 0.2 micrometer, and HfO_2 particles consisted of several grains. One difference was that the grain boundaries appeared more glassy than those of compositions containing ZrO_2 (Y_2O_3). Results of a semiquantitative analysis are shown in Fig. 15. The presence of Mg in the HfO_2 grains was unexpected. This qualitative observation is valid, although the quantity is uncertain because the dispersive energy of the two elements are adjacent to each other, and because one is a light element and the other is a heavy element (Fig. 16).

The average 4-point MOR at room temperature was 876 MPa with a standard deviation of 34 MPa (4 samples). The average 3-point strength was 917 MPa with a standard deviation of 144 MPa (6 samples).

The 3-point strength of two samples at 1200 C was 555 and 577 MPa, which averages 62% retention of room temperature strength. This is 20% better retention than that for a comparable composition with ZrO_2 instead of HfO_2.
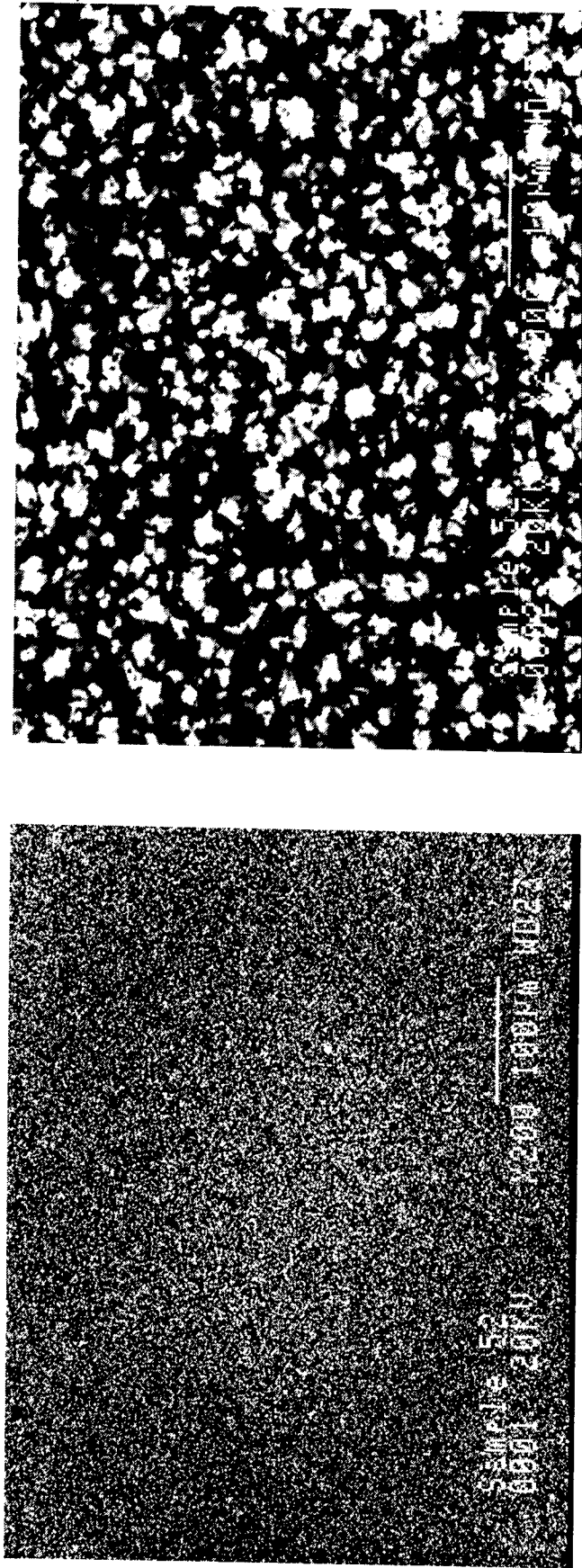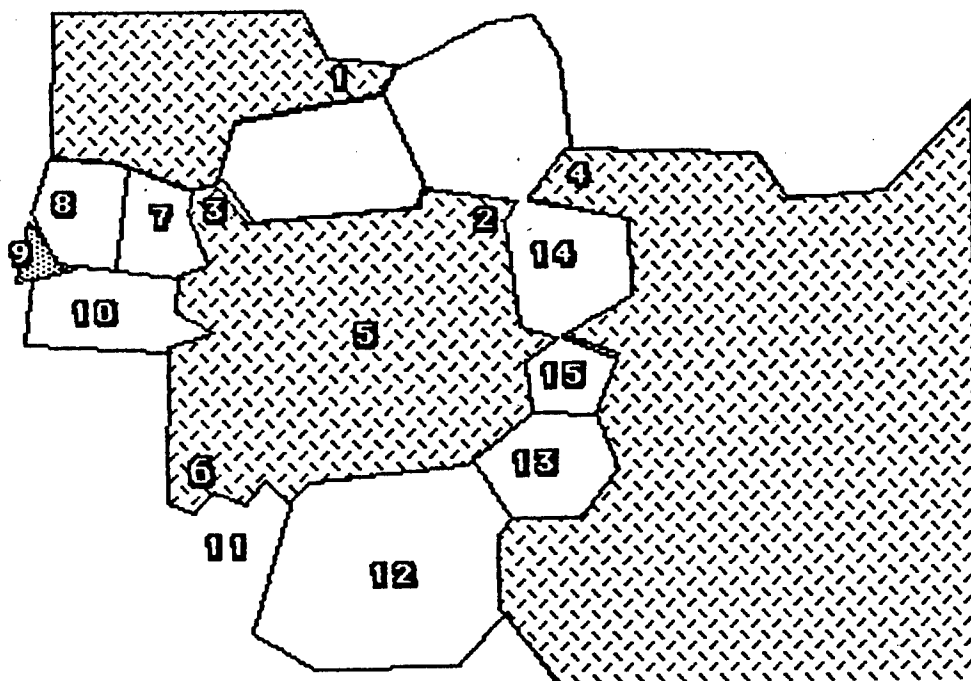
Figure 14. Microstructure of Si_3N_4/HfO_2 Composite

Semiquantitative Analysis (cation %)

No.	Hf	Mg	Y	Si	Al	
1	89	2	9			
2	88	3	9			
3	86	4	10			
4	86	2	12			
5	89	3	8			
6	87	3	10			
7						
8				97	3	
9	9		21	57	12	Grain boundary triple point
10				96	4	
11				96	4	
12				97	3	
13						
14				95	5	
15				96	4	

Figure 15. Semiquantitative Analysis of Si_3N_4 + HfO_2 (10 m/o Y_2O_3) + 4 w/o Al_2O_3
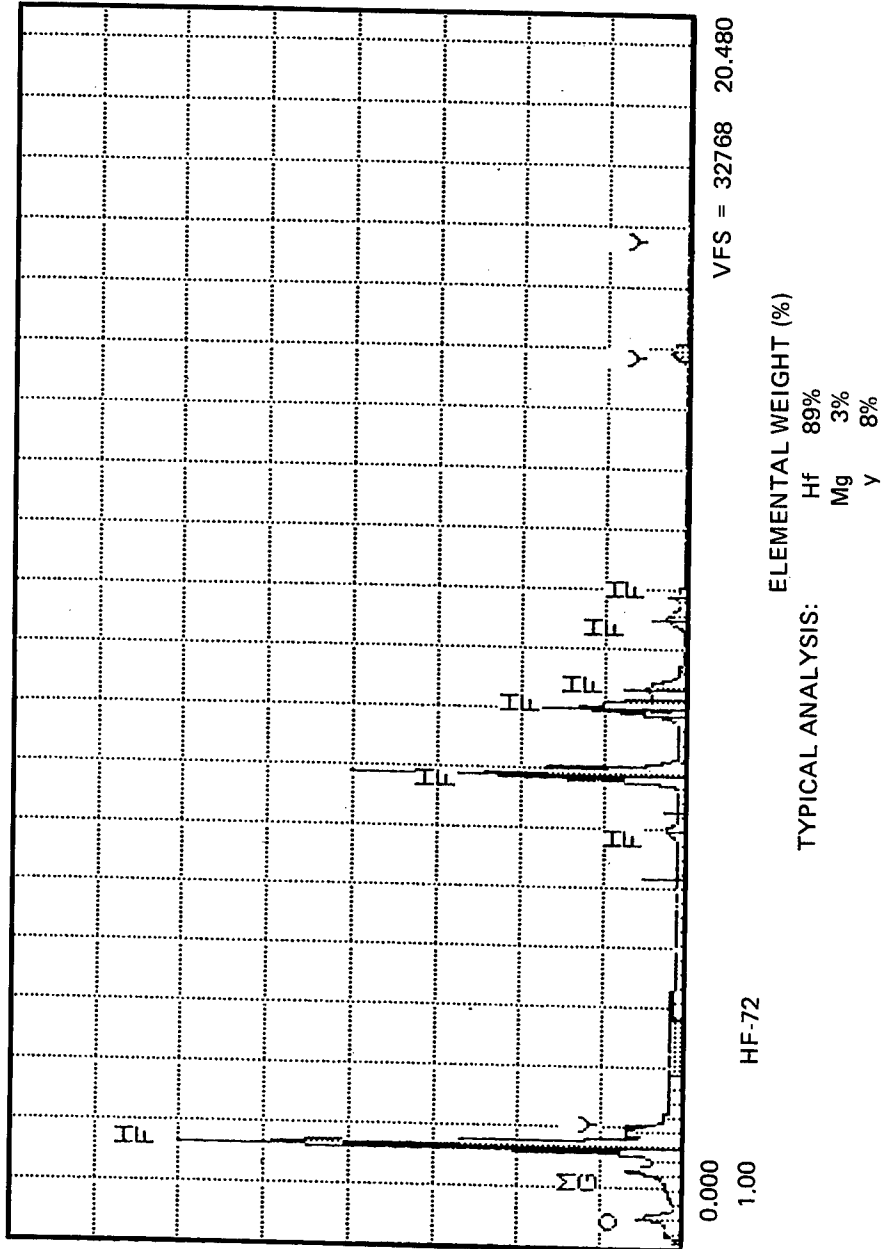
Figure 16. Energy Dispersive Analysis of a HfO_2 Grain

The strength at 1400 C was 220 and 203 MPa. While this was higher than comparable ZrO_2 composites, the use of a more refractory sintering aid, such as Y_2O_3 + SiO_2, will be necessary to improve strength at 1400 C.

Samples were aged in air at 700 C to determine whether there was any microcracking at intermediate temperatures. Results showed no indication of degradation; in fact, strength increased at each duration that was tested (Fig. 17). The average room-temperature strengths of bars aged at 700 C in air are listed in Table 12. The average strength after aging 500 h was 20% higher than that of unaged samples.

ZrO_2 (CaO)

Hot-Pressed Composites

Early in the program, increased toughness could not be obtained in Si_3N_4/-ZrO_2 (Y_2O_3) composites without microcracking, so a ZrO_2 alloying agent with a divalent cation was evaluated. The only two available ZrO_2 powders were alloyed with CaO or MgO. Success was immediate with the CaO-alloyed composition and the results are reported in this section. Results of the MgO-alloyed composition are reported in the next major section of this report.

The ZrO_2 powder*, which contained 5 w/o CaO, was too coarse for colloidal suspension processing. Batches containing Si_3N_4 plus 15, 30, and 45 w/o ZrO_2 (5 w/o CaO) were prepared by ball-milling using ZrO_2 milling media and polyethylene jars. Initial samples were densified by hot pressing and near full density was achieved at 1700 C, 1 h. Two and one-half percent MgO was added as a sintering aid and to keep the CaO in the ZrO_2 grains from diffusing to the grain boundaries during densification. The results showed significant increases in both fracture toughness and strength.

_____

*Zircoa Grade B
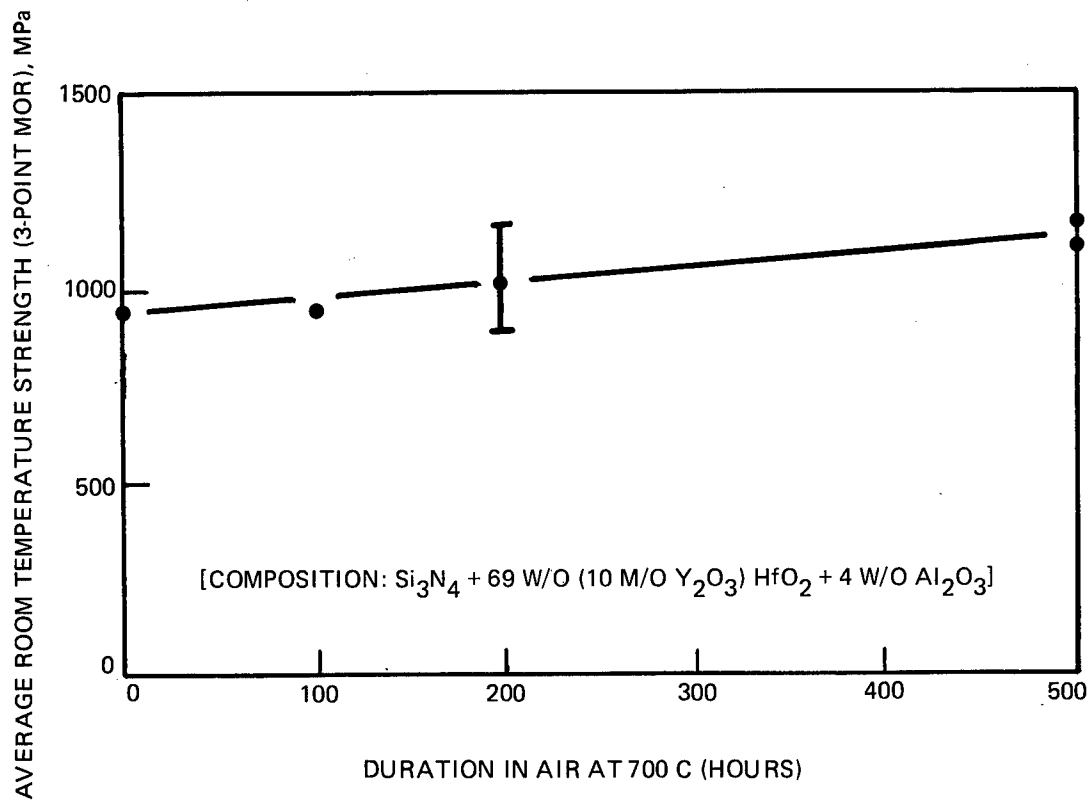
87-239

Figure 17. Evidence of Stability at Intermediate Temperatures of
Si₃N₄ + HfO₂ Composites

The fracture toughness of all samples was substantially higher than that of the Si_3N_4 matrix. The baseline matrix toughness is 4.1 MPa $m^{1/2}$. Toughness was measured and calculated by the same diamond indentation technique (Ref. 5) on NC-132 samples. Toughness values measured on as-hot-pressed samples and samples subjected to selected heat treat conditions are shown in Fig. 18. All of these samples, except the NC132, were composed of Si_3N_4 + 45 w/o ZrO_2 (5 w/o CaO) + 2.5 w/o MgO.

A large portion of the high measured toughness in the aged samples is due to surface compressive stresses that develop as Zr-oxynitride oxidizes to form monoclinic ZrO_2 on the surface. Toughness was measured at 12.5 MPa $m^{1/2}$ on the surface of a specimen aged at 1350 C for 2 h. Toughness was measured after 0.25 mm of the surface was removed by polishing, and this was repeated until the toughness level reached the level of the material in the as-hot pressed condition, which was 8.9 MPa $m^{1/2}$. This level of toughness was reached 1 mm below the original surface. Toughness was not affected by annealing at an intermediate temperature of 700 C for 120 h.

Toughness for the three loadings of ZrO_2 (5 w/o CaO) and for the matrix material without the ZrO_2 is shown in Fig. 19. Toughness increases from that of NC-132 Si_3N_4, 4.1 MPa $m^{1/2}$, to 6.3 MPa $m^{1/2}$ with a loading of only 15 w/o. Toughness then increases nearly linearly to 7 MPa $m^{1/2}$ at the highest loading of 45 w/o. Thus, even a small amount of ZrO_2 results in substantial increases in fracture toughness.

Flexural strengths of Si_3N_4 composites with 45 w/o ZrO_2 modified with 5 w/o CaO are given in Table 14. These samples were tested in either the as-hot-pressed or after-heat-treatment conditions. Heat treatment consisted of 1350 C for 2 h followed by 700 C for 261 h exposure in an air environment.

The 4-point modulus of rupture was measured as a function of (1) volume loading of ZrO_2 and (2) exposure to oxidation at 700 C for durations to 250 h. The strength of these compositions is degraded by microcracking at moderate temperatures, and a temperature of 700 C was selected to study this microcracking phenomenon. The degree of strength degradation for volume loadings
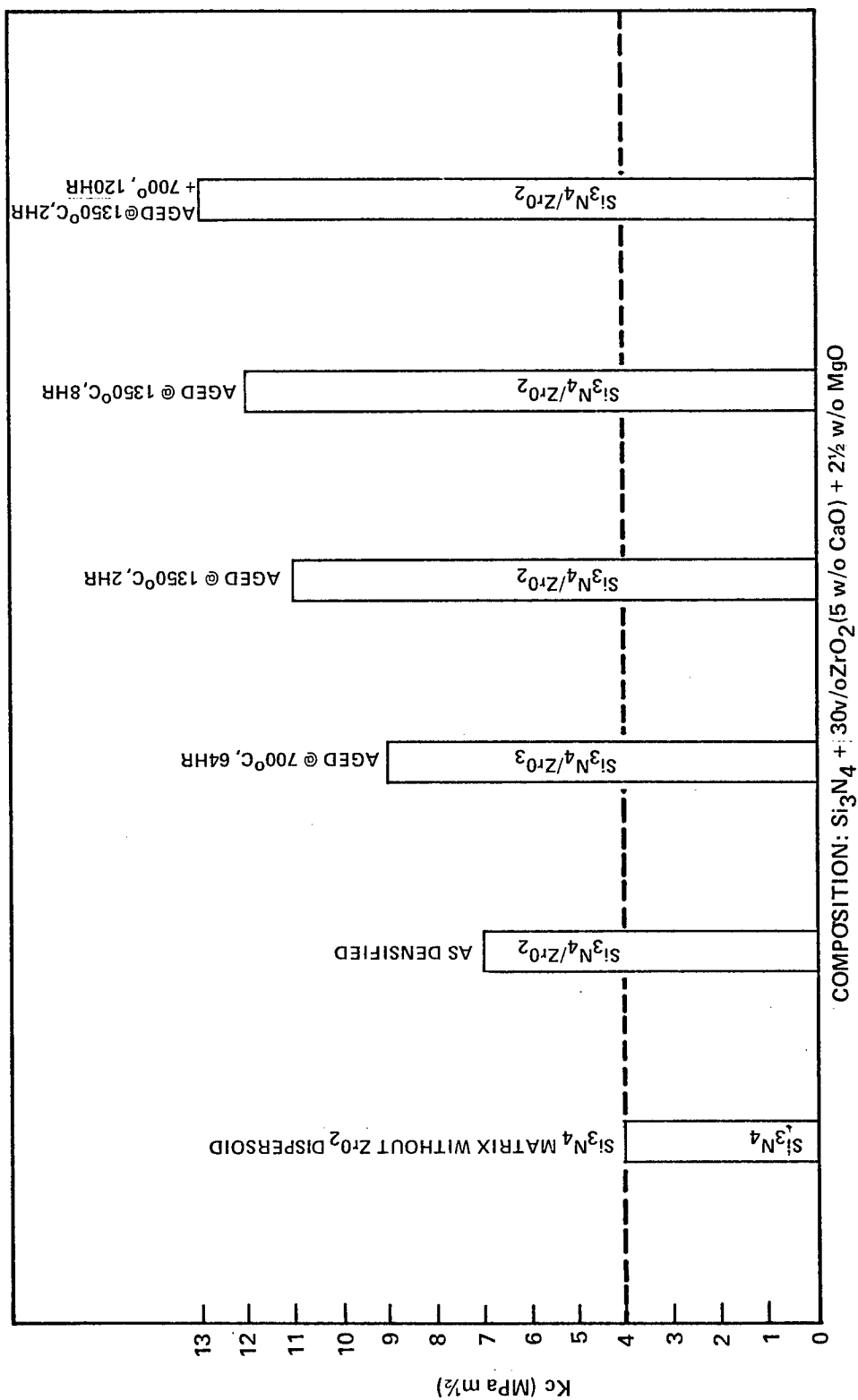
Figure 18. Effect of ZrO_2 Additions and Post Sintering Heat Treatments on Si_3N_4 Fracture Toughness

COMPOSITION: Si_3N_4 + 30v/oZrO_2(5 w/o CaO) + 2½ w/o MgO
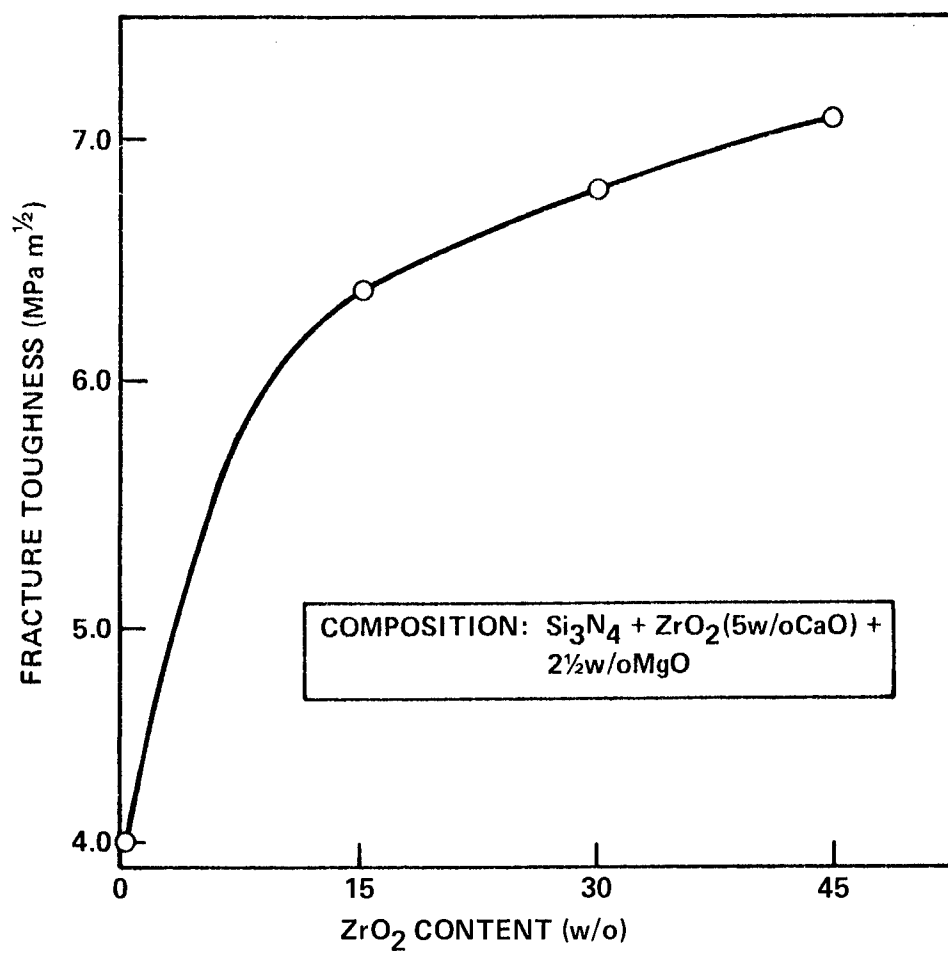
Figure 19. Fracture Toughness vs ZrO₂ Content

Table 14. Strength of Hot-Pressed Si_3N_4 + 45 w/o ZrO_2
(5 w/o CaO) + 2-1/2 w/o MgO

HOT PRESS RUN (NO.)	MOR (MPa) AS HOT PRESSED		MOR (MPa) HEAT TREATED 1350°C, 2 HR + 700°C, 261 HR	
	4-POINT	3-POINT	4-POINT	3-POINT
4	118	—	—	—
15	115	132	—	—
16	118	130	—	—
17	120	130	119	134
18	124	147	158	183

NOTE: HEAT TREATING AT ELEVATED TEMPERATURES ELIMINATES
INTERMEDIATE — TEMPERATURE DEGRADATION

of 15, 30, and 45 w/o ZrO_2 is plotted in Fig. 20. Reduction in MOR at a volume loading of 45 w/o ZrO_2 is substantial, but the degradation can be reduced by pre-aging at an elevated temperature. A temperature of 1350 C was selected for evaluation. The strength of samples aged at 1350 C for 2 h and then exposed at 700 C for selected periods is plotted in Fig. 21. There is no apparent reduction in strength at volume loadings of 15 and 30 w/o ZrO_2. The strength of the 45 w/o ZrO_2 composite, on the other hand, decreased about 33% as a result of heating at 700 C in air. Densification at higher temperatures reduced the occurrence of this when using Y_2O_3 alloyed ZrO_2 additions. XRD analyses showed that the major phases in the as-hot-pressed material were beta-Si_3N_4, cubic, and sometimes tetragonal ZrO_2. Monoclinic ZrO_2 was a minor phase and it increased to a major phase during heat treatment. Monoclinic phase was seldom observed in the composites containing ZrO_2 alloyed with Y_2O_3.

Large black inclusions and agglomerated microporosity were observed in the microstructure of these materials. The agglomerated microstructure created a mottled appearance to the unaided eye.

Sintered Material Using Coarse ZrO_2

Samples of the same compositions, 15, 30, and 45 w/o ZrO_2 (5 w/o CaO), + 2-1/2 w/o MgO, were sintered at 1800 C, 1 h. The 15 and 30 w/o compositions sintered to near theoretical densities but not as high as the densities of hot-pressed material (Table 15). The 45 w/o ZrO_2 composition, on the other hand, was extremely porous when sintered at 1800 C. It also lost weight during sintering, while the 15 and 30 w/o compositions gained small amounts of weight. Another batch of material was prepared and sintered with results in line with the other two compositions. This 45 w/o composition was sintered at five different temperatures from 1700 C to 1825 C (Fig. 22). Comparable behavior was not observed.
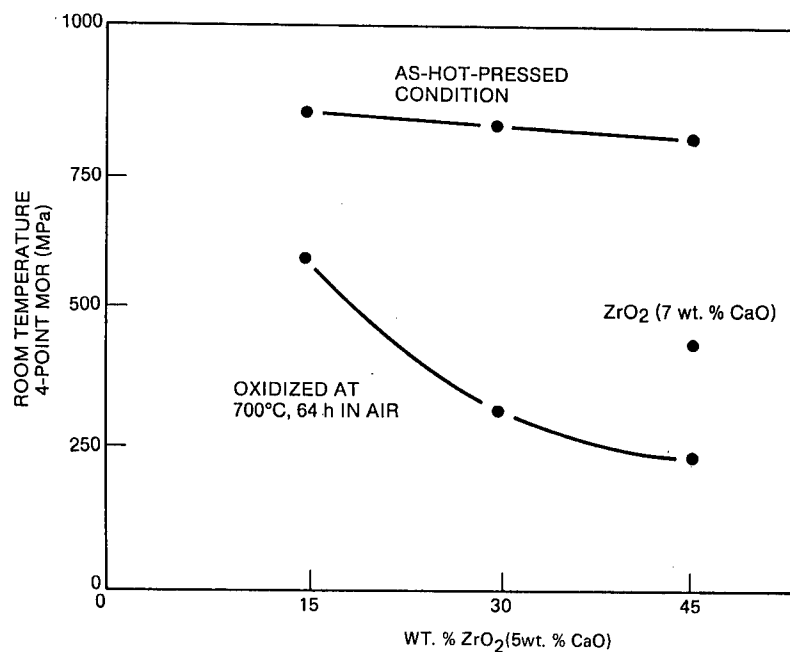
Figure 20.   Room Temperature Strength vs
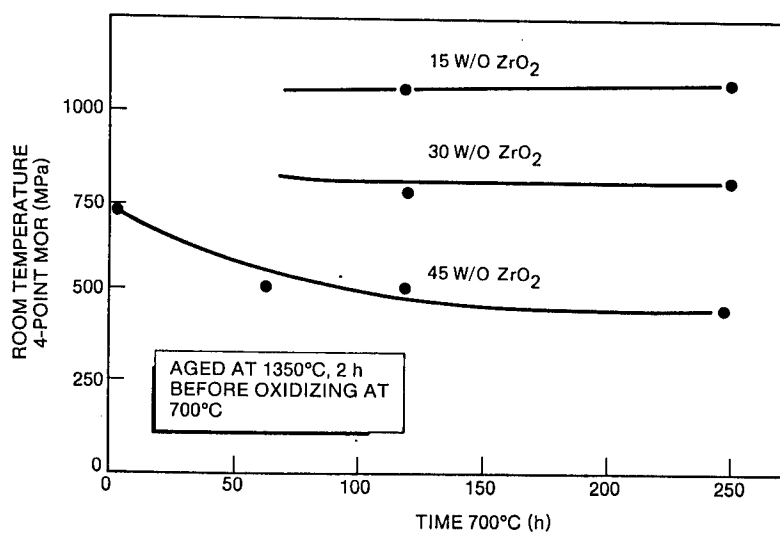ZrO$_2$ Particulate Content

Figure 21.   Room Temperature Strength of
Si$_3$N$_4$ + ZrO$_2$ (5 w/o CaO) Composites
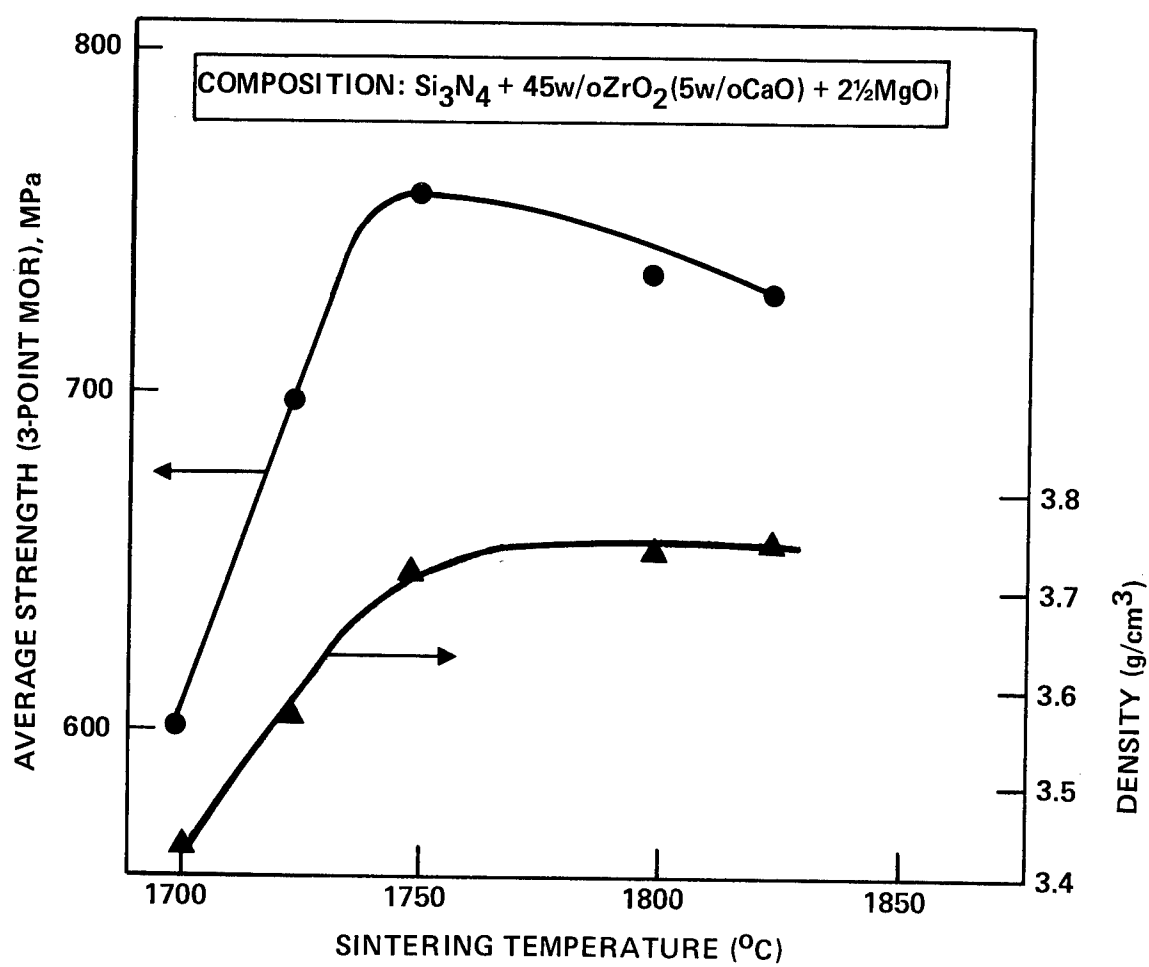vs Duration at 700 C in Air

Figure 22. Effect of Sintering on Strength and Density

Table 15. Results of 1800 C Sintering

$Zr0_2$ Content* (w/o)	Wt. Change (%)	Density (g/cm^3)	Strength (3-Pt. MOR) (MPa)	Comments
15	+0.03	3.15	668	Considerable Agglomerated Porosity
30	+0.06	3.56	779	Considerable Agglomerated Porosity
45	NA	3.73	730	Excessive Porosity

*Zircoa Grade B powder

The microstructures of the three compositions, 15, 30, and 45 w/o, are shown in Fig. 23. All of the compositions exhibited agglomerated microporosity (Fig. 24), much more than was observed in the hot-pressed materials. The data in Fig. 22 show that sintered density increased with temperature to 1750 C. Increased sintering temperatures resulted in little density change but decreased strength. Even at a sintering temperature of 1825 C, the density remained below that of hot-pressed material, which was 3.83 g/cm^3.

In spite of the agglomerated microporosity and the black inclusions, the room-temperature strength was over 700 MPa. Average strength of the 45 w/o composite also is shown in Fig. 22. The density increased only slightly above 1750 C, and the strength peaked at 1750 C, then decreased with increasing sintering temperature. As was the case for the $Zr0_2$ (Y_2O_3) cor posites, the compositions containing 30 w/o were the strongest (Fig. 25). Strengths were 670, 780, and 730 MPa for the compositions 15, 30, and 45 w/o, respectively. The decrease in strength observed for sintering temperatures above 1750 C for the 45 w/o $Zr0_2$ loading agrees with results for the Y_2O_3 alloyed $Zr0_2$ additions.

The strength at elevated temperatures was relatively low because an appreciable amount of CaO diffuses into the grain boundaries during sintering. Strengths of these materials to 1200 C are shown in Fig. 26. Strength dropped rapidly after 600 C.
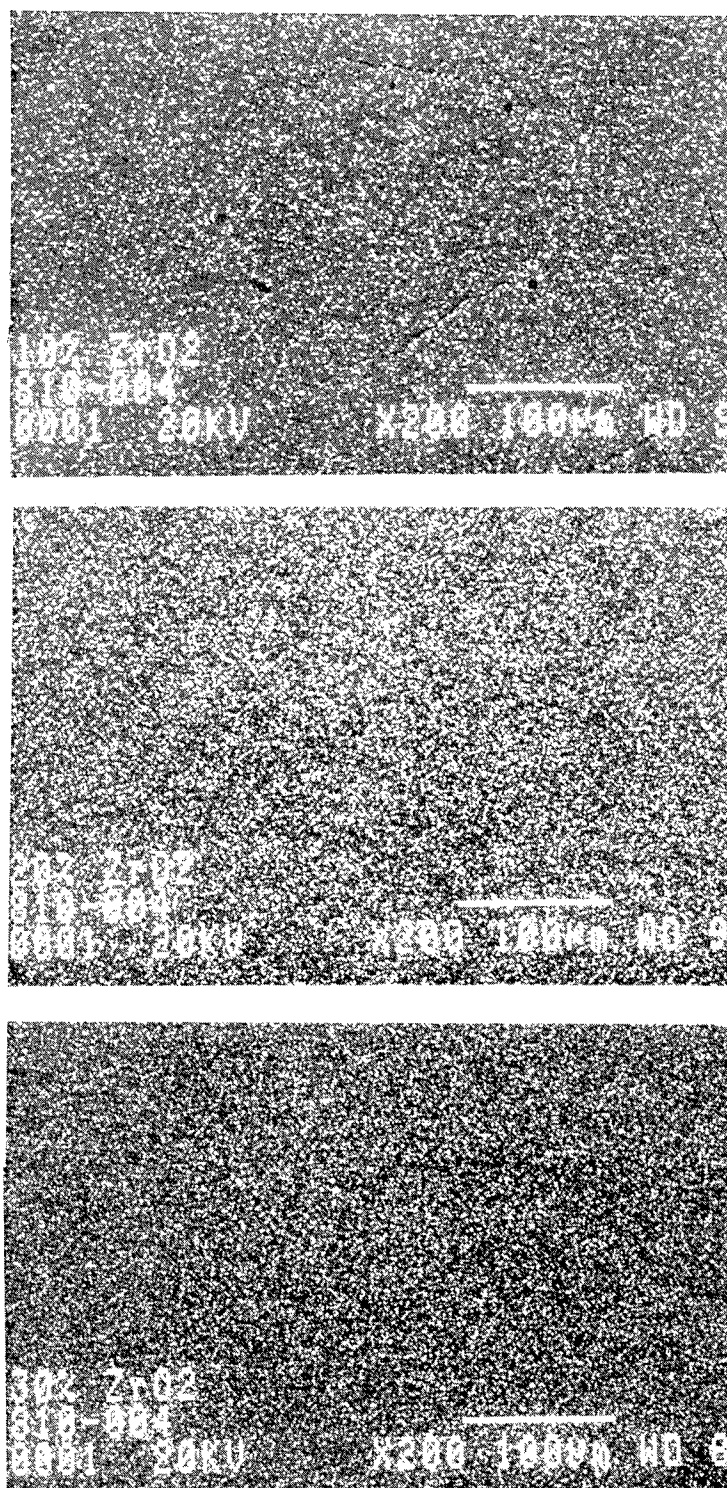
Figure 23. Dispersions of 15, 30, and 45 w/o ZrO$_2$ Grains
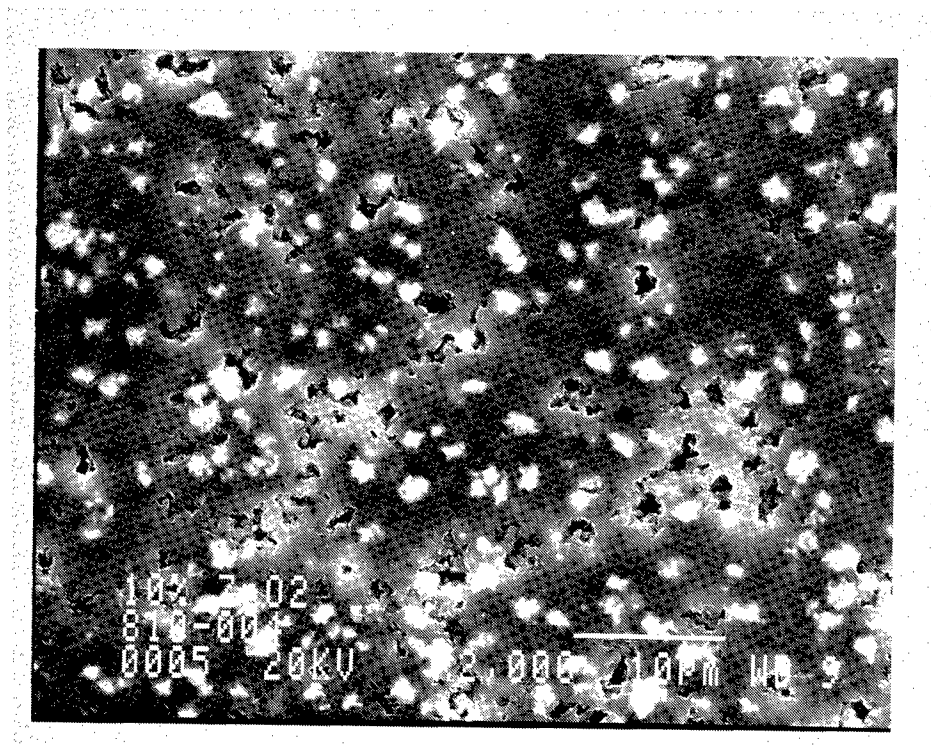
Figure 24. Polished Surface of Sintered Si_3N_4 + 15 w/o ZrO_2 (5 w/o CaO) + 2-1/2 w/o MgO Showing High Porosity Region

AVERAGE STRENGTH (3-POINT MOR), MPa

ZIRCONIA CONTENT (W/O)
[v/o ZrO₂ (5 w/o CaO)]

COMPOSITION: Si_3N_4 + ZrO_2(5w/oCaO) + 2½w/oMgO
SINTERING PARAMETERS: 1800C, 1h

Figure 25. Strength as a Function of ZrO_2 Content

Figure 26.   Strength as a Function of Temperature and ZrO_2 Content

Intermediate-temperature oxidation degradation was not observed in the sintered material, but aging was carried out only to 250 h (Fig. 27). This is, however, in agreement with results with material containing Y_2O_3 as the alloying agent, as reported in the preceding section. Degradation was pronounced in the hot-pressed materials, which were de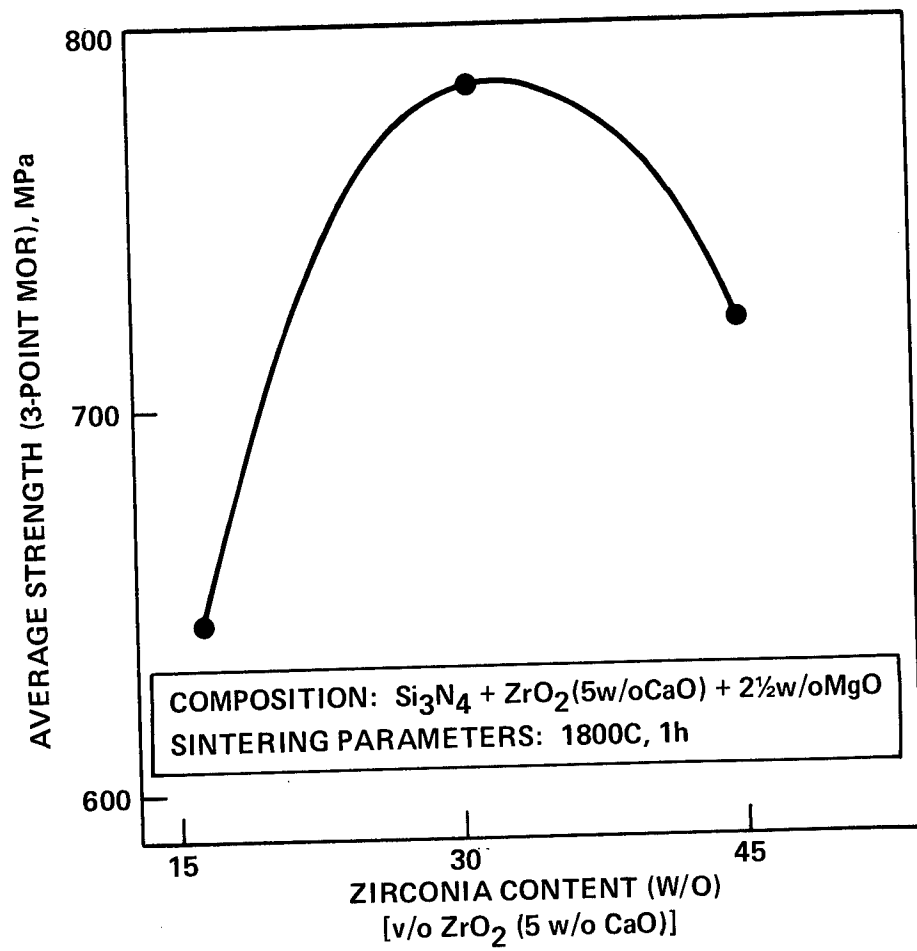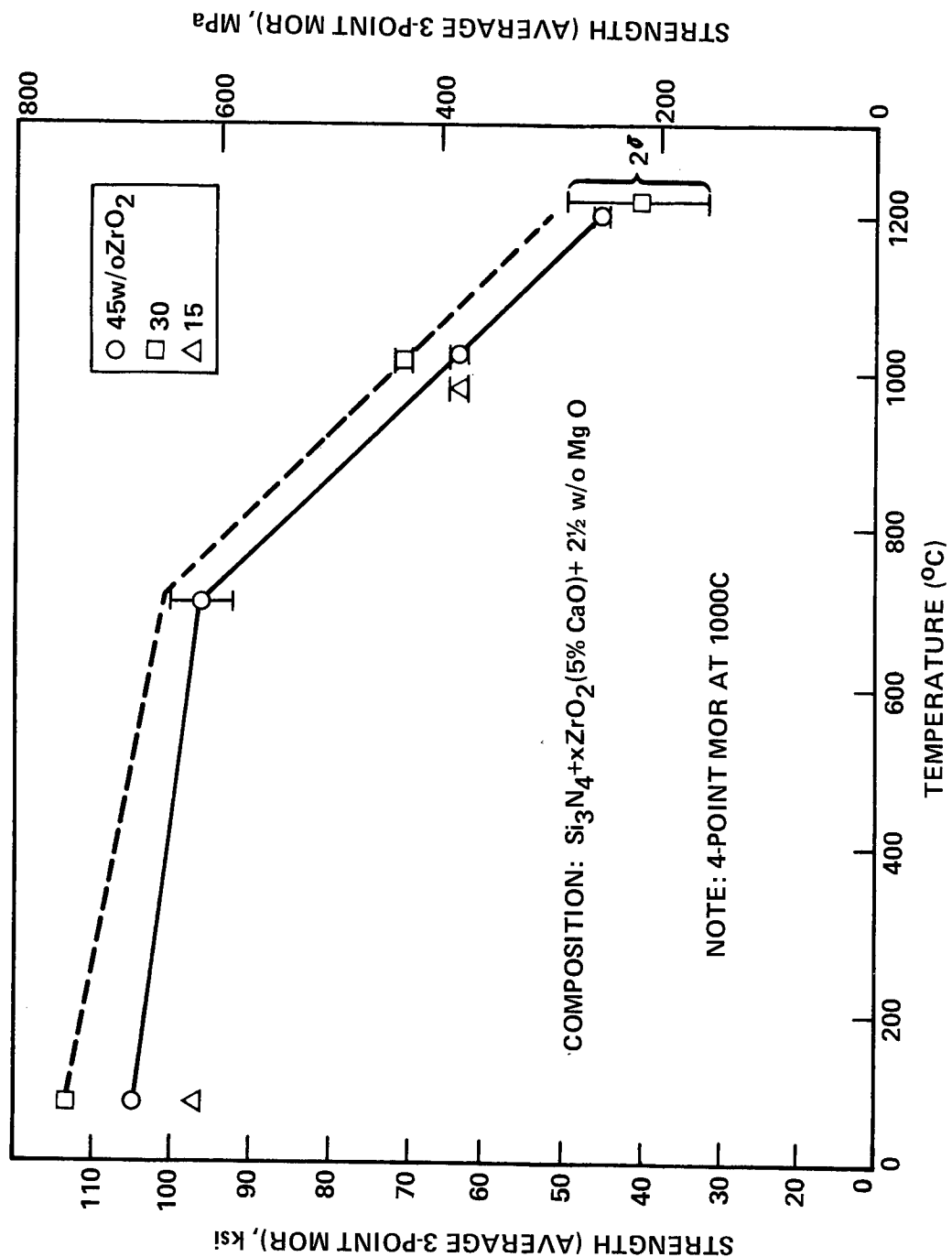nsified at 1700 C, while it was not observed in the material that was sintered at 1800 C. The composites were more stable when densified at 1800 C or above.

Fracture toughness of the sintered materials was at the same high level as that of the hot-pressed material. The toughness, measured according to the Anstis relationship (Ref. 5), of the 45 w/o composition was 7.5 MPa $M^{1/2}$. When aged in air at 1200 C for 2 h, it increased to 11.8 MPa $m^{1/2}$.

Sintered Composite with Submicron ZrO_2 (CaO)

Submicron, high-purity ZrO_2 powders containing 3.5, 6.2, and 10 w/o CaO were obtained. Batches of Si_3N_4 + 45 w/o ZrO_2 (xCaO) + 2.5 w/o MgO were colloidally prepared, and disk-shaped samples were prepared by pressure filtration. These disks were then dried and sintered at 1800 C, 1860 C, and 1900 C for 1 h. Properties of the sintered samples are presented in Table 16. A sintering temperature of 1860 C was required to obtain a high density for the composition containing 10 w/o CaO; a temperature of 1900 C was required for the composition containing 6.2 w/o CaO, while the composition containing 3.5 w/o did not sinter to a high density, even at 1900 C.

Examination under a high-power light microscope showed that these samples did not exhibit the agglomerated microporosity as the previous samples made with the coarse, less pure powder. A secondary phase that appeared as black inclusions was observed in the new samples made from the high-purity, submicron ZrO_2, however. The black inclusions were found to be composed of Fe and Ti. Subsequent investigation of the Ti-alloy ultrasonic horn showed signs of wear.
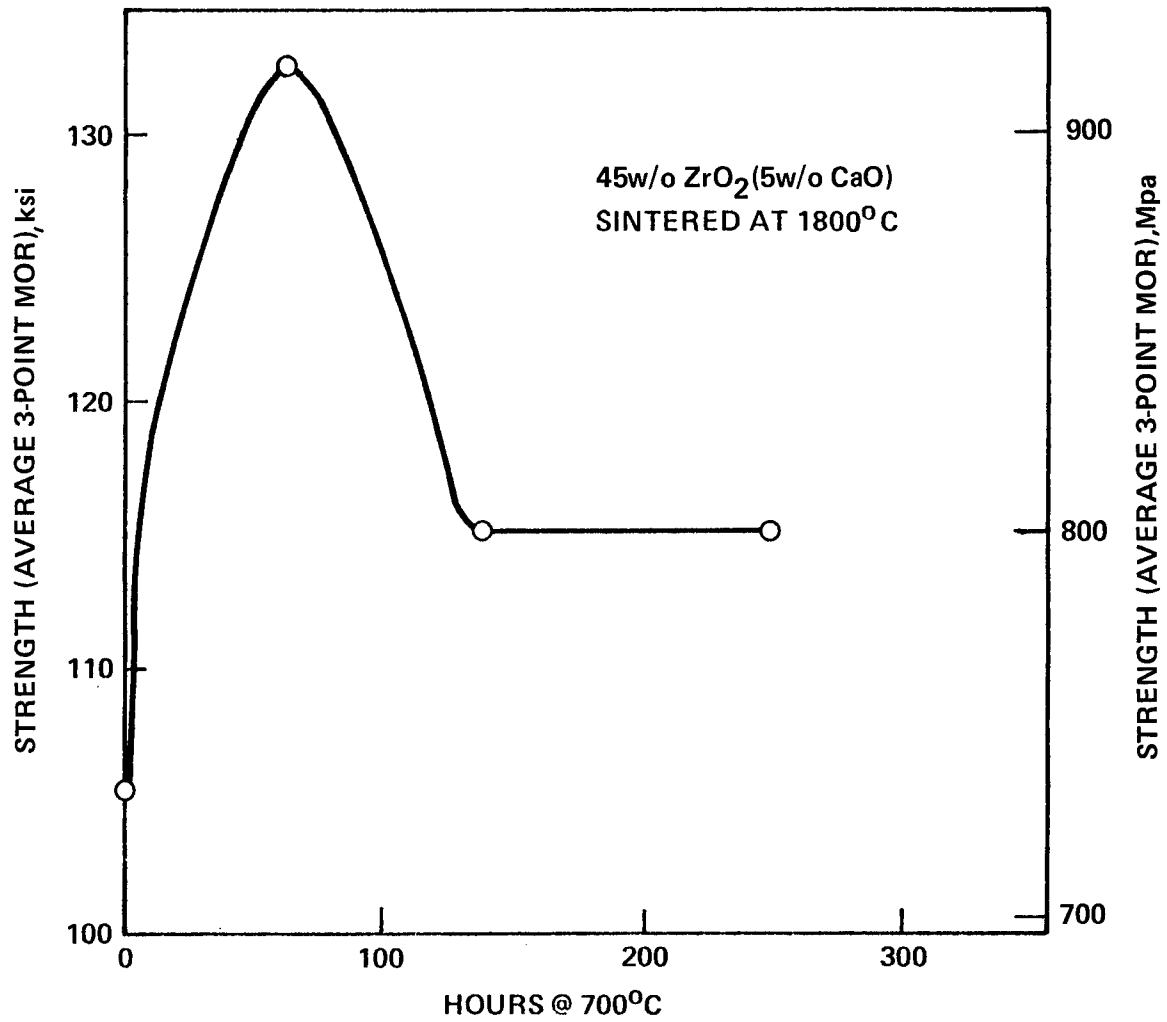
Figure 27.   Aged Composites Show No Microcracking

Table 16. Sintering Results for ZrO_2 (CaO) Dispersed Phase Composites

Sinter Temperature (°C)	CaO Alloy (w/o)	Wt Loss (%)	Porosity (%)	Density (g/cm³)	Room-Temperature Strength (Avg. 3-Pt. MOR) (MPa)
1800	3.5	3.3	21	2.89	-
	6.2	2.5	14	3.29	-
	10	1.8	10	3.48	-
1860	3.5	4.5	6.9	3.40	682
	6.2	1.2	0.2	3.66	792
	10	0.8	0.1	3.83	723
1900	3.5	7.1	8.9	3.44	675
	6.2	1.3	0.2	3.80	772
	10	1.1	1.7	3.78	655

*Si_3N_4 + 45 w/o ZrO_2 (CaO) + 2-1/2 MgO
Note: All fracture origins were at metal inclusions (Fe, Ni, Cr, Ti)

Room-temperature strength is also presented in Table 16. Maximum strength, 792 MPa, was obtained for the 6.2 w/o CaO composition sintered at 1860 C. All failures originated at large, black metal inclusions. The sintered density and strength are plotted in Fig. 28 as a function of sintering temperature. The highest density was exhibited by the 10 w/o CaO composition because there is more CaO in the grain boundaries. However, the strength of the 10 w/o composition was lower than that of the 6.2 w/o composition. Strength decreased for each composition when the sintering temperature was raised from 1860 C to 1900 C.

Toughness was measured (Ref. 5) and the results are plotted in Fig. 29. Toughness was highest, 8.5 MPa $m^{1/2}$, for the composition containing 6.2 w/o CaO alloy, while the toughness was lowest, 6.8 MPa $m^{1/2}$, for the composition containing 10 w/o CaO alloy. These toughness values represent a 100 and a 60% increase, respectively. The composite with 6.2 w/o CaO alloy did not respond
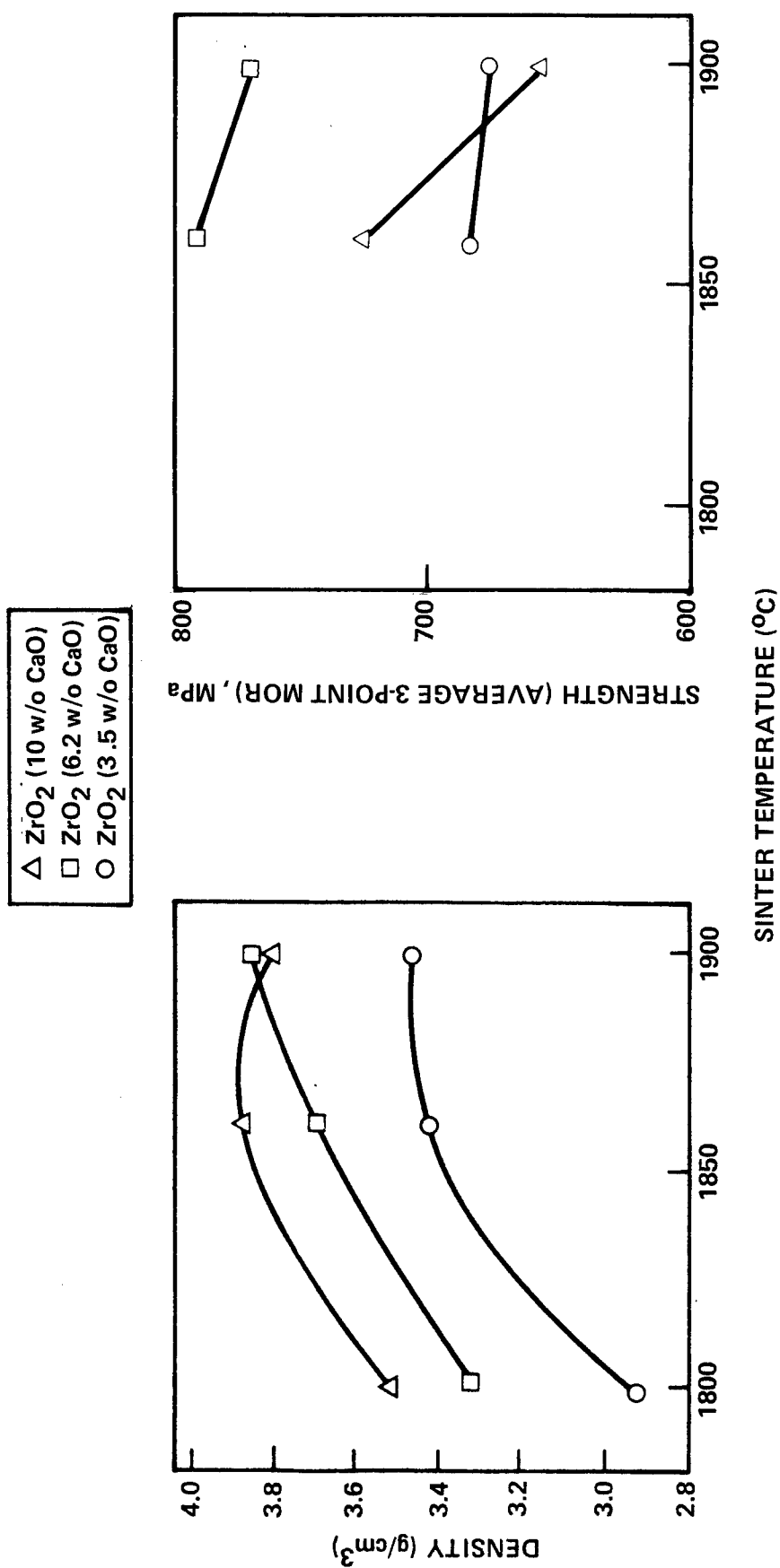
Figure 28. Strength and Density vs Sintering Temperature
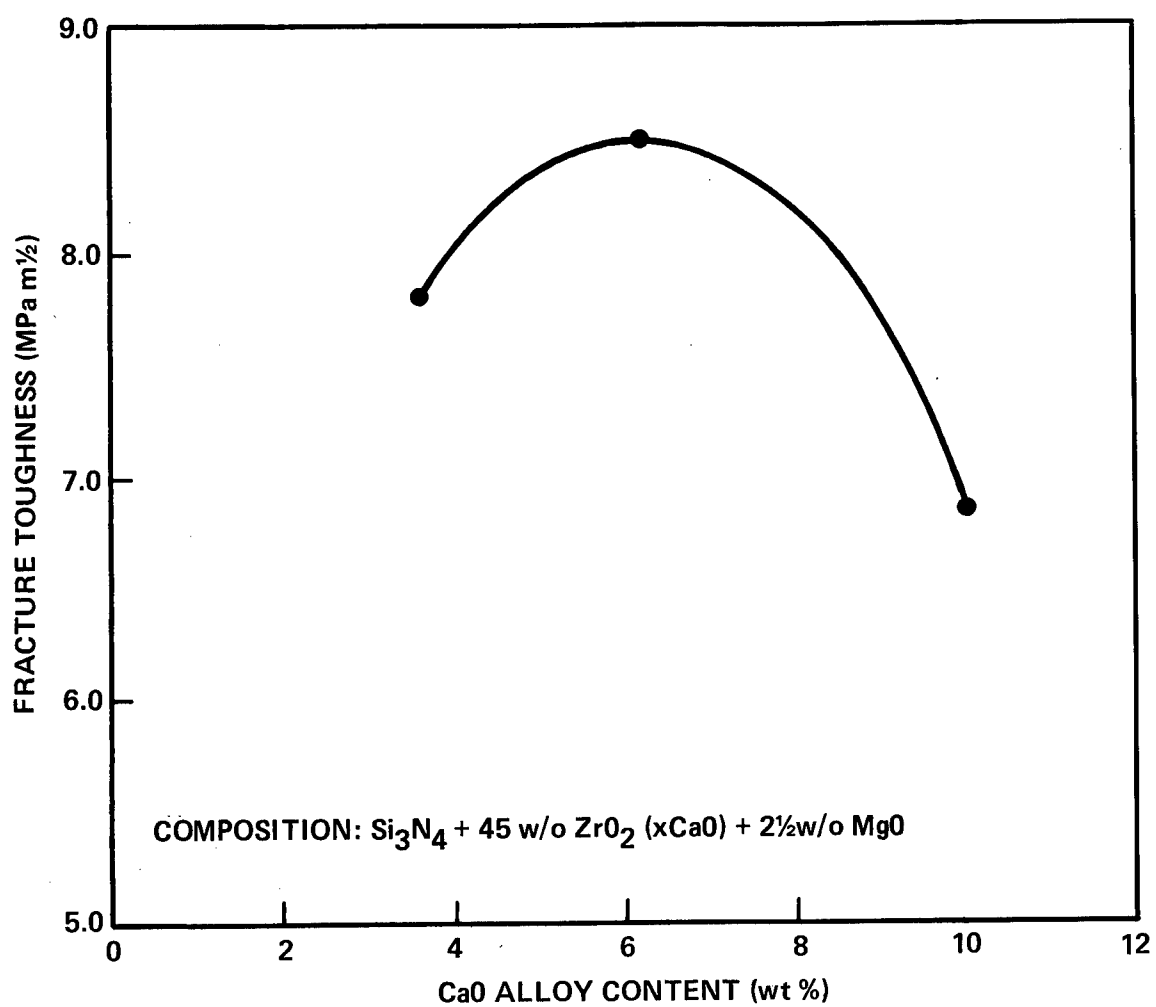Composition: $Si_3N_4 + ZrO_2$ (XCaO) + 2.5 w/o MgO

Figure 29. Fracture Toughness vs CaO Content in the ZrO_2

to heat treatment at 1350 C as did the composite made with the coarse 5 w/o CaO powder. In fact, toughness decreased slightly after the heat treatment.

TEM studies of the composite microstructure were conducted. The presence of monoclinic phase was confirmed by convergent beam diffraction and the mono-clinic laths extended across the entire zirconia grain. The ZrO_2 grains were depleted of CaO (Fig. 30).

OTHER DISPERSED PHASES

<u>ZrO_2 (5 w/o MgO)</u>

MgO as an alloying agent for ZrO_2 or HfO_2 offers potential advantages over CaO. An appreciable amount of the alloying constituent will diffuse out of the ZrO_2 grains during sintering and react with the other compounds in the grain boundaries. MgO would be expected to form more refractory and oxida-tion-resistant compositions than would CaO. However, the ZrO_2 (MgO) system was not pursued because the first samples that were made cracked. The results of the Si_3N_4/ZrO_2 (MgO) samples are presented to show that this system did indicate high fracture toughness.

The only powder that could be obtained for evaluation early in the program was a relatively coarse powder, average particle size of 22 micrometers, contain-ing 5 w/o MgO*. Due to the particle size, the colloidal processing method could not be used. A water slurry of the composition Si_3N_4 + 45 w/o ZrO_2 (5 w/o MgO) plus 2.5 w/o MgO as a sintering aid was prepared by milling for 16 h using ZrO_2 milling material. Disks, 3.8 cm in diameter, were pre-pared by pressure filtration, dried, and hot-pressed at 1550 C for 1/4 h; at 1600 C for 1 h; and at 1700 C for 1 h. Fracture toughness was exceptionally high (Table 17), 7.6 MPa $m^{1/2}$ in the as-hot-pressed condition, and as high as 13.4 MPa $m^{1/2}$ after aging at 1350 C for 2 h. This apparent toughness is double and triple that of the Si_3N_4 matrix.

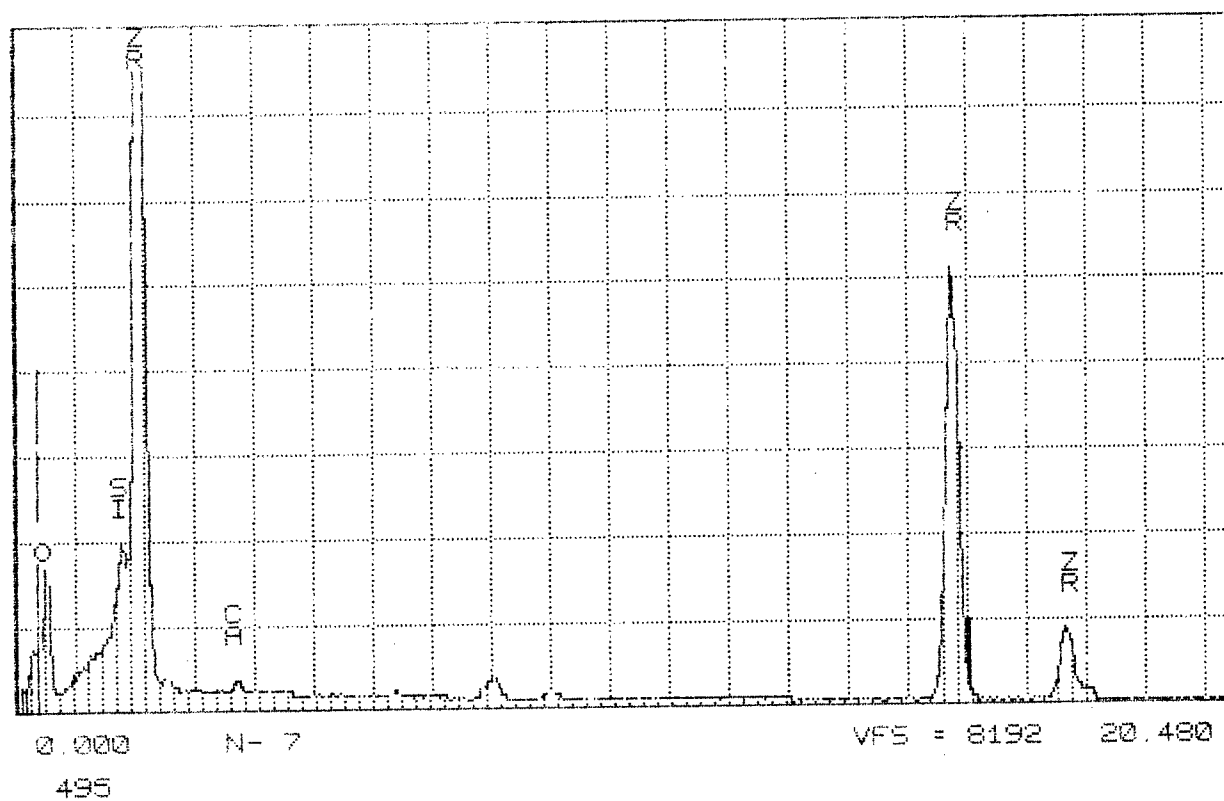*SCMG5 Grade, Magnesium Electron, Inc., Flemington, NJ

Figure 30. Semiquantitative Analysis Shows Low Ca Content
in Monoclinic ZrO_2 grain

Table 17. Results of Hot Pressed Si_3N_4 + 45 w/o ZrO_2
(5 w/o MgO) + 2-1/2 w/o MgO Composite

Properties	Hot-Pressing Temperature (C)		
	1700	1600	1550
Density (g/cm³)	3.87	3.91	4.08
Fracture Toughness* (MPa m$^{1/2}$)			
As-Hot-Pressed Condition	7.6	6.4	3.9
Aged at 1350 C, 2 h in air	10.1	13.4	9.2
3-Point MOR (MPa)			
As-Hot Pressed	138 to 696	599	324
Aged at 700 C, 64 h in air	103 to 620	186	69
Aged at 1350 C, 2 h in air	–	–	413
Aged at 1350 C, 2 h + 700 C, 64 h in air	–	41 to 241	41

*Diamond indentation per Anstis (Ref. 5)

Strength, on the other hand, was low and erratic. These low and erratic results were believed to be due to microcracking that occurred during hot pressing. The sample hot pressed at 1600 C cracked audibly into two pieces while at temperature. Density was highest at the lowest hot-pressing temperature.

$HfO_2-ZrO_2-TiO_2$

A composite with a zero thermal expansion coefficient to 1800 C was developed and patented (Ref. 12) at Rocketdyne for rocket nozzle applications in the mid 1960s. The intent of this experiment was to use this composition, 60 m/o HfO_2-20 m/o ZrO_2-20 m/o TiO_2, as a dispersion in Si_3N_4 to cause toughening. Submicron powder was obtained and a composition of Si_3N_4 + 30 v/o dispersion + 4 w/o Al_2O_3 was prepared by the colloidal processing method. A 3.8 cm diameter disk was prepared by pressure filtration, dried, and hot pressed to near full density. The material was very dark and appeared to be uniform. The fracture toughness, however, was low, only 2.7 MPa m$^{1/2}$, and samples turned into powder when oxidized in air at 700 C. For these reasons, investigation of this composition was abandoned.

*Wah Chang, Albany, OR

THERMOPHYSICAL PROPERTIES

Thermal diffusivity and thermal expansion were measured and are reported in this section.

THERMAL DIFFUSIVITY

Thermal diffusivity of four samples was measured by the laser flash method* from room temperature to 1300 C. Results are listed in Table 18. Sample composites included Si_3N_4 + 30 and 45 w/o ZrO_2 (12 w/o Y_2O_3) + 4 w/o Al_2O_3 and Si_3N_4 + 30 and 45 w/o ZrO_2 (6.2 w/o CaO) + 2.5 w/o MgO. Data for the Y_2O_3 alloyed composites are plotted in Fig. 31 and 32, along with data for both single-phase Si_3N_4 and ZrO_2 (Y_2O_3). The Si_3N_4 data were measured on grade NC132 material (Ref. 14) and the ZrO_2 data were measured on ZrO_2 material alloyed with 5.3 w/o Y_2O_3 (Ref. 13). The thermal diffusivity values for the composites show a significant deviation from the rule of mixtures. The 30 and 45 w/o additions of ZrO_2 result in significant reductions of thermal diffusivity. Thermal diffusivity values for the CaO alloyed compositions, on the other hand, fall on or near the straight line connecting the Si_3N_4 and ZrO_2 end members.

THERMAL EXPANSION

Thermal expansion was measured** on samples of three different compositions, using an Orton Automatic Recording Dilatometer. Total sampl length was 51 mm. Samples were made in two end-to-end bars. A single bar, 51 mm long, could not be produced due to the limited diameter of the pressure filtration die. NC-132 material, supplied by Norton Co. (lot 3931), was one of the three samples and it, also, was in two pieces. The measured coefficients are summarized in Table 19. The measured expansion value for the NC-132 reference

---

*Dr. D. P. H. Hasselman, Virginia Polytechnic Institute and State University, Blacksburg, VA
**Measurements performed at Emhart Corp., Windsor, CT

Table 18. Thermal Diffusivity of Si_3N_4

Sample A		Sample B		Sample C		Sample D	
Temp. (°C)	T.D. (cm^2s^{-1})	Temp. (°C)	T.D. (cm^2s^{-1})	Temp. (°C)	T.D. (cm^2s^{-1})	Temp. (°C)	T.D. (cm^2s^{-1})
25	0.0658	25	0.0628	25	0.1480	25	0.1480
300	0.0466	304	0.0428	300	0.0890	311	0.0753
404	0.0431	400	0.0356	404	0.0749	404	0.0650
505	0.0414	505	0.0308	502	0.0656	500	0.0541
609	0.0390	600	0.0281	601	0.0586	604	0.0472
706	0.0361	705	0.0252	700	0.0517	702	0.0424
803	0.0325	807	0.0237	800	0.0446	807	0.0388
906	0.0298	905	0.0223	900	0.0403	902	0.0371
1004	0.0277	1002	0.0208	1002	0.0366	1003	0.0341
1100	0.0258	1100	0.0192	1100	0.0339	1100	0.0310
1200	0.0239	1200	0.0176	1200	0.0312	1200	0.0284
1300	0.0220	1300	0.0172	1300	0.0284	1300	0.0266

	Density (g/cm^3)	Composition
A	3.53	Si_3N_4 + 30 w/o ZrO_2 (12 w/o Y_2O_3) + 4 w/o Al_2O_3
B	3.91	Si_3N_4 + 45 w/o ZrO_2 (12 w/o Y_2O_3) + 4 w/o Al_2O_3
C	3.50	Si_3N_4 + 30 w/o ZrO_2 (6.2 w/o CaO) + 2-1/2 w/o MgO
D	3.66	Si_3N_4 + 45 w/o ZrO_2 (6.2 w/o CaO) + 2-1/2 w/o MgO

Table 19. Coefficient of Thermal Expansion

	Coefficient (10^{-6}/C) (25 to 725 C)
● NC-132	2.90
● Si_3N_4 + 30 w/o ZrO_2 (12 w/o Y_2O_3) + 4 w/o Al_2O_3	4.20
● Si_3N_4 + 45 w/o ZrO_2 (6.2 w/o CaO) + 2-1/2 w/o MgO	4.20
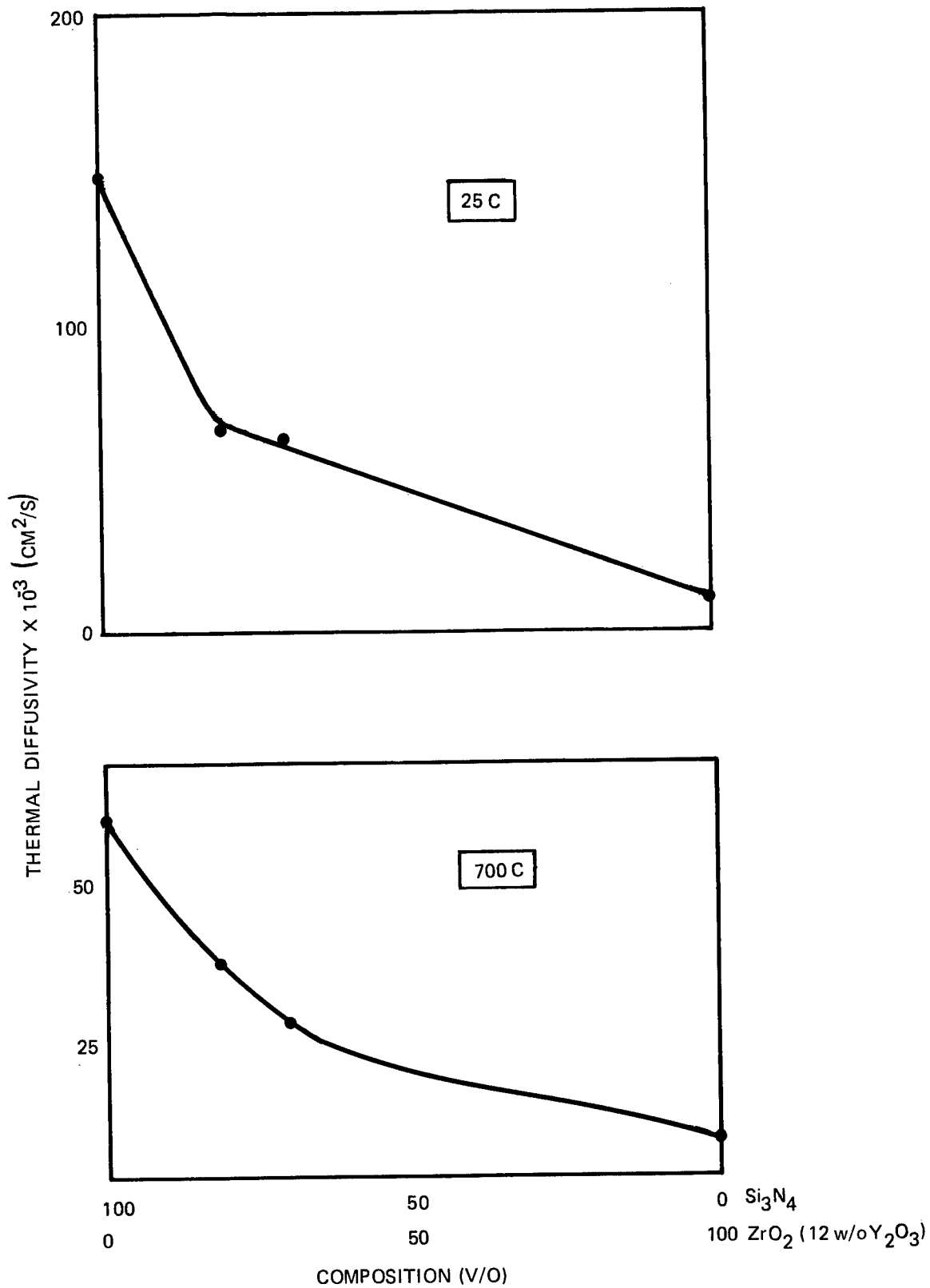
Figure 31. Thermal Diffusivity of Si_3N_4 + ZrO_2 (Y_2O_3) Composites at 25 C and 700 C
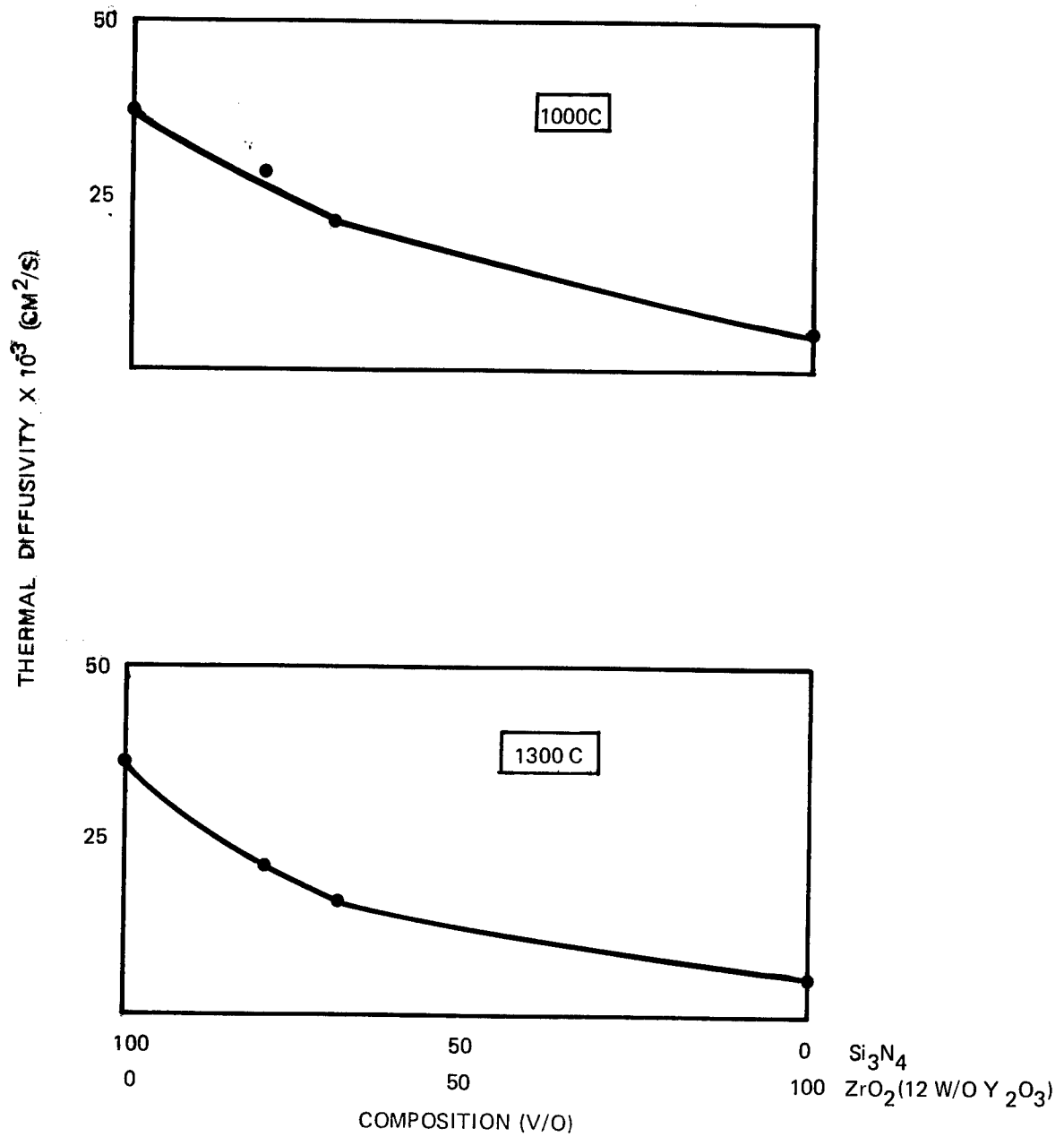
Figure 32. Thermal Diffusivity of Si_3N_4/ZrO_2 (Y_2O_3) Composites at 1000 C and 1300 C

sample (Fig. 34) agreed closely with published data. The other two sample compositions were Si_3N_4 + 30 w/o ZrO_2 (12 w/o Y_2O_3) + 4 w/o Al_2O_3 and Si_3N_4 + 45 w/o ZrO_2 (6.2 w/o CaO) + 2-1/2 w/o MgO. The thermal expansion coefficients, 25 to 725 C, were calculated from Fig. 35 and 36. The composite values followed the rule of mixtures (Fig. 33). The 30 w/o ZrO_2 composite in Fig. 33 was alloyed with 12 w/o Y_2O_3 and X-ray diffraction analysis showed that the ZrO_2 particles were cubic phase. The 30 w/o ZrO_2 composition in Fig. 33 was alloyed with 6.2 w/o CaO and X-ray diffraction showed that the ZrO_2 particles were mostly cubic with a minor amount of monoclinic phase present. Thus, the expansion coefficient was below the line connecting NC132 and cubic ZrO_2 end point compositions, and it was closer to the line connecting the NC132 and monoclinic-ZrO_2 end points.

The fact that the thermal expansion for the composites is relatively low for a structural ceramic material indicates that these composites have potentially excellent resistance to thermal shock. These composites have an exceptionally high figure of merit for thermal shock resistance due to their combination of low thermal expansion, high strength, and high toughness compared with monolithic Si_3N_4, which exhibits, by far, the best resistance to thermal shock of high-temperature monolithic ceramics (Ref. 15).
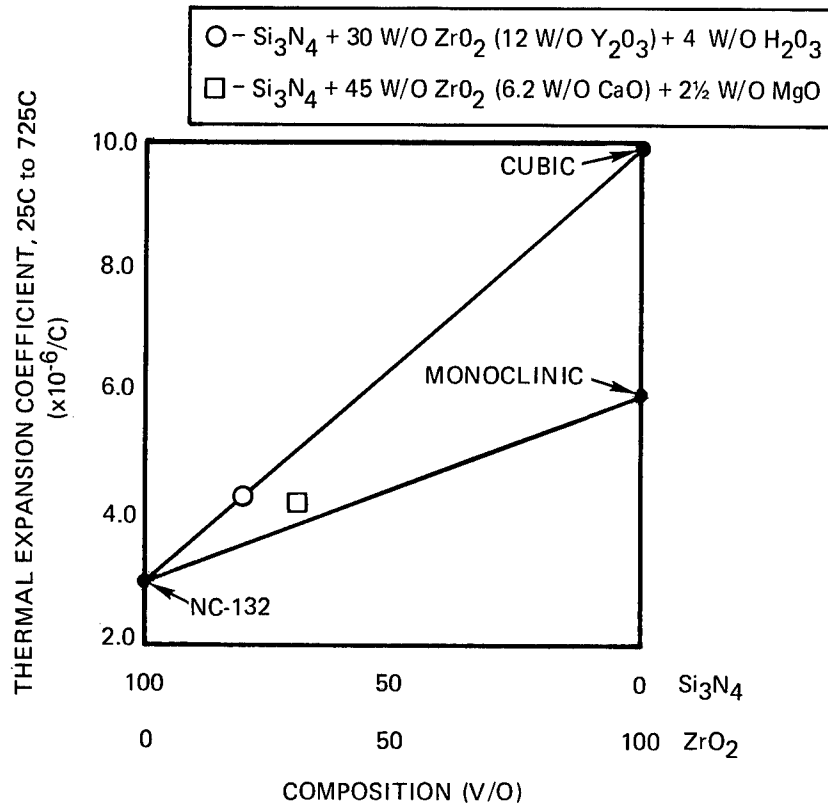
Figure 33. Thermal Expansion Coefficient of Si₃N₄
            Composites Comply with Rule of Mixtures
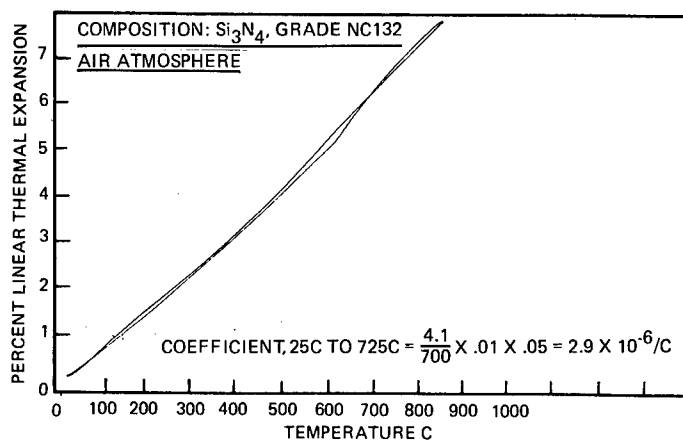
Figure 34.   Dilatometer Record for NC-132
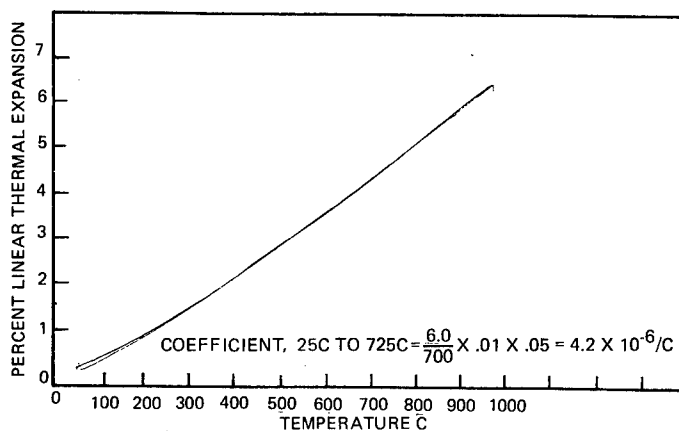
Figure 35.   Dilatometer Record for Si$_3$N$_4$ + 30 w/o ZrO$_2$
(12 w/o Y$_2$O$_3$) + 4 w/o Al$_2$O$_3$
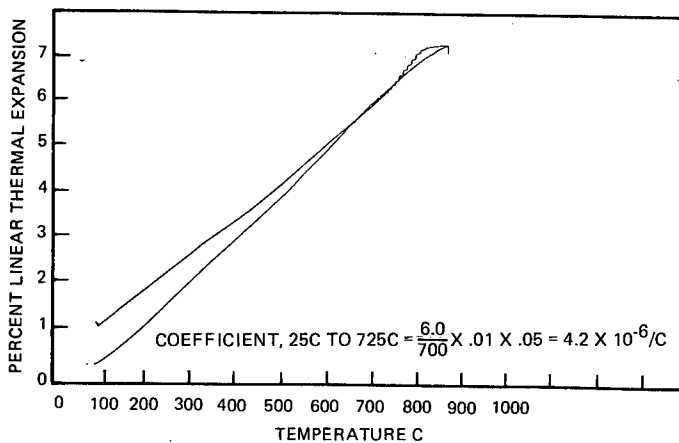
Figure 36.   Dilatometer Record for Si$_3$N$_4$ + 45 w/o ZrO$_2$
(6.2 w/o CaO) + 2-1/2 w/o MgO

INJECTION MOLDING

One of the primary objectives of this program was to demonstrate fabrication using a high-volume, low-cost process. The colloidal processing methods used in this program are compatible with two conventional fabrication methods, injection molding and slip casting plus sintering. The injection molding method was selected for this program because Rocketdyne has been active in injection molding of Si_3N_4 for a decade and has been successful in producing a number of demonstration shapes of Si_3N_4 such as turbine blades and vanes.

Ideally, a water soluble plasticizer/binder system should be used so that it can be mixed directly with the Si_3N_4/ZrO_2 powders which are suspended in water. However, a water-base system was not available so the suspended slurries of Si_3N_4/ZrO_2 had to be dried before mixing with the plasticizer/binder systems. Mixing was performed in a heated sigma blade-type machine. The maximum volume loading that could be attained was 50% solids. A higher loading would be preferred. The green bodies sintered to near full density but the shrinkage would have been less had the starting green density been higher.

The material molded well, and no major problems were encountered in making MOR bars. Binder removal was normal, and MOR bars sintered to an average density of 3.89 g/cm^3, which is 96% of theoretical. Average weight loss was 1.5%, and the average measured open porosity was less than 0.1%. Examination of polished sections showed that the microstructure was homogeneous and the ZrO_2 grains were well dispersed (Fig. 37).

MOR bars were made with an existing die which was designed for making metal tensile specimens shaped like flat, thin, dog bones. The dumbbell ends were cut off in the green state, and the center section was used for MOR bars. The resultant MOR specimen is satisfactory, and Rocketdyne has used it for a decade to generate strength data. A disadvantage of this bar is that it is not a standard geometry that can be directly compared to data reported by other laboratories. The typical size of these injection molded bars is 2.2 mm x
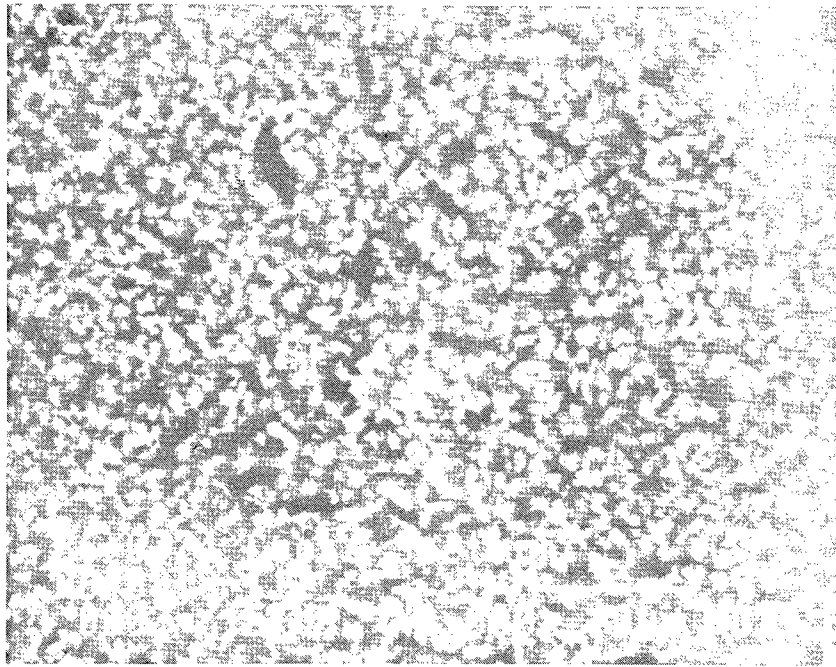
Figure 37. Microstructure of Injection Molded Si_3N_4 + 45 w/o ZrO_2 (12 w/o Y_2O_3) + 4 w/o Al_2O_3

6.4 mm x 50 mm long. Thus, they are a slab rather than a beam. Unpublished data generated by the author using NC430 grade SiC bars, one-half having been diamond ground to the injection-molded slab geometry and one-half having been diamond ground to a similar size but having a cross section more like a conventional MOR bar, showed that the flexural strength of the same material when measured in a slab configuration was 20% lower.

The 4-point MOR data are listed in Table 20. The strength of samples densified in sintering runs No. 36 and 41 were similar, and they were grouped together. The strengths of samples densified in sintering run No. 45, however, were lower and are listed separately. The reason for the difference in strength is unknown. Samples tested in the as-sintered condition were covered with a very thin film of zirconium nitride. Four-point MOR was 429 MPa and 356 MPa, respectively. When the surfaces were tested in the ground condition, the strength increased to 595 MPa and 538 MPa. Figures 38 and 39 show the texture of the surface of injection-molded MOR bars in the as-sintered and ground conditions.

Analyses were conducted on fractured and polished surfaces of injection-molded bars using the scanning electron microscope to identify the source of fracture-causing flaws. Few flaws were found but the population was enough that one or more would always be found within the high-stress region of the test bar, and these flaws were large. One category of flaws was metal inclusions composed of Fe and Ti (Fig. 40), which probably originated from the titanium alloy ultrasonic mixing horn. Other metal surfaces were coated with a hard abrasion-resistant layer of chromium. A second category of flaws was low-density regions caused by incomplete mixing of the powder and plasticizer (Fig. 41). This was verified by inspecting the powder/plasticizer before injection molding under low-power magnification. White inclusions were analyzed by energy-dispersive X-ray analyses which showed that the composition was the same as that of the composite mixture. In other words, these were plasticizer-rich nodules that left a pore-like structure after the plasticizer was removed. The third category of flaws was worm-like pores caused by dust contamination during processing (Fig. 42).

Table 20. Results of Injection Molding Study

Sinter Run No.	Procedure	Surface Condition	Number of Samples	Average Strength (4-Point MOR)[3] (MPa)	Standard Deviation (MPa)	Weight Loss During Sintering (%)	Sintered Density (g/cm^3)	Open Porosity (%)
36 and 41	Standard	As-sintered	9	429	47	1.1	3.89	0.01
36 and 41	Standard	Ground	8	595	96	-	-	-
45	Standard	As-sintered	4	356	51	1.6	3.90	0.1
45	Isopressed[1]	As-sintered	8	354	56	-	-	-
45	Isopressed	Ground[2]	5	538	41	-	-	-

Notes:

1. The MOR bars were isostatically pressed at 345 MPa after binder removal and before sintering.

2. Grinding exposed a few large surface pores.

3. Typical sample size 2.2 mm x 6.4 mm x 50 mm

Outer span = 31.6 mm
Inner span = 10.3 mm

Composition: Si_3N_4 + 45 w/o ZrO_2 (12 w/o Y_2O_3) + 4 w/o Al_2O_3

Sintering parameters: 1800 C 1 h
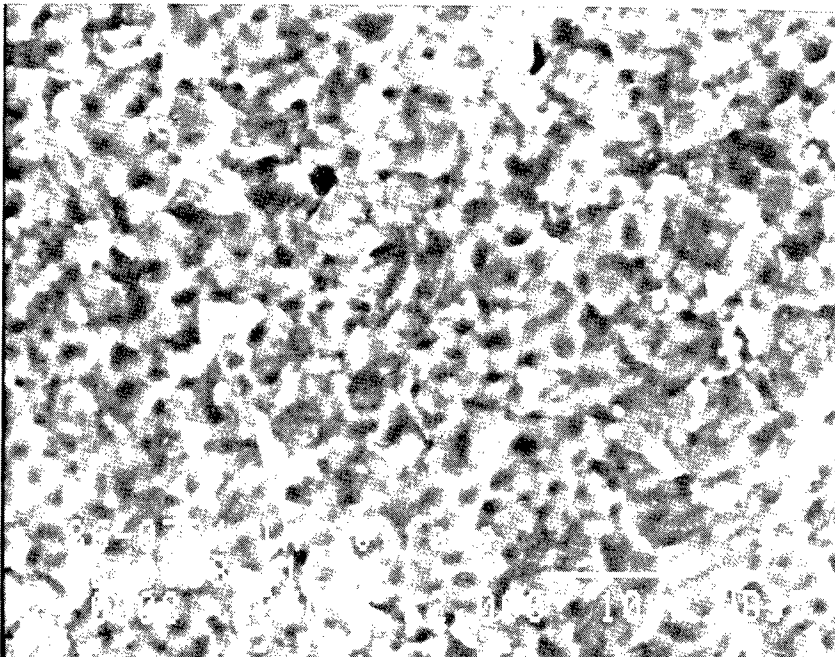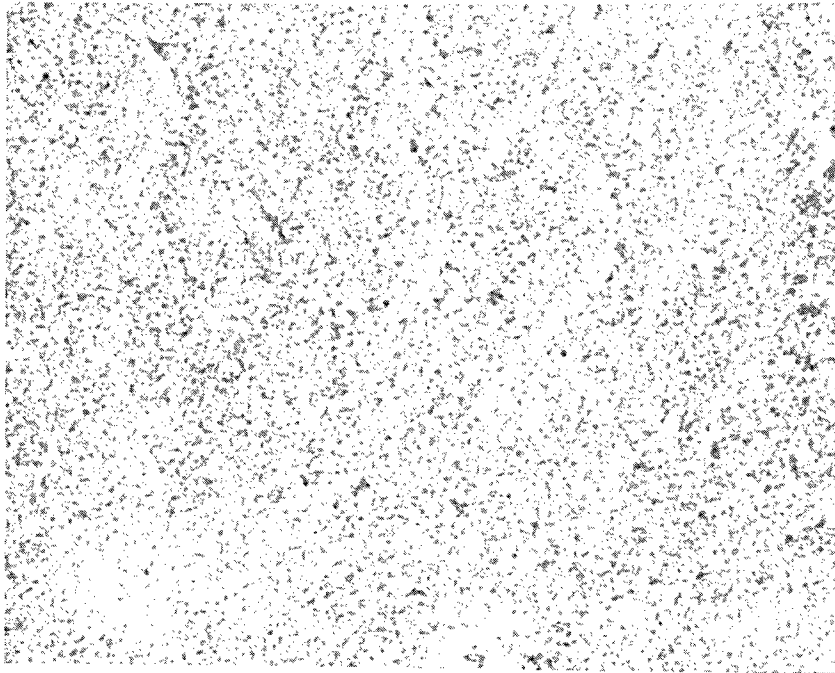
Figure 38.   Photomicrographs of Injection-Molded
Bar in the As-Sintered Condition
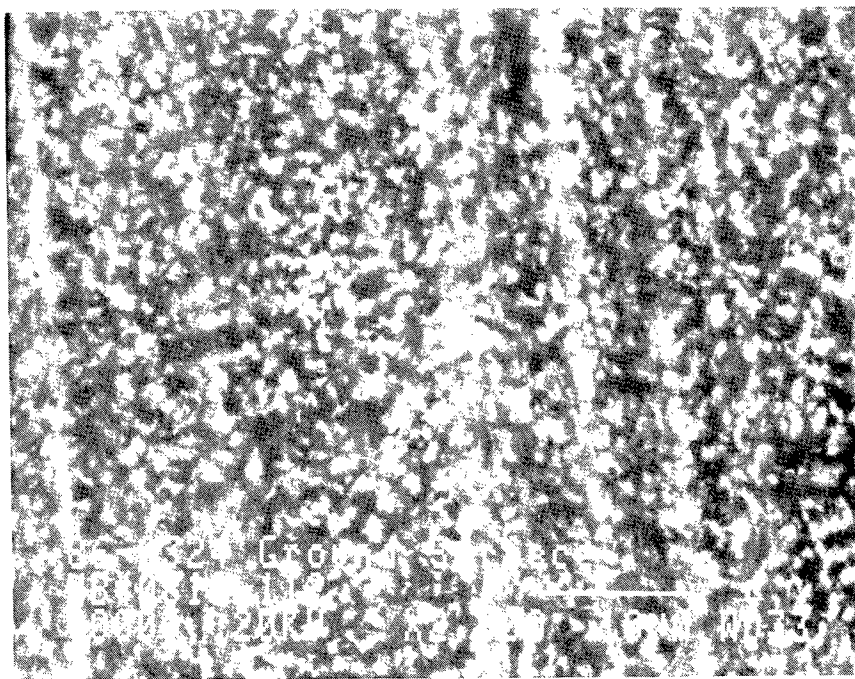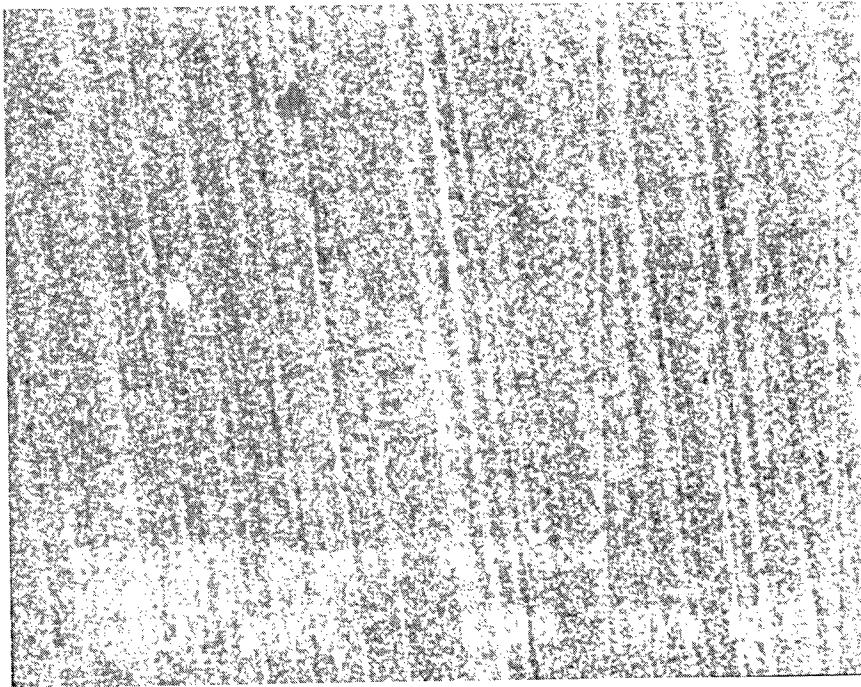
Figure 39. Photomicrographs of Injection-Molded
Bar After Grinding
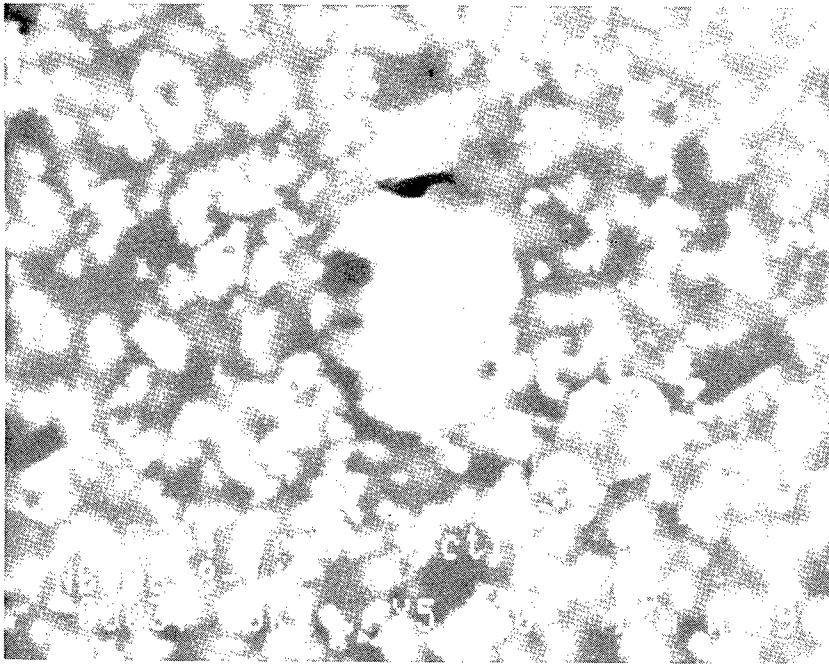
Figure 40. Metal Inclusion in Polished
Section of Injection-Molded Material
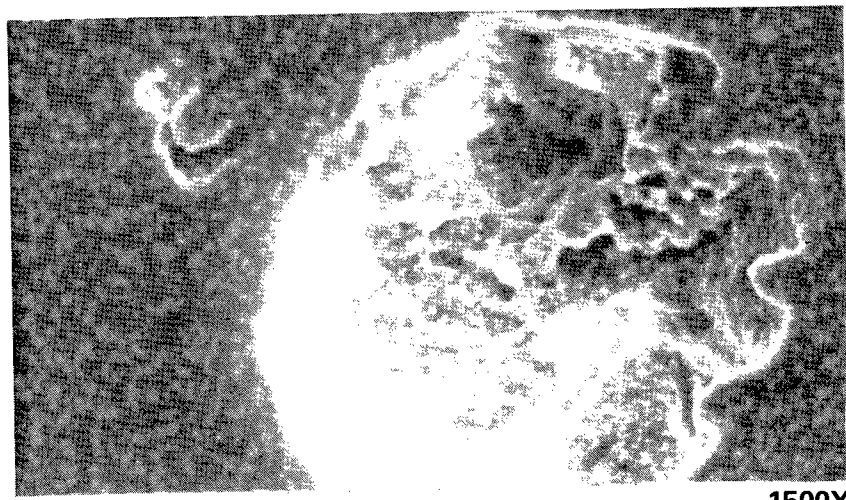
1500X

2000X
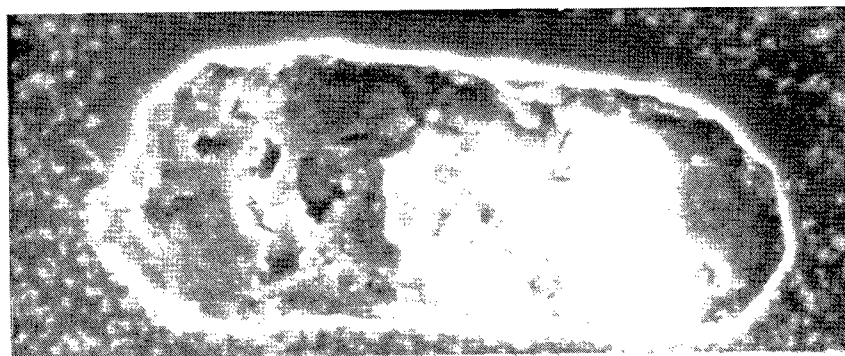
2000X

Figure 41. Low-Density Flaws in
Injection-Molded Material
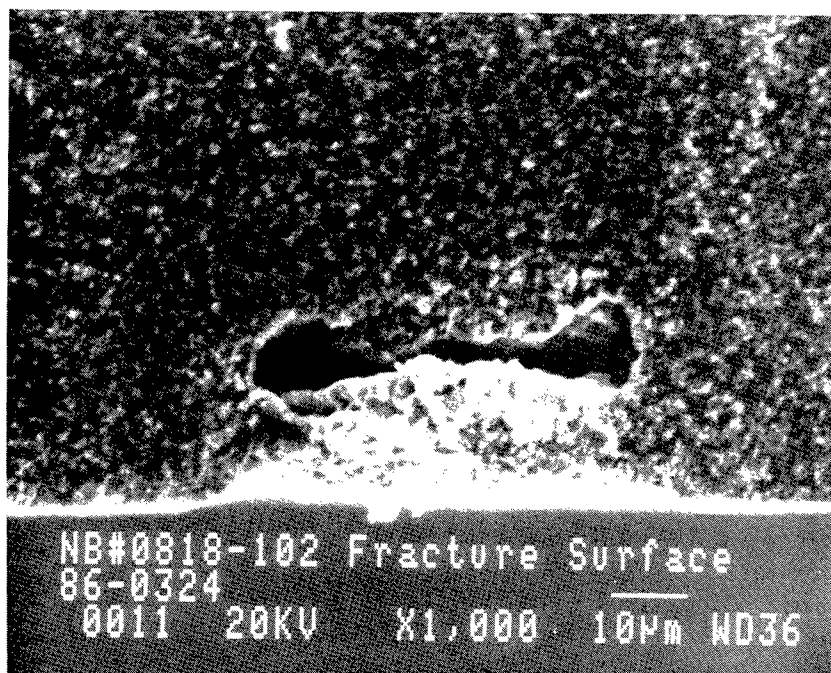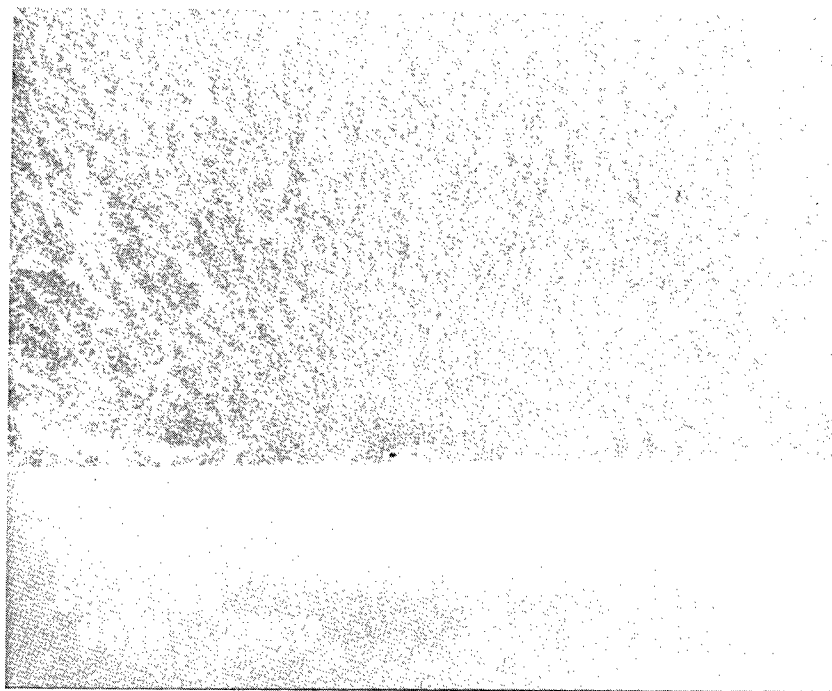
Figure 42.   Large Pore Fracture Origin in
Injection-Molded Sample

Low-power examination of samples after burnout of the plasticizer indicated
that some pores might be created during the burnout operation. It was postu-
lated that these, as well as other types of pores, could be eliminated by iso-
statically pressing the green flexure test bars after the burnout operation
and before the sintering operation. The strengths of sintered bars prepared
by this modification are listed in Table 20. No improvement was indicated as
a result of the isopressing operation.

CONCLUSIONS

Two composite systems composed of Si_3N_4 plus a dispersion of ZrO_2 particles were shown to exhibit improved properties over those of the Si_3N_4 matrix:

1. Colloidal processing produced composites with excellent dispersion and homogeneity.

2. Compositions of Si_3N_4 + 30 and 45 w/o ZrO_2 stabilized with Y_2O_3 exhibited:

   a. An increase in toughness to 6 MPa $m^{1/2}$ over the untoughened Si_3N_4 value of 4.1 MPa $m^{1/2}$.

   b. Room-temperature strengths as high as 1000 MPa.

   c. High strength to 1000 C with Al_2O_3 as the sintering aid, and no loss in strength to 1400 C with a mixture of Y_2O_3 + SiO_2 as the sintering aid.

   d. Significantly lower thermal diffusivity (lower than predicted by rule of mixtures).

   e. Capability of increasing strength another 40% by heat treatment for low to moderate temperature applications.

   f. Injection molding possibilities.

3. Compositions of Si_3N_4 + 15, 30, or 45 w/o ZrO_2 stabilized with CaO exhibited:

   a. Increases in apparent toughness to 7 MPa $m^{1/2}$ without post-heat treatment.

   b. Potential toughness increases to 14 MPa $m^{1/2}$ with heat treatment.

   c. Room-temperature strength as high as 780 MPa.

   d. Potential for low-temperature (<700 C) application.

4. Successful substitution of HfO_2 (Y_2O_3) for ZrO_2 (Y_2O_3) with associated strength gain.

RECOMMENDATIONS

1. Ensure Long-Term Stability. Composites of Si_3N_4 and ZrO_2 stabilized with Y_2O_3 and sintered at 1750 C and 1800 C must be completely characterized by TEM and SEM analyses. Differences in microcompositions must be determined to understand the microcracking mechanism that is present in material sintered at the lower temperature. This information is essential to ensure formulation and fabrication of composites that will demonstrate long-term stability at intermediate temperatures. The possibility of crack healing needs further evaluation.

2. Optimize Toughness. The Y_2O_3 stabilizer content in ZrO_2 and sintering conditions should be optimized to yield maximum toughness with long-term stability.

3. Develop Improved High-Temperature Toughness. Optimize HfO_2 additions for use in place of, or in combination with, ZrO_2.

4. Increase High-Temperature Strength. Submicron powders of Y_2O_3 and SiO_2 must be obtained so that these oxides can be added by colloidal processing rather than by ball-milling.

5. Demonstrate High-Volume, Low-Cost Fabrication. The colloidal processing method lends itself to slip casting. Slip casting of the colloidal suspensions should be developed.

6. Demonstrate Superior High-Temperature Properties. Measure creep, stress-rupture strength, and resistance to thermal shock.

7. Confirm existence of transformation toughening mechanism in samples containing dispersions of partially stabilized zirconia, e.g., having less than 9 w/o Y_2O_3 in the Y_2O_3 stabilized system.

REFERENCES

1. Rice, R. W., <u>An Assessment of the Use of Ceramics in Heat Engines</u>, NRL Memorandum Report 4499, 18 May 1981.

2. Lange, F. F., "Compressive Surface Stresses Developed in Ceramics by an Oxidation-Induced Phase Change," <u>J. Am. Cer. Soc.</u>, <u>63</u> (1-2) 38-40 (1980).

3. Gilles, J. C., "Zirconium Oxynitride Preparation by Solid-State Reaction and Structure," <u>Bull. Soc. Chim., France</u>, 2118-22, 1962.

4. Lange, F. F., L. K. L. Falk, and B. I. Davis, "Structural Ceramics Composites Based on $Si_3N_4-ZrO_2(+ Y_2O_3)$ Compositions," <u>J. Mater. Res.</u>, <u>2</u> (1) 66-76 (1987).

5. Anstis, G. R., et al., "A Critical Evaluation of Indentation Techniques for Measuring Fracture Toughness: I Direct Crack Measurements Strength Method," <u>J. Am. Cer. Soc.</u>, <u>64</u> (9) 533-39 (1981).

6. Cook, R. F., and B. R. Lawn, "A Modified Indentation Toughness Technique," <u>Comm. of the Am. Cer. Soc.</u>, 200-01, November 1983.

7. Miller, R. A., R. G. Garlick, and J. L. Smialek, "Phase Distribution in Plasma-Sprayed Zirconia-Yttria," <u>Am. Cer. Soc. Bull.</u>, <u>62</u> (12) 1355-58 (1983).

8. Lange, F. F., and S. C. Singhal, U.S. Patent 4,102.698, 20 July 1978.

9. Larsen, D. C., and J. W. Adams, "Property Screening and Evaluation of Ceramic Turbine Engine Materials," IIT Research Institute, ITR No. 8, Contract No. F33615-79-C-5100.

10. Clarke, D. R., F. F. Lange, and G. D. Schnittgrund, "Strengthening of a Sintered Silicon Nitride by a Post-Fabrication Heat Treatment," Comm. Am Cer. Soc., 51-52, April 1982.

11. Engineering Property Data on Selected Ceramics, Volume III, Single Oxides, Battelle, Columbus, Ohio, July 1981.

12. Carniglia, S. C., S. D. Brown, and T. F. Schroeder, "Phase Equilibria and Physical Properties of Oxygen-Deficient Zirconia & Thoria," J. Am. Cer. Soc., 54 (1) 13-17 (1971).

13. Hasselman, D. P. H., "Thermal Diffusivity and Conductivity of Dense Poly-crystalline ZrO_2 Ceramics: A Survey," Am. Cer. Soc. Bull., 66 (5) 799-806 (1987).

14. Miller, D. G., et al., Brittle Materials Design High-Temperature Gas Turbine, AMMRC CTR 76-32, Final Report, Vol. IV--Material Technology, p.122, 1976.

15. Carpenter, H. W., Ceramic Turbine Elements, Final Report, RI/RD84-164, Rocketdyne Division, Rockwell International, Contract No. NAS-8-35327, June 1984.

INTERNAL DISTRIBUTION

1-2.	Central Research Library	44.	R. R. Judkins
3.	Document Reference Section	45.	M. A. Karnitz
4-5.	Laboratory Records Department	46.	H. D. Kimrey, Jr.
6.	Laboratory Records, ORNL RC	47.	T. G. Kollie
7.	ORNL Patent Section	48.	T. B. Lindemer
8.	L. F. Allard, Jr.	49.	K. C. Liu
9.	B. R. Appleton	50.	E. L. Long, Jr.
10.	R. L. Beatty	51.	W. D. Manly
11.	P. F. Becher	52.	R. W. McClung
12.	T. M. Besmann	53.	D. L. McElroy
13.	P. J. Blau	54.	J. R. Merriman
14.	A. Bleier	55.	A. J. Moorhead
15.	E. E. Bloom	56.	T. A. Nolan
16.	K. W. Boling	57.	J. L. Rich
17.	R. A. Bradley	58.	C. R. Richmond
18.	C. R. Brinkman	59.	J. M. Robbins
19.	V. R. Bullington	60.	M. W. Rosenthal
20.	A. J. Caputo	61.	M. L. Santella
21.	R. S. Carlsmith	62-80.	A. C. Schaffhauser
22.	P. T. Carlson	81.	G. M. Slaughter
23.	J. V. Cathcart	82.	W. B. Snyder, Jr.
24.	G. M. Caton	83.	E. J. Soderstrom
25.	R. H. Cooper	84.	D. P. Stinton
26.	S. A. David	85.	R. W. Swindeman
27.	J. H. DeVan	86.	V. J. Tennery
28.	W. P. Eatherly	87-89.	P. T. Thornton
29.	J. I. Federer	90.	T. N. Tiegs
30.	W. Fulkerson	91.	J. R. Weir, Jr.
31.	R. L. Graves	92.	F. W. Wiffen
32.	D. L. Greene	93.	R. K. Williams
33.	M. A. Janney	94.	S. G. Winslow
34-43.	D. R. Johnson	95.	C. S. Yust

EXTERNAL DISTRIBUTION

96. Donald F. Adams
University of Wyoming
Laramie, WY 82071

97. Jane W. Adams
Corning Glass Works
Corning, NY 14831

98. Donald J. Adrian
High Velocity Corporation
701 Scarboro Road
Oak Ridge, TN 37830

99. Bruce J. Agle
Sundstrand Corporation
Turbomach Division
4400 Ruffin Road
PO Box 85757
San Diego, CA 92138-5757

100. Richard L. Allor
Ford Motor Company
20000 Rotunda Drive
PO Box 2053
Dearborn, MI 48121-2053

101. Richard T. Alpaugh
     U.S. Department of Energy
     Forrestal Building CE-151
     1000 Independence Avenue
     Washington, DC 20585

102. H. Arbabi·
     Brunel University
     Uxbridge Middlesex
     UNITED KINGDOM UB8 3PH

103. V. S. Avva
     North Carolina Agricultural and
     Technical State University
     Greensboro, NC 27411

104. John M. Bailey
     Caterpillar Inc.
     Technical Center
     Post Office Box 1875
     Peoria, IL 61656-1875

105. Murray Bailey
     NASA Lewis Research Center
     21000 Brookpark Road
     MS: 77-6
     Cleveland, OH 44135

106. R. R. Baker
     Ceradyne, Inc.
     3169 Red Hill Avenue
     Costa Mesa, CA 92626

107. J. Gary Baldoni
     GTE Laboratories, Inc.
     40 Sylvan Road
     Waltham, MA 02254

108. A. L. Bement, Jr.
     TRW, Inc.
     23555 Euclid Avenue
     Cleveland, OH 44117

109. M. Bentele
     Xamag, Inc.
     259 Melville Avenue
     Fairfield, CT 06430

110. Clifton G. Bergeron
     University of Illinois
     105 South Goodwin Avenue
     204 Ceramics Building
     Urbana, IL 61801

111. William D. Bjorndahl
     TRW, Inc.
     One Space Park
     Building 01, Room 2060
     Redondo Beach, CA 90278

112. James A. Black
     American Matrix, Inc.
     118 Sherlake Drive
     Knoxville, TN 37922

113. Dan Blake
     Solar Energy Research
       Institute
     1617 Cole Boulevard
     Golden, CO 80401

114. Keith Blandford
     Boride Products, Inc.
     2879 Aero Park Drive
     Traverse City, MI 49684

115. John Blum
     Norton Company
     High Performance Ceramics
     Goddard Road
     Northboro, MA 01532-1545

116. Paul N. Blumberg
     Integral Technologies Inc.
     415 East Plaza Drive
     Westmont, IL 60559

117. Wolfgang D. G. Boecker
     Standard Oil Engineered
       Materials Company
     Post Office Box 832
     Niagara Falls, NY 14302

118. Han Juergen Bossmeyer
BMW Technologies, Inc.
800 South Street
Waltham, MA 02154

119. J.A.M. Boulet
University of Tennessee
310 Perkins Hall
Knoxville, TN 37996

120. Raymond J. Bratton
Westinghouse Electric
Corporation
1310 Beulah Road
Pittsburgh, PA 15235

121. Catherine E. Brown
E. 1. DuPont de Nemours &
Company
Wilmington, DE 19898

122. J. J. Brown
Virginia Polytechnic Institute
and State University
Blacksburg, VA 24061

123. W. Bryzik
U.S. Army Tank Automotive
Command
Warren, MI 48090

124. S. T. Buljan
GTE Laboratories, Inc.
40 Sylvan Road
Waltham, MA 02254

125. John M. Byrne, Jr.
PPG Industries, Inc.
One PPG Place
Pittsburgh, PA 15272

126. Donald J. Campbell
Air Force Wright
Aeronautical Laboratory
AFWAL/POX
Wright-Patterson AFB
OH 45433

127. Roger Cannon
Rutgers University
Post Office Box 909
Bowser Road
Piscataway, NJ 08855-0909

128-132. Harry W. Carpenter
19945 Acre Street
Northridge, CA 91324

133. David Carruthers
Allied-Signal Aerospace
Company
Garrett Engine Division
111 South 34th Street
Post Office Box 5217
Phoenix, AZ 85010

134. Jere G. Castor
Allied-Signal Aerospace
Company
Garrett Engine Company
111 South 34th Street
Post Office Box 5217
Phoenix, AZ 85010

135. Se-Tak Chang
Sundstrand Corporation
Turbomach Division
4400 Ruffin Road
San Diego, CA 92138-5757

136. R. J. Charles
General Electric Company
Post Office Box 8
Schenectady, NY 12301

137. En-sheng Chen
B&C Engineering Research
13906 Dentwood Drive
Houston, TX 77014

138. Albert A. Che nes
U.S. Department of Energy
Forrestal Building CE-151
1000 Independence Avenue
Washington, DC 20585

139. Frank Childs
EG&G, Inc.
Post Office Box 1625
Idaho Falls, ID 83415

140. Gilbert Y. Chin
Bell Telephone Laboratories
Murray Hill, NJ 07974

141. Melvin H. Chiogioji
U.S. Department of Energy
Forrestal Building CE-15
1000 Independence Avenue, SW
Washington, DC 20585

142. William J. Chmura
The Torrington Company
59 Field Street
Torrington, CT 06790

143. Eugene V. Clark
Turbine Metal Technology, Inc.
7327 Elmo Street
Tujunga, CA 91042-2204

144. William L. Cleary
ORI, Inc.
1375 Piccard Drive
Rockville, MD 20850

145. Jack L. Clem
J. M. Huber Corporation
PO Box 2831
Borger, TX 79008-2831

146. Philip R. Compton
National Aeronautics and
Space Administration
Washington, DC 20546

147. Harry E. Cook
Chrysler Motors Corporation
1200 Chrysler Drive
Highland Park, MI 48288-1118

148. Stephen Copley
University of
Southern California
Los Angeles, CA 90089-0241

149. John A. Coppola
Standard Oil Engineered
Materials Company
Structural Ceramics Division
PO Box 1054, Bldg 91-2
Niagara Falls, NY 14302

150. Normand D. Corbin
Norton Company
High Performance Ceramics
Goddard Road
Northboro, MA 01532-1545

151. Charles H. Craig
Defense Technology Security
Administration
400 Army-Navy Drive
Suite 300
Arlington, VA 22202

152. William J. Croft
U.S. Army Materials
Technology Laboratory
Arsenal Street
Watertown, MA 02172

153. Gary M. Crosbie
Ford Motor Company
20000 Rotunda Drive
PO Box 2053, Room S-2079
Dearborn, MI 48121-2053

154. Floyd W. Crouse, Jr.
U.S. Department of Energy
PO Box 880
Morgantown, WV 26505

155. Raymond Cutler
Ceramatec, Inc.
163 West 1700 South
Salt Lake City, UT 84115

156. David A. Dalman
The Dow Chemical Company
Midland, MI 48640

157. James I. Dalton
Reynolds Metals Company
Fourth and Canal Streets
PO Box 27003
Richmond, VA 23261

158. Stephen C. Danforth
Rutgers University
Post Office Box 909
Bowser Road
Piscataway, NJ 08854

159. Stanley J. Dapkunas
National Bureau of Standards
Gaithersburg, MD 20899

160. Robert F. Davis
North Carolina State University
232 Riddick Laboratory
Box 7907
Raleigh, NC 27695

161. Evelyn M. DeLiso
Rutgers University
PO Box 909
Bowser Road
Piscataway, NJ 08854

162. Alan L. Dragoo
National Bureau of Standards
Gaithersburg, MD 20899

163. Keith F. Dufrane
Battelle Columbus Laboratories
505 King Avenue
Columbus, OH 43201

164. Edmund M. Dunn
GTE Laboratories Inc.
40 Sylvan Road
Waltham, MA 02254

165. Jeremy D. Dunning
Indiana Memorial Union 662
Indiana University
Bloomington, IN 47405

166. Dr. Sunil Dutta
NASA Lewis Research Center
21000 Brookpark Road
MS: 49-3
Cleveland, OH 44135

167. Paul N. Dyer
Air Products and Chemicals, Inc.
PO Box 538
Allentown, PA 18105

168. Robert J. Eagan
Sandia National Laboratories
Department 1840
PO Box 5800
Albuquerque, NM 87185

169. Christopher A. Ebel
Norton Company
High Performance Ceramics
Goddard Road
Northboro, MA 01532-1545

170. J. J. Eberhardt
U.S. Department of Energy
Forrestal Building CE-12
1000 Independence Avenue, SW
Washington, DC 20585

171. E. E. Ecklund
U.S. Department of Energy
Forrestal Building CE-151
1000 Independence Avenue
Washington, DC 20585

172. William A. Ellingson
Argonne National Laboratory
9700 South Cass Avenue
Argonne, IL 60439

173. Graydon A. Elliott
U.S. Army Research and
Technology Laboratory
(AVSCOM)
Fort Eustis, VA 23604

174. A. Erdely
26 Av. Gore des Eaux-Vives
1208 Geneva
SWITZERLAND

175. Charles D. Estes
U.S. Senate
Washington, DC 20510

176. Peggy Evanich
National Aeronautics and
Space Administration
Washington, DC 20546

177. Anthony G. Evans
University of California
Santa Barbara, CA 93106

178. Robert C. Evans
NASA Lewis Research Center
21000 Brookpark Road
MS: 77-6
Cleveland, OH 44135

179. Katherine T. Faber
Ohio State University
2041 College Road
Columbus, OH 43210

180. John W. Fairbanks
U.S. Department of Energy
Forrestal Building CE-151
1000 Independence Avenue
Washington, DC 20585

181. Larry Farrell
Babcock and Wilcox
Old Forrest Road
Lynchburg, VA 24505

182. H. W. Foglesong
Dow Corning Corporation
3901 South Saginaw Road
Midland, MI 48686

183. Thomas F. Foltz
Avco Corporation
Two Industrial Avenue
Lowell, MA 01851

184. Robert G. Frank
Technology Assessment Group
10793 Bentley Pass Lane
Cincinnati, OH 45140

185. Douglas W. Freitag
LTV Aerospace and Defense
Company
PO Box 225907
MS: TH-85
Dallas, TX 75265

186. George E. Gazza
U.S. Army Materials
Technology Laboratory
405 Arsenal Street
Watertown, MA 02172

187. Charles M. Gilmore
The George Washington
University
Washington, DC 20052

188. Paul Glance
Concept Analysis
950 Stephenson Highway
Troy, MI 48007-7013

189. Fred M. Glaser
U.S. Department of Energy
Washington, DC 20545

190. Joseph W. Glatz
Naval Air Propulsion
Test Center
Box 7176, PE 34
Trenton, NJ 08628

191. W. M. Goldberger
Superior Graphite Company
2175 East Broad Street
Columbus, OH 43209

192. Stephen T. Gonczy
Allied Signal Research Center
50 UOP Plaza
Des Plaines, IL 60016-6187

193. Robert J. Gottschall
U.S. Department of Energy
MS: G-256
Washington, DC 20545

194. Dr. Earl Graham
Cleveland State University
Uclid Ave East 24th Street
Cleveland, OH 44115

195. Kenneth Green
Coors Ceramics Company
17750 West 32nd Street
Golden, CO 80401

196. Robert E. Green, Jr.
Center for Nondestructive
Evaluation
Maryland Hall 107
The Johns Hopkins University
Baltimore, MD 21218

197. Lance E. Groseclose
General Motors Corporation
PO Box 420
Indianapolis, IN 46206-0420

198. T. D. Gulden
GA Technologies, Inc.
PO Box 81608
San Diego, CA 92138

199. P. Ulf Gummeson
Hoeganaes
River Road and Taylors Lane
Riverton, NJ 08077

200. Bimleshwar P. Gupta
Solar Heat Research Division
Solar Energy Research Institute
1617 Cole Boulevard
Golden, CO 80401

201. M. D. Gurney
NIPER
PO Box 2128
Bartlesville, OK 74005

202. John P. Gyekenyesi
NASA Lewis Research Center
21000 Brookpark Road
Cleveland, OH 44135

203. J. J. Habeeb
Esso Petroleum Canada
PO Box 3022
Sarina, Ontario
CANADA N7T 7MI

204. H. T. Hahn
Pennsylvania State University
227 Hammond Building
University Park, PA 16802

205. Nabil S. Hakim
General Motors Corporation
36880 Ecorse Road
Romulus, MI 48174

206. John W. Halloran
Ceramic Process Systems
840 Memorial Drive
Cambridge, MA 02139-3758

207. Kay Hardman-Rhyne
DARPA
1400 Wilson Boulevard
Arlington, VA 22209

208. R. A. Harmon
25 Schalren Drive
Latham, NY 12110

209. Stephen D. Hartline
Norton Company
High Performance Ceramics
Goddard Road
Northboro, MA 01532-1545

210. Willard E. Hauth
Dow Corning Corporation
3901 South Siginaw Road
Midland, MI 48640

211. Kevin L. Haynes
McDonnell Douglas
Astronautics Company
Box 516 E456/HQ/3N/MS329
Saint Louis, MO 63166

212. Norman L. Hecht
University of Dayton
Research Institute
300 College Park
Dayton, OH 45469-0001

213. S. S. Hecker
Los Alamos National
Laboratory
PO Box 1663
Los Alamos, NM 87545

214. Peter W. Heitman
General Motors Corporation
PO Box 420, W-5
Indianapolis, IN 46206-0420

215. Richard L. Helferich
The Duriron Company,
Incorporated
PO Box 1145
Dayton, OH 45401

216. H. E. Helms
General Motors Corporation
PO Box 420
Indianapolis, IN 46206-0420

217. Thomas L. Henson
GTE Products Corporation
Hawes Street
Towanda, PA 18848-0504

218. Thomas P. Herbell
NASA Lewis Research Center
21000 Brookpark Road
MS: 49-3
Cleveland, OH 44135

219. Hendrik Heystek
Bureau of Mines
Tuscaloosa Research Center
PO Box L
University, AL 35486

220. Robert V. Hillery
General Electric Company
One Neumann Way
PO Box 156301
Cincinnati, OH 45215

221. Jonathan W. Hinton
Standard Oil Engineered
Materials Company
Structural Ceramics Division
PO Box 1054
Niagara Falls, NY 14302

222. George Hsu
Jet Propulsion Laboratory
4800 Oak Grove Drive
MS: 512-103
Pasadena, CA 91109

223. Stephen M. Hsu
National Bureau of Standards
Gaithersburg, MD 20899

224. Harold A. Huckins
Princeton Advanced
Technology, Inc.
56 Finley Road
Princeton, NJ 08540

225. Fred Huettic
Advanced Ceramic
Technology, Inc.
17 Deerfield Road
East Brunswick, NJ 08816

226. O. Richard Hughes
Celanese Research Company
86 Morris Avenue
Summit, NJ 07901

227. Joseph E. Hunter, Jr.
General Motors Corporation
12 Mile and Mound Roads
Warren, MI 48090-9055

228. Louis C. Ianniello
U.S. Department of Energy
Washington, DC 20545

229. Robert H. Insley
Champion Spark Plug Company
20000 Conner Avenue
Detroit, MI 48234

230. D. M. Jacques
Norton Company
HPC Library
Goddard Road
Northboro, MA 01532-1545

231. Curt A. Johnson
General Electric Company
PO Box 8
Schenectady, NY 12301

232. Douglas C. Johnson
Sundstrand Corporation
4400 Ruffin Road
PO Box 85757
San Diego, CA 92138-5757

233. Larry Johnson
Argonne National Laboratory
9700 South Cass Avenue
Bldg 362
Argonne, IL 60439

234. R. A. Johnson
General Motors Corporation
PO Box 420
Indianapolis, IN 46206-0420

235. L. A. Joo
Great Lakes Research
Corporation
Post Office Box 1031
Elizabethton, TN 37643

236. A. David Joseph
Sealed Power Corporation
100 Terrace Plaza
Muskegon, MI 49443

237. Roy Kamo
Adiabatics, Inc.
630 South Mapleton
Columbus, IN 47201

238. Allan Katz
Air Force Wright
Aeronautical Laboratory
Materials Laboratory,
AFWAL/MLLM
Wright-Patterson AFB, OH 45433

239. R. N. Katz
U.S. Army Materials
Technology Laboratory
405 Arsenal Street
Watertown, MA 02172

240. Mr. Kawaguchi
Tokai Carbon
375 Park Avenue
Suite 3802
New York, NY 10152

241. P. Victor Kelsey
Aluminum Company of America
Alcoa Technical Center B
Alcoa Center, PA 15061

242. Frederick L. Kennard, III
General Motors Corporation
1300 North Dort Highway
Flint, MI 48556

243. J. R. Kidwell
Allied-Signal Aerospace
Company
Garrett Engine Division
111 South 34th Street
Post Office Box 5217
Phoenix, AZ 85010

244. Max Klein
Gas Research Institute
8600 West Bryn Mawr Avenue
Chicago, IL 60631

245. C. E. Knapp
Norton Company
8001 Daly Street
Niagara Falls, Ontario
CANADA

246. A. S. Kobayashi
University of Washington
Seattle, WA 98195

247. David M. Kotchick
AiResearch Manufacturing
Company
2525 West 190th Street
Torrance, CA 90509

248. Bruce Kramer
George Washington University
Washington, DC 20052

249. Saunders B. Kramer
U.S. Department of Energy
Forrestal Building CE-151
1000 Independence Avenue
Washington, DC 20585

250. D. M. Kreiner
Allied-Signal Aerospace
Company
Garrett Engine Division
111 South 34th Street
PO Box 5217
Phoenix, AZ 85010

251. Pieter Krijgsman
Ceramic Design Int.
Hold., Ltd.
PO Box 68
8050 AB Hattem
THE NETHERLANDS

252. W. J. Lackey
Georgia Tech Research
Institute
Atlanta, GA 30332

253. Everett A. Lake
Air Force Wright
Aeronautical Laboratory
AFWAL/POOS
Wright-Patterson AFB
OH 45433

254. Hari S. Lamba
General Motors Corporation
Electro-Motive Division
LaGrange, IL 60525

255. James Lankford
Southwest Research Institute
6220 Culebra Road
PO Drawer 28510
San Antonio, TX 78284

256. John G. Lanning
Corning Glass Works
Corning, NY 14831

257. David C. Larsen
Corning Glass Works
Sullivan Park, FR-51
Corning, NY 14831

258. Dr. S. K. Lau
Standard Oil Engineered
Materials Company
Technology Division
Box 832
Niagara Falls, NY 14302

259. Harry A. Lawler
Standard Oil Engineered
Materials Company
Structural Ceramics Division
PO Box 1054, Bldg 91-2
Niagara Falls, NY 14302

260. Alan Lawley
Drexel University
Philadelphia, PA 19104

261. Daniel Lee Temescon
2850 7th Street
Berkeley, CA 94710

262. June-Gunn Lee
Korea Advanced Institute of
Science and Technology
PO Box 131
Dong Dac Mun, Seoul
KOREA

263. E. M. Lenoe
Air Force Office of Scientific
Research
APO San Francisco
CA 96503-0110

264. Stanley R. Levine
NASA Lewis Research Center
21000 Brookpark Road
Cleveland, OH 44135

265. David Lewis
Naval Research Laboratory
4555 Overlook Avenue, SW
Washington, DC 20375

266. Winston W. Liang
AMERCOM, Inc.
8948 Fullbright Avenue
Chatsworth, CA 91311

267. Bill Long
Babcock and Wilcox
PO Box 1260
Lynchburg, VA 24505

268. L. A. Lott
EG&G, Inc.
PO Box 1625
Idaho Falls, ID 83415

269. Bryan K. Luftglass
Chem Systems, Inc.
303 South Broadway
Tarrytown, NY 10591

270. Robert Lundberg
Svenska Silikatforsknings-
institutet
Swedish Institute for
Silicate Research
Box 5403
S-402 29 Gothenburg
SWEDEN

271. Michael J. Lynch
General Electric Company
PO Box 414, 7B-36
Milwaukee, WI 53201

272. James W. MacBeth
Standard Oil Engineered
    Materials Company
Structural Ceramics Division
Box 1054
Niagara Falls, NY 14302

273. Vincent L. Magnotta
Air Products and Chemicals, Inc.
PO Box 538
Allentown, PA 18105

274. Tai-il Mah
Universal Energy Systems
4401 Dayton-Xenia Road
Dayton, OH 45432

275. L. Manes
Commission of the European
    Communities
Ispra Establishment
1-21020 Ispra (Varese)
ITALY

276. Gerald R. Martin
Fleetguard, Inc.
Cookeville, TN 38501

277. Dr. John L. Mason
Allied-Signal Aerospace Company
AiResearch Los Angeles Division
2525 West 190th Street
Torrance, CA 90509

278. J. McCauley
U.S. Army Materials Technology
    Laboratory
DRXMR-MC
Arsenal Street
Watertown, MA 02172-0001

279. William J. McDonough
Keramont
4233 South Fremont Avenue
Tucson, AZ 85714

280. Bryan J. McEntire
Norton Company
TRW Ceramics
Goddard Road
Northboro, MA 01532-1545

281. Thomas D. McGee
Iowa State University
Ames, IA 50011

282. H. Christopher McGowan
Advanced Ceramic
    Technology, Inc.
17 Deerfield Road
East Brunswick, NJ 08816

283. Malcolm G. McLaren
Rutgers University
PO Box 909
Bowser Road
Piscataway, NJ 08854

284. Arthur F. McLean
6225 N Camino Almonte
Tucson, AZ 85718

285. Brian L. Mehosky
Standard Oil Engineered
    Materials Company
4440 Warrensville Center Road
Cleveland, OH 44128

286. P. K. Mehrotra
Kennametal, Inc.
PO Box 639
Greensburg, PA 15601

287. Joseph J. Meindl
Reynolds International, Inc.
PO Box 27002
6603 West Broad Street
Richmond, VA 23261

288. D. Messier
U.S. Army Materials
    Technology Laboratory
DRXMR-MC
Arsenal Street
Watertown, MA 02172

289. Arthur G. Metcalfe
Solar Turbines, Inc.
2200 Pacific Highway
PO Box 80966
San Diego, CA 92138

290. Thomas N. Meyer
Aluminum Company of America
Alcoa Technical Center
Alcoa Center, PA 15069

291. W. Miloscia
Standard Oil Engineered
Materials Company
4440 Warrensville Center Road
Cleveland, OH 44128

292. Bill Moehle
Ethyl Corporation
451 Florida Avenue
Ethyl Tower
Baton Rouge, LA 70801

293. Helen Moeller
Babcock and Wilcox
PO Box 11165
Lynchburg, VA 24506-1165

294. Frederick E. Moreno
Turbo Energy Systems, Inc.
350 Second Street, Suite 5
Los Altos, CA 94022

295. Peter E. D. Morgan
Rockwell International
1049 Camino Dos Rios
PO Box 1085
Thousand Oaks, CA 91360

296. Lawrence M. Murphy
Thermal Systems Research
Branch
Solar Energy Research
Institute
1617 Cole Boulevard
Golden, CO 80401

297. Solomon Musikant
General Electric Company
PO Box 8555
MS: U-1219
Philadelphia, PA 19101

298. Pero Nannelli
Pennwalt Corporation
900 First Avenue
PO Box C
King of Prussia, PA 19406-0018

299. Robert M. Neilson, Jr.
EG&G Idaho, Inc.
PO Box 1625
Idaho Falls, ID 83415

300. William D. Nix
Stanford University
Stanford, CA 94305

301. Richard D. Nixdorf
American Matrix, Inc.
118 Sherlake Drive
Knoxville, TN 37922

302. Brian M. O'Connor
The Lubrizol Corporation
29400 Lakeland Boulevard
Wickliffe, OH 44092

303. W. Richard Ott
Alfred University
Alfred, NY 14802

304. Muktesh Paliwal
GTE Products Corporation
Hawes Street
Towanda, PA 18848-0504

305. Hayne Palmour III
North Carolina State
University
2158 Burlington Engineering
Laboratories
PO Box 5995
Raleigh, NC 27607

306. Joseph N. Panzarino
Norton Company
Goddard Road
Northboro, MA 01532-1545

307. Pellegrino Papa
Corning Glass Works
Corning, NY 14831

308. James G. Paschal
     Reynolds Metals Company
     PO Box 76154
     Atlanta, GA 30358

309. Arvid E. Pasto
     GTE Laboratories, Inc.
     40 Sylvan Road
     Waltham, MA 02254

310. Donald O. Patten
     Norton Company
     High Performance Ceramics
     Goddard Road
     Northboro, MA 01532-1545

311. James W. Patten
     Cummins Engine Company, Inc.
     Box 3005, Mail Code 50183
     Columbus, IN 47202-3005

312. Timothy M. Pattison
     Textron Lycoming
     MS: LSM1
     550 Main Street
     Stratford, CT 06497

313. Robert A. Penty
     Eastman Kodak Company
     901 Elmgrove Road
     Rochester, NY 14650

314. Gary R. Peterson
     U.S. Department of Energy
     785 DOE Place
     Idaho Falls, ID 83402

315. R. Byron Pipes
     University of Delaware
     2001 Spencer Laboratory
     Newark, DE 19716

316. Robert C. Pohanka
     Office of Naval Research
     800 North Quincy St, Code 431
     Arlington, VA 22217

317. Stephen C. Pred
     ICD Group, Inc.
     1100 Valley Brook Avenue
     Lyndhurst, NJ 07071

318. Karl M. Prewo
     United Technologies
       Corporation
     Silver Lane, MS: 24
     East Hartford, CT 06108

319. Hubert B. Probst
     NASA Lewis Research Center
     21000 Brookpark Road
     Cleveland, OH 44135

320. Carr Lane Quackenbush
     Norton Company
     High Performance Ceramics
     Goddard Road
     Northboro, MA 01532-1545

321. Brian Quigy
     National Aeronautics and
       Space Administration
     Washington, DC 20546

322. George Quinn
     U.S. Army Materials
       Technology Laboratory
     Arsenal Street
     Watertown, MA 02172

323. Dennis T. Quinto
     Kennametal, Inc.
     PO Box 639
     Greensburg, PA 15601

324. S. Venkat Raman
     Air Products and
       Chemicals, Inc.
     PO Box 538
     Allentown, PA 18105

325. Dennis Readey
     Ohio State University
     2041 College Road

326. Robert R. Reeber
     U.S. Army Research Office
     PO Box 12211
     Research Triangle Park
        NC 27709

327. K. L. Reifsnider
     Virginia Polytechnic Institute
        and State University
     Blacksburg, VA 24061

328. Paul Rempes
     Williams International
     2280 West Maple
     MS: 6-5
     Walled Lake, MI 48088

329. T. M. Resetar
     U.S. Army Materials
        Technology Laboratory
     DAXMA-MC
     Arsenal Street
     Watertown, MA 02172

330. K. T. Rhee
     Rutgers University
     PO Box 909
     Bowser Road
     Piscataway, NJ 08854

331. Roy W. Rice
     W. R. Grace and Company
     7379 Route 32
     Columbus, MD 21044

332. David W. Richerson
     Ceramatec, Inc.
     163 West 1700 South
     Salt Lake City, UT 84115

333. Paul Rieth
     Ferro Corporation
     661 Willet Road
     Buffalo, NY 14218-9990

334. Michael A. Rigdon
     Institute for Defense Analyses
     1801 Beauregard Street
     Alexandria, VA 22311

335. John E. Ritter, Jr.
     University of Massachusetts
     Amherst, MA 01003

336. Giulio A. Rossi
     Norton Company
     High Performance Ceramics
     Goddard Road
     Northboro, MA 01532-1545

337. Barry R. Rossing
     Lanxide Corporation
     Tralee Industrial Park
     Newark, DE 19711

338. David J. Rowcliffe
     SRI International
     333 Ravenswood Avenue
     Menlo Park, CA 94025

339. Donald W. Roy
     Coors Ceramics Company
     17750 West 32nd Street
     Golden, CO 80401

340. Bruce Rubinger
     Gobal
     50 Milk Street, 15th Floor
     Boston, MA 02109

341. Robert Ruh
        Air Force Wright
        Aeronautical Laboratory
     Materials Laboratory
        AFWAL/M LLM
     Wright-Patterson AFB,
        OH 45433

342. Robert J. Russell, Sr.
     Norton Company
     High Performance Ceramics
     Goddard Road
     Northboro, MA 01532-1545

343. George P. Safol
     Westinghouse Electric
        Corporation
     Pittsburgh, PA 15235

344. J. Sankar
     North Carolina Agricultural
        and Technical State
        University
     Greensboro, NC 27411

345. Maxine L. Savitz
     Garrett Processing Company
     Ceramic Components Division
     19800 South Van Ness Avenue
     Torrance, CA 90509

346. Richard Schapery
     Texas A&M University
     College Station, TX 77843

347. J. L. Schienle
     Allied-Signal Aerospace
        Company
     Garrett Auxiliary Power
        Division
     2739 East Washington Street
     PO Box 5227
     Phoenix, AZ 85010

348. Liselotte J. Schioler
     Aerojet Tech Systems Company
     PO Box 13222
     Dept. 9990, Bldg. 2019-A2
     Sacramento, CA 95813

349. Richard A. Schmidt
     Battelle Columbus
        Laboratories
     505 King Avenue
     Columbus, OH, 43201-2693

350. Arnie Schneck
     Deere and Company
        Technical Center
     PO Box 128
     Wood-Ridge, NJ 07075

351. Matthew Schreiner
     Gas Research Institute
     8600 West Bryn Mawr Avenue
     Chicago, IL 60631

352. John Schuldies
     Industrial Ceramic
        Technology, Inc.
     37 Enterprise Drive
     Ann Arbor, MI 48103

353-363. R. B. Schulz
     U.S. Department of Energy
     Forrestal Building CE-151
     1000 Independence Avenue
     Washington, DC 20585

364. Murray A. Schwartz
     Bureau of Mines
     2401 Eye Street, N.W.
     Washington, DC 20241

365. Douglas B. Schwarz
     The Dow Chemical Company
     52 Building
     Midland, MI 48674

366. Thomas M. Sebestyen
     U.S. Army Tank
        Automotive Command
     AMSTA-RGRT
     Warren, MI 48397-5000

367. Brian Seegmiller
     Coors Ceramics Company
     17750 West 32nd Street
     Golden, CO 80401

368. S. G. Seshadri
     Standard Oil Engineered
        Materials Company
     PO Box 832
     Niagara Falls, NY 14302

369. Peter T. B. Shaffer
     Advanced Refractory
        Technologies, Inc.
     699 Hertel Avenue
     Buffalo, NY 14207

370. Maurice E. Shank
     United Technologies
        Corporation
     East Hartford, CT 06108

371. Laurel M. Sheppard
     Advanced Materials and
        Processes
     Route 87
     Metals Park, OH 44073

372-376. Dinesh K. Shetty
     The University of Utah
     Salt Lake City, UT 84112

377. Wesley J.C. Shuster
Thermo Electron Corporation
115 Eames Street
PO Box 340
Wilmington, MA 01887

378. Jack D. Sibold
Coors Ceramics Company
17750 West 32nd Street
Golden, CO 80401

379. Neal Sigmon
U.S. House of Representatives
Rayburn Building, Room B308
Washington, DC 20515

380. Richard Silberglitt
Quest Research Corporation
1651 Old Meadow Road
McLean, VA 22102

381. Maurice J. Sinnott
University of Michigan
438 West Engineering Building
Ann Arbor, MI 48109-2136

382. S. R. Skaggs
Los Alamos National Laboratory
PO Box 1663
Los Alamos, NM 87545

383. J. Thomas Smith
GTE Laboratories, Inc.
40 Sylvan Road
Waltham, MA 02254

384. Jay R. Smyth
Allied-Signal Aerospace
Company
Garrett Auxiliary Power
Division
2739 East Washington Street
PO Box 5227
MS: 93-172/1302-2K
Phoenix, AZ 85010

385. Rafal Sobotowski
Standard Oil Engineered
Materials Company
3092 Broadway Avenue
Cleveland, OH 44115

386. Thomas M. Sopko
Lubrizol Enterprises, Inc.
29400 Lakeland Boulevard
Wickliffe, OH 44092

387. Boyd W. Sorenson
Du Pont Company
Experimental Stat, Bldg 304
Wilmington, DE 19898

388. Dr. Richard M. Spriggs
Center for Advanced
Ceramic Technology
New York State College
of Ceramics at
Alfred University
Alfred, NY 14802

389. M. Srinivasan
Standard Oil Engineered
Materials Company
PO Box 832
Niagara Falls, NY 14302

390. Gordon L. Starr
Cummins Engine Company, Inc.
Box 3005, Mail Code 50183
Columbus, IN 47202-3005

391. Harold L. Stocker
General Motors Corporation
PO Box 420, T-23
Indinapolis, IN 46206-0420

392. Paul D. Stone
The Dow Chemical Company
1801 Building
Midland, MI 48674

393. Roger Storm
Standard Oil Engineered
Materials Company
PO Box 832
Niagara Falls, NY 14302

394. E. E. Strain
Allied-Signal Aerospace
Company
Garrett Engine Division
111 South 34th Street
PO Box 5217
MS: 301-2N
Phoenix, AZ 85010

395. Thomas N. Strom
NASA Lewis Research Center
21000 Brookpark Road, 77-6
Cleveland, OH 44135

396. Jerry Strong
Albright & Wilson
PO Box 26229
Richmond, VA 23260

397. Richard Suddeth
Boeing Motor Airplane Company
PO Box 7730
MS: K-76-67
Wichita, KS 67277

398. Paul Sutor
Midwest Research Institute
425 Volker Boulevard
Kansas City, MO 64116

399. J. J. Swab
U.S. Army Materials
  Technology Laboratory
405 Arsenal Street
Watertown, MA 02172

400. John W. Swain, Jr.
Kollmorgen Corporation
PCK Technology Division
15424 Garrison Lane
Southgate, MI 48915

401. Lewis Swank
Ford Motor Company
20000 Rotunda Drive
PO Box 2053
Building SRL, Room S2023
Dearborn, MI 48121-2053

402. Stephen R. Tan
ICI Advanced Materials
PO Box 11
The Heath, Runcorn
Cheshire
ENGLAND WA7 4QE

403. Anthony C. Taylor
U.S. House of Representatives
Rayburn Building, Room 2321
Washington, DC 20515

404. W. H. Thielbahr
U.S. Department of Energy
550 2nd Street
Idaho Falls, ID 83401

405. John K. Tien
Columbia University
1137 S.W. Mudd Building
New York, NY 10027

406. T. Y. Tien
University of Michigan
Dow Building
Ann Arbor, MI 48109-2136

407. Julian M. Tishkoff
Air Force Office of
  Scientific Research
(AFOSR/WC) Bolling AFB
Washington, DC 20332

408. Louis E. Toth
National Science Foundation
1800 G Street, N.W.
Washington, DC 20550

409. Richard E. Tressler
Pennsylvania State University
201 Steidle Building
University Park, PA 16802

410. Donald R. Uhlmann
Massachusetts Institute
  of Technology
77 Massachusetts Avenue
Cambridge, MA 02139

411. Edward C. Van Reuth
Technology Strategies, Inc.
10722 Shingle Oak Court
Burke, VA 22015

412. Thomas Vasilos
Avco Corporation
201 Towell Street
Wilmington, MA 01887

413. V. Venkateswaran
Standard Oil Engineered
  Materials Company
PO Box 832
Niagara Falls, NY 14302

414. John B. Wachtman, Jr.
     Rutgers University
     PO Box 909
     Bowser Road
     Piscataway, NJ 08854

415. Richard B. Wallace
     36880 Ecorse Road
     Romulus, MI 48174

416. Harlan L. Watson
     U.S. House of Representatives
     Rayburn Building, Suite 2321
     Washington, DC 20515

417. John D. Watson
     BHP Research & New Technology
     Melbourne Research
        Laboratories
     245 Wellington Road
     Mulgrave, Vic. 3170
     AUSTRALIA

418. Albert R. C. Westwood
     Martin Marietta Laboratories
     1450 South Rolling Road
     Baltimore, MD 21227

419. Thomas J. Whalen
     Ford Motor Company
     20000 Rotunda Drive
     PO Box 2053
     Dearborn, MI 48121-2053

420. Sheldon M. Wiederhorn
     National Bureau of Standards
     Gaithersburg, MD 20899

421. James C. Williams
     Carnegie-Mellon University
     Schenley Park
     Pittsburgh, PA 15213

422. Roger R. Wills
     TRW, Inc.
     Valve Division
     1455 East 185th Street
     Cleveland, OH 44110

423. J. M. Wimmer
     Allied-Signal Aerospace
        Company
     Garrett Engine Division
     111 South 34th Street
     Post Office Box 5217

424. David Wirth
     Coors Ceramics Company
     17750 West 32nd Street
     Golden, CO 80401

425. Thomas J. Wissing
     Eaton Corporation
     26201 Northwestern Highway
     Post Office Box 766
     Southfield, MI 48037

426. Dale Wittmer
     Southern Illinois University
        at Carbondale
     Department of Mechanical
        Engineering and
        Energy Processes
     Carbondale, IL 62901

427. George W. Wolter
     Howmet Turbine Components
        Corporation
     699 Benston Road
     Whitehall, MI 49461

428. James C. Wood
     NASA Lewis Research Center
     21000 Brookpark Road
     MS: 500-210
        Cleveland, OH 44135

429. Roger P. Worthen
     Eaton Corporation
     26201 Northwestern Highway
     PO Box 766
     Southfield, MI 48076

430. Thomas M. Yonushonis
Cummins Engine Company, Inc.
Box 3005, Mail Code 50183
Columbus, IN 47202-3005

431. Don Zabierek
Air Force Wright
   Aeronautical Laboratory
AFWAL/POTC
Wright-Patterson AFB
   OH 45433

432. Charles Zeh
U.S. Department of Energy
PO Box 880
Morgantown, WV 26505

433. Anne Marie Zerega
U.S. Department of Energy
Forrestal Building CE-15
1000 Independence Avenue
Washington, DC 20585

434. Martin Zlotnick
Nichols Research Corporation
8618 Westwood Center Dr.
Suite 200
Vienna, VA 22180-2222

435. Klaus M. Zwilsky
National Research Council
2101 Constitution Avenue
Washington, DC 20418

436. Department of Energy
Oak Ridge Operations Office
Assistant Manager for Energy
   Research and Development
PO Box 2001
Oak Ridge, TN 37831

437-446. Department of Energy
Office of Scientific and
   Technical Information
Office of Information Services
PO Box 62
Oak Ridge, TN 37831

For distribution by microfiche
as shown in DOE/TIC-4500,
Distribution Category UC-95.